Published for SISSA by Springer

Received: December 22, 2025
Revised: August 21, 2026
Accepted: September 22, 2026
Published: October 21, 2026

Search for $t\bar{t}$ resonances in final states with exactly one or two leptons using 140 fb^{-1} of pp collision data at $\sqrt{s} = 13$ TeV with the ATLAS experiment

The ATLAS collaboration

Full author list at the end of the paper

E-mail: atlas.publications@cern.ch

Abstract: A search for heavy spin-1 and spin-2 resonances decaying into a top-antitop-quark pair has been performed with 140 fb^{-1} of proton-proton collision data collected by the ATLAS experiment at the Large Hadron Collider at a centre-of-mass energy of $\sqrt{s} = 13$ TeV. Final states with either exactly one electron or muon, or exactly two leptons (ee, $\mu\mu$ or $e\mu$), large missing transverse momentum, and two jets, at least one of which must be identified as likely containing a b-hadron decay, are considered. The search targets resonances with both narrow and broad widths relative to the detector resolution, and with masses in the range of 0.4–5.0 TeV. No significant deviation from the Standard Model prediction is observed. Exclusion limits are set on the production cross-section times branching ratio for hypothetical Z' bosons, Kaluza-Klein gravitons, and Kaluza-Klein gluons that decay into top-quark pairs.

Keywords: Beyond Standard Model, Hadron-Hadron Scattering

ArXiv ePrint: 2512.17856

Open Access, Copyright CERN,
for the benefit of the ATLAS Collaboration.
Article funded by SCOAP^3.

https://doi.org/10.1007/JHEP10(2026)219

JHEP10(2026)219

Contents

1 Introduction **2**

2 Theoretical framework **3**
- 2.1 Spin-1 colour singlet 4
- 2.2 Spin-2 colour singlet 4
- 2.3 Spin-1 colour octet 5

3 ATLAS detector **6**

4 Data and simulated event samples **7**

5 Object reconstruction **10**

6 Event selection and categorisation **13**
- 6.1 Event selection and categorisation in the 1-lepton channel 13
- 6.2 Event selection and categorisation in the 2-lepton channel 17

7 Observables **20**
- 7.1 Observables in the 1-lepton channel 20
- 7.2 Observables in the 2-lepton channel 21

8 Data-driven estimation of background contributions **22**
- 8.1 W + jets background in the 1-lepton channel 22
- 8.2 Fakes background in the 1-lepton channel 24
- 8.3 Z + jets background in the 2-lepton channel 25

9 Statistical analysis **26**

10 Systematic uncertainties **26**
- 10.1 Modelling uncertainties 26
- 10.2 Experimental uncertainties 30
- 10.3 Uncertainty correlation scheme 31

11 Results **31**
- 11.1 Uncertainty impact 31
- 11.2 Constraints on selected benchmark models 34

12 Conclusion **37**

The ATLAS collaboration **48**

JHEP10(2026)219

1 Introduction

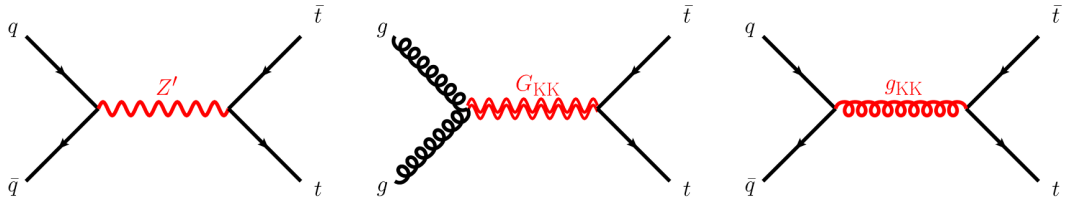
New heavy particles coupling strongly to the top quark are predicted in numerous extensions of the Standard Model (SM) of particle physics. Such models are proposed to address open questions of the SM, such as the large difference between the scales of electroweak interactions at $\mathcal{O}(100)$ GeV and gravity at $\mathcal{O}(10^{19})$ GeV, known as the Planck scale [1, 2]. Models include, for example, topcolor-assisted-technicolor (TC2) [3–6] and Randall-Sundrum (RS) models of warped extra dimensions [7, 8], predicting one or several additional heavy bosons, such as a spin-1 Z' particle, a spin-2 Kaluza-Klein (KK) graviton (G_{KK}), or a spin-1 KK gluon (g_{KK}). The new states can have strong or preferential couplings to the top quark, the heaviest elementary particle of the SM. Resonant production of a top-antitop-quark pair ($t\bar{t}$), if observed, would thus provide a smoking-gun signature of phenomena beyond the SM. Searches for this process are therefore an integral part of the experimental programme at the Large Hadron Collider (LHC) [9], which now provides unique access to heavy resonances with masses in the multi-TeV range.

Searches for heavy resonances decaying into a $t\bar{t}$ pair have previously been conducted with the ATLAS and CMS experiments using proton-proton (pp) collisions at $\sqrt{s} = 7$ TeV [10–15], 8 TeV [16–19], and 13 TeV [20–24]. Both experiments have performed the searches in the fully-hadronic and single-lepton final states, while the CMS Collaboration has also included the dileptonic final states. ATLAS and CMS have also recently performed dedicated searches for (pseudo-)scalar resonances [25, 26], focusing on signals with masses below 2 TeV and where interference between the signal and the SM $t\bar{t}$ background is known to be significant. These signals are hence not considered in this paper. In the search performed by CMS, a significant deviation from the SM expected limits for a $t\bar{t}$ mass less than approximately 400 GeV was observed. This was later shown by CMS [27] to be consistent with a colour-singlet, quasi-bound state of top quarks, predicted in the SM. The mild tension observed by ATLAS [28] and CMS [29] between the data and simulation in the quantum entanglement studies is also partially relieved by the inclusion of the pseudo-scalar state. In this paper, the focus is on searches for resonant signals with masses above 400 GeV; the inclusion of the quasi-bound state as a background was tested and has no impact on the results of this paper.

This paper presents a search for $t\bar{t}$ resonances across the $t\bar{t}$ invariant mass spectrum, $m_{t\bar{t}}$, from 0.4 TeV to 5.0 TeV. The search is performed using 140 fb^{-1} of pp collision data recorded in 2015–2018 at $\sqrt{s} = 13$ TeV with the ATLAS detector at the LHC, and uses the single-lepton and dilepton final states, complementing the fully-hadronic ATLAS search. The results in this paper consider spin-1 and spin-2 signal models and are valid for the case when interference is negligible. It is the first time in Run 2 that the dilepton channel has been included in an ATLAS search for these types of resonances, and both the single-lepton and dilepton channels use the full Run-2 data for the first time. Additionally, the single-lepton channel improves on the previous 36 fb^{-1} analysis through improved $t\bar{t}$ reconstruction and the addition of validation regions to better evaluate the background modelling.

The search presented in this paper targets events in which one top quark decays semi-leptonically and the other hadronically (1-lepton channel), as well as events in which both top quarks decay leptonically (2-lepton channel). Here, leptonic top-quark decays are defined as the top-quark decays resulting in a prompt electron (e) or muon (μ), either directly from

JHEP10(2026)219



(a) (b) (c)

Figure 1. Representative leading-order Feynman diagrams for the s-channel production and subsequent decay to $t\bar{t}$ of the (a) Z'_{TC2} , (b) G_{KK}, and (c) g_{KK} signals.

the W boson decay or via secondary decays of leptonically-decaying τ-leptons. Hadronic top-quark decays in the 1-lepton channel are targeted using separate analysis strategies for resolved and merged topologies that are combined to maximise the sensitivity for the $m_{t\bar{t}}$ range from 400 GeV up to values of several TeV. In the range $m_{t\bar{t}} > 2$ TeV, the top quarks are highly Lorentz boosted, resulting in the decay products merging into a single jet. Therefore, an advanced multivariate classifier based on a deep neural network is used to identify the hadronic top-quark decays with these highly collimated decay products [30]. The dominant background in both channels arises from SM $t\bar{t}$ production.

This paper is structured as follows. In section 2, the benchmark models used for the interpretation of the results of this search are introduced. In sections 3 and 4, the ATLAS detector as well as the data and simulated event samples are described. The object reconstruction, event selection, categorisation and reconstruction of observables, and the estimate of background processes are described in sections 5 to 8. The description of the statistical analysis is provided in section 9 and the systematic uncertainties are detailed in section 10. Finally, results are presented and discussed in section 11, where, in the absence of any significant excess, exclusion limits on the production cross-section times branching ratio for the hypothetical new particles are presented at the 95% confidence level.

2 Theoretical framework

The search presented in this paper is designed to be sensitive to the production of different types of spin-1 and spin-2, s-channel resonances decaying to $t\bar{t}$. The selection efficiency and acceptance can differ depending on the properties of the new resonance, such as its spin, width, or production mode. Therefore, the sensitivity to three types of new particle was evaluated to quantify the performance of the search. The benchmark models adopted in this search are colour-singlet and colour-octet bosons with spin-1 or spin-2 and masses ranging from 400 GeV to 5 TeV. Two benchmark models with a narrow relative resonance width, Γ/m, below the experimental resolution of $\Gamma/m \approx \mathcal{O}(10\%)$ are used, in addition to a model predicting wide resonances with a relative width of $\Gamma/m = 30\%$. Figure 1 shows example Feynman diagrams for the three benchmark models considered, and the following section details the theoretical motivation for such models.

JHEP10(2026)219

2.1 Spin-1 colour singlet

Spin-1, electrically neutral, colour-singlet vector bosons, referred to as Z' bosons, are predicted in various extensions of the SM, such as topcolor-assisted-technicolor models [3, 4]. The benchmark model used in this paper is the same as in previous searches for $t\bar{t}$ resonances [11, 12, 17, 19–21, 24] and is referred to as Model IV in ref. [5], with production cross-section calculations for the LHC provided by ref. [6]. The model predicts a leptophobic Z' boson, referred to as Z'_{TC2}, which is mainly produced via $q\bar{q}$ annihilation and decays into first- and third-generation quarks. The properties of the boson are controlled by three parameters: the top-color tilting parameter, $\cot\theta_H$, which controls the width and the production cross-section, and f_1 and f_2, which are related to the coupling to up-type and down-type quarks, respectively. In the benchmark considered in this and previous papers, f_1 is set to 1 and f_2 to 0 to maximise the branching fraction of the $Z'_{\mathrm{TC2}} \to t\bar{t}$ decay, which reaches 33%. The parameter $\cot\theta_H$ is tuned for each mass point such that the resonance has a width of 3% of its mass [6]. Given that this width is smaller than the experimental resolution, the Z'_{TC2} signal considered in this paper can also be used to set limits on the production cross-section times branching ratio for a Z'_{TC2} signal with other widths that are also below the experimental resolution by rescaling the theory production cross-section. The predicted next-to-leading-order (NLO) $Z'_{\mathrm{TC2}} \to t\bar{t}$ production cross-section for a Z'_{TC2} mass of 4 TeV is about 7.6 fb for a width of $\Gamma/m = 3\%$ and about 2.0 fb for a width of $\Gamma/m = 1\%$.

The strongest mass constraints on this model have been derived by the ATLAS Collaboration using the search in fully-hadronic final states on 139 fb^{-1} of $\sqrt{s} = 13$ TeV data [24]. This search excluded Z'_{TC2} bosons with 1% and 3% relative widths with masses up to 3.9 TeV and 4.7 TeV, respectively. The CMS Collaboration excluded Z'_{TC2} bosons with masses up to 3.80 TeV for a decay width of 1% using the combination of all three decay channels on 35.9 fb^{-1} of $\sqrt{s} = 13$ TeV data [23]. In the 1-lepton decay channel, the ATLAS Collaboration excluded Z'_{TC2} signals of width 1% with masses up to 3.0 TeV, using 36 fb^{-1} of data [20] and no previous search in the 2-lepton decay channel has been performed by the ATLAS Collaboration. Dijet searches performed by ATLAS [31–33] and CMS [34] also place constraints on leptophobic Z' bosons. ATLAS has provided direct sensitivity comparisons in the context of a simplified model with a dark matter Z' mediator that has flavour-universal couplings to all quarks, and this shows similar sensitivities between flavour-inclusive dijet searches and $t\bar{t}$ searches at high masses [35]. Given that the Z'_{TC2} model considered in this paper couples preferentially to top quarks, leading to approximately twice the branching ratio as that to bottom quarks, $t\bar{t}$ searches will be more sensitive than dijet searches for models with preferential couplings to $t\bar{t}$.

2.2 Spin-2 colour singlet

Spin-2, colour-singlet bosons are predicted in models that postulate extra dimensions of space leading to Kaluza-Klein (KK) excitations of the graviton. This search considers a Randall-Sundrum (RS) model with a single warped extra dimension, where the SM fields are in the bulk and the fermions are localised appropriately to explain the flavour structure of the SM [7, 36, 37]. The type of KK graviton predicted in this RS model is referred to as a "bulk" RS graviton, or G_{KK}, and it is characterised by its mass, $m_{G_{\mathrm{KK}}}$, and the dimensionless

JHEP10(2026)219

coupling of the KK gravitons to the SM fields, $k/\overline{M}_{\mathrm{Pl}}$, where $\overline{M}_{\mathrm{Pl}} = M_{\mathrm{Pl}}/8\pi$ is the reduced Planck mass and k is the curvature of the warped extra dimension. Larger values of $k/\overline{M}_{\mathrm{Pl}}$ yield a larger production cross-section and a larger resonance width. In RS models with SM fields in the bulk, values of $k/\overline{M}_{\mathrm{Pl}} \sim 1$ ensure that higher-order corrections to this model can be neglected [36]. For these KK gravitons, decays into light fermions are suppressed and the branching ratio to photons is negligible. In this and previous ATLAS papers, $k/\overline{M}_{\mathrm{Pl}} = 1.0$, a choice that maximises the production cross-section while keeping the resonance width below the experimental resolution. In the mass range 0.4–3 TeV considered for the KK graviton in this paper, the width varies between 3% and 6% of the mass. The primary production mode is gg fusion, while the primary decay modes are those to $t\bar{t}$, WW, ZZ, and hh. The branching ratio of the G_{KK} decay into a $t\bar{t}$ pair increases rapidly from 18% to 50% for masses between 0.4 and 0.6 TeV, reaching a plateau at 68% for masses larger than 1 TeV.

A previous search in the 1-lepton channel using 36 fb^{-1} of ATLAS data [20] excluded bulk RS gravitons with masses in the range of 0.45–0.65 TeV. A complementary search on the same ATLAS data sample targeting the decays $G_{\mathrm{KK}} \to WW, ZZ$ [38] excluded masses up to 2.3 TeV. A dijet search [31] considered the G_{KK} benchmark with $k/\overline{M}_{\mathrm{Pl}} = 0.2$ decaying into a bottom quark-anti-quark pair, and excluded these signals with masses up to 2.8 TeV. A CMS search on 35.6 fb^{-1} of $\sqrt{s} = 13$ TeV data targeting the decay $G_{\mathrm{KK}} \to ZZ$ [39] excluded the G_{KK} signal with $k/\overline{M}_{\mathrm{Pl}} = 0.5$ up to 0.8 TeV.[1] The model used in this paper and the papers mentioned above is itself ruled out by precision electroweak tests; nevertheless, it provides a useful generic benchmark that allows interpretations assuming some custodial symmetry to circumvent the electroweak constraints.

2.3 Spin-1 colour octet

Spin-1 colour-octet bosons are predicted in models with extra dimensions of space leading to KK excitations of the gluon [8, 40]. The benchmark model chosen in this paper, which is consistent with the benchmark choices in previous ATLAS publications, is an RS model with a single warped extra dimension, where the SM fields propagate in the bulk. The parameters of the model are also consistent with that of the G_{KK} model described above. The primary production mode of these KK gluons, referred to as g_{KK}, is via $q\bar{q}$ annihilation. The strong coupling of the g_{KK} to light quarks is set to $g_q = 0.2g_s$, where g_s is the SM gluon coupling to quarks and the couplings correspond to the configuration given in eq. (3) of ref. [8]. The left-handed coupling to the top quark is fixed at $g_{t,\mathrm{L}} = g_s$, and the right-handed coupling to the top quark, $g_{t,\mathrm{R}}$, is chosen to obtain a width of 30% to obtain benchmark predictions for a broad resonance. For the configuration described here, this sets $g_{t,\mathrm{L}} = g_{t,\mathrm{R}}$. This is fully consistent with the previous ATLAS searches for a g_{KK} signal [20, 21]. The branching fraction to $t\bar{t}$ in this case amounts to 92.5%.

A previous search in the 1-lepton channel using 36 fb^{-1} of ATLAS data [20] excluded KK gluon masses lower than 3.7 TeV in this benchmark model. The CMS Collaboration searched for similar resonances in 35.9 fb^{-1} of $\sqrt{s} = 13$ TeV data [23] using a combination of the three $t\bar{t}$ decay channels, excluding g_{KK} signals with masses up to 4.55 TeV. This is a

[1] The G_{KK} benchmark was not considered by the CMS Collaboration in their latest $t\bar{t}$ resonance searches [23].

JHEP10(2026)219

slightly different benchmark model than that used in this paper, which leads to a natural width of 15–20% and a smaller production cross-section times branching fraction [41].

3 ATLAS detector

The ATLAS detector [42] at the LHC covers nearly the entire solid angle around the collision point.[2] It consists of an inner tracking detector surrounded by a thin superconducting solenoid, electromagnetic and hadronic calorimeters, and a muon spectrometer incorporating three large superconducting air-core toroidal magnets.

The inner-detector system (ID) is immersed in a 2 T axial magnetic field and provides charged-particle tracking in the range $|\eta| < 2.5$. The high-granularity silicon pixel detector covers the vertex region and typically provides four measurements per track, the first hit generally being in the insertable B-layer (IBL) installed before Run 2 [43, 44]. It is followed by the SemiConductor Tracker (SCT), which usually provides eight measurements per track. These silicon detectors are complemented by the transition radiation tracker (TRT), which enables radially extended track reconstruction up to $|\eta| = 2.0$. The TRT also provides electron identification information based on the fraction of hits (typically 30 in total) above a higher energy-deposit threshold corresponding to transition radiation.

The calorimeter system covers the pseudorapidity range $|\eta| < 4.9$. Within the region $|\eta| < 3.2$, electromagnetic calorimetry is provided by barrel and endcap high-granularity lead/liquid-argon (LAr) calorimeters, with an additional thin LAr presampler covering $|\eta| < 1.8$ to correct for energy loss in material upstream of the calorimeters. Hadronic calorimetry is provided by the steel/scintillator-tile calorimeter, segmented into three barrel structures within $|\eta| < 1.7$, and two copper/LAr hadronic endcap calorimeters. The solid angle coverage is completed with forward copper/LAr and tungsten/LAr calorimeter modules optimised for electromagnetic and hadronic energy measurements, respectively.

The muon spectrometer (MS) comprises separate trigger and high-precision tracking chambers measuring the deflection of muons in a magnetic field generated by the superconducting air-core toroidal magnets. The field integral of the toroids ranges between 2.0 and 6.0 T m across most of the detector. Three layers of precision chambers, each consisting of layers of monitored drift tubes, cover the region $|\eta| < 2.7$, complemented by cathode-strip chambers in the forward region, where the background is highest. The muon trigger system covers the range $|\eta| < 2.4$ with resistive-plate chambers in the barrel, and thin-gap chambers in the endcap regions.

The luminosity is measured mainly by the LUCID-2 [45] detector that records Cherenkov light produced in the quartz windows of photomultipliers located close to the beampipe.

Events were selected by the first-level trigger system implemented in custom hardware, followed by selections made by algorithms implemented in software in the high-level trigger [46].

[2] ATLAS uses a right-handed coordinate system with its origin at the nominal interaction point (IP) in the centre of the detector and the z-axis along the beam pipe. The x-axis points from the IP to the centre of the LHC ring, and the y-axis points upwards. Polar coordinates (r, ϕ) are used in the transverse plane, ϕ being the azimuthal angle around the z-axis. The pseudorapidity is defined in terms of the polar angle θ as $\eta = -\ln\tan(\theta/2)$ and is equal to the rapidity $y = \frac{1}{2}\ln\left(\frac{E+p_z}{E-p_z}\right)$ in the relativistic limit. Angular distance is measured in units of $\Delta R \equiv \sqrt{(\Delta y)^2 + (\Delta\phi)^2}$.

JHEP10(2026)219

The first-level trigger accepted events from the 40 MHz bunch crossings at a rate close to 100 kHz, which the high-level trigger further reduced in order to record complete events to disk at about 1.25 kHz.

A software suite [47] is used in data simulation, in the reconstruction and analysis of real and simulated data, in detector operations, and in the trigger and data acquisition systems of the experiment.

4 Data and simulated event samples

Data from pp collisions at $\sqrt{s} = 13$ TeV corresponding to an integrated luminosity of 140 fb^{-1}, collected in the years 2015 to 2018 with the ATLAS detector, are analysed in the context of this search. The uncertainty in the combined 2015–2018 integrated luminosity is 0.83% [48], obtained primarily using the LUCID-2 detector [45], and complemented by measurements provided by the inner detector and the calorimeters. The average number of interactions per bunch crossing (pile-up) in this data sample is $\langle\mu\rangle = 33.7$. All detector subsystems were required to be operational during data taking [49].

Candidate events for both the 1- and 2-lepton channels are selected using single-muon [50] and single-electron [51] triggers. These triggers require a muon or an electron with momentum transverse to the beamlime, p_{T}, or energy transverse to the beamline, E_{T}, respectively, above a certain threshold and satisfying certain quality and, for some triggers, lepton isolation requirements. The triggers with the lowest p_{T} (E_{T}) threshold require $p_{\mathrm{T}}(E_{\mathrm{T}}) > 26$ GeV for muons (electrons) in 2016–2018 and $p_{\mathrm{T}}(E_{\mathrm{T}}) > 20(24)$ GeV in 2015, and include a lepton isolation requirement that is not applied for triggers with higher thresholds. The trigger efficiency is mostly constant in the transverse momentum for leptons with $p_{\mathrm{T}} > 28$ GeV, but can vary with η.

Monte Carlo (MC) simulated event samples are used to model the signal and background processes. Unless otherwise stated, the top-quark mass was always set to $m_{\mathrm{top}} = 172.5$ GeV; samples that used Pythia [52] for the generation used the A14 set of tuned parameters (tune) [53] with the NNPDF2.3lo [54] set of parton distribution functions (PDFs); and all samples that did not use Sherpa [55] used EvtGen [56] to model the decays of bottom and charm hadrons. The ATLAS simulation infrastructure [47] was used to simulate the detector and its response. Signal and nominal background samples as well as several alternative background samples used to assess systematic uncertainties were produced with a detailed Geant4 [57] detector simulation. A faster simulation based on a parameterisation of the calorimeter response and Geant4 for the other detector systems [47] was used for the remaining alternative background samples. Pile-up effects were modelled by overlaying minimum-bias events simulated using the soft QCD processes of Pythia 8.186 with the NNPDF2.3lo set of PDFs and the A3 tune [58]. The pile-up profiles match the ones of each data sample between 2015 and 2018. The same offline reconstruction methods used for data were applied to the simulated event samples. Corrections were applied to the simulated events to match the selection efficiencies, energy and mass scales and resolutions of reconstructed simulated particles to those measured in data control samples. An overview of the generator choices for the signal and background processes can be found in table 1, with further details given in the following.

JHEP10(2026)219

Process	ME generator	ME order	PDF set (ME)	PS and hadronisation	UE tune
Signal Z'_{TC2}	MadGraph 2.9.3	LO	NNPDF2.3lo	Pythia 8.245	A14
Signal g_{KK}	MadGraph 2.9.3	LO	NNPDF2.3lo	Pythia 8.245	A14
Signal G_{KK}	MadGraph 2.2.3	LO	NNPDF2.3lo	Pythia 8.210	A14
$t\bar{t}$	Powheg Box v2	NLO	NNPDF3.0nlo	Pythia 8.230	A14
Single top (Wt)	Powheg Box v2	NLO	NNPDF3.0nlo	Pythia 8.307	A14
Single top (s-channel)	Powheg Box v2	NLO	NNPDF3.0nlo	Pythia 8.230	A14
Single top (t-channel)	Powheg Box v2	NLO	NNPDF3.0nlo	Pythia 8.230	A14
Diboson	Sherpa 2.2.1/2.2.2	MEPS@NLO	NNPDF3.0nnlo	Sherpa	author tune
$W+$jets	Sherpa 2.2.11	MEPS@NLO	NNPDF3.0nnlo	Sherpa	author tune
$Z+$jets	Sherpa 2.2.1/2.2.11	MEPS@NLO	NNPDF3.0nnlo	Sherpa	author tune
$t\bar{t}+V$	MadGraph5_aMC@NLO 2.3.3	NLO	NNPDF3.0nlo	Pythia 8.210	A14
$t\bar{t}+H$	Powheg Box v2	NLO	NNPDF3.0nlo	Pythia 8.230	A14

Table 1. List of matrix element (ME) generators and the order of the strong coupling constant in the perturbative calculation, parton distribution function (PDF) sets, parton shower (PS) and hadronisation generator, and underlying event (UE) tune for the different signal and background processes.

The dominant background process is SM $t\bar{t}$ production. Smaller background components arise from single vector-boson (W, Z) production in association with hadronic jets, referred to as $W/Z+$jets, and single top-quark production (single top). There are also background processes in both channels that lead to at least one mis-identified or non-prompt lepton that satisfies the lepton identification and isolation criteria applied in this search, referred to as *fakes* in this paper. These mostly originate from strong multijet production in the 1-lepton channel and from single-lepton $t\bar{t}$ events in the 2-lepton channel. Single top and $W+$jets production can also lead to these mis-identified or non-prompt leptons. Minor backgrounds from $t\bar{t}+V$, $t\bar{t}+H$ and diboson (WW, ZZ, WZ) production are also considered. All background components, except the fakes in the 1-lepton channel (see section 8.2), are modelled using MC simulation. Data-driven corrections are applied to the MC-based estimates of the $W+$jets background in the 1-lepton channel (see section 8.1) and the $Z+$jets background in the 2-lepton channel (see section 8.3) to correct the $W+$jets normalisation and $Z+$jets shape, respectively.

SM $t\bar{t}$ production was generated at NLO accuracy in QCD using Powheg Box v2 [59–63] with the NNPDF3.0nlo [64] PDF set and the h_{damp} parameter set to $1.5\,m_{\mathrm{top}}$ [65].[3] The functional form of the renormalisation and factorisation scales was set to the default scale $\sqrt{m_{\mathrm{top}}^2+p_{\mathrm{T}}^2}$. The top quarks were decayed in Powheg Box, thus preserving their spin correlations. The matrix element (ME) generator is interfaced with Pythia 8.230 [66] to model the parton shower (PS), hadronisation, and the underlying event (UE).

Alternative SM $t\bar{t}$ samples obtained with different generator choices and settings are used to estimate systematic uncertainties related to the modelling of this main background component. The details can be found in section 10.1.

The top-quark kinematics in the nominal and all alternative SM $t\bar{t}$ samples were corrected to more accurate differential predictions calculated at next-to-next-to-leading-

[3]The h_{damp} parameter controls the p_{T} of the first additional emission beyond the leading-order Feynman diagram in the parton shower and therefore regulates the high-p_{T} emission against which the $t\bar{t}$ system recoils.

JHEP10(2026)219

order (NNLO) QCD and NLO electroweak (EW) accuracy for a top-quark mass value of m_{top} =173.3 GeV [67]. The difference between the m_{top} value used in the reweighting and the value of 172.5 GeV used in the NLO MC generation was found to have no impact on the analysis sensitivity. The corrections were applied as event-by-event weights that were obtained via an iterative recursive reweighting procedure in the differential distributions of the (anti)top-quark p_{T} and $m_{t\bar{t}}$, referred to as *NNLO reweighting*, following the same procedure as described in ref. [25]. The systematic uncertainties related to the NNLO reweighting procedure are listed in section 10.1.

All reweighted $t\bar{t}$ samples were additionally normalised to the cross-section prediction at NNLO in QCD, including the resummation of next-to-next-to-leading logarithmic (NNLL) soft-gluon terms calculated using Top++ 2.0 [68–74], corresponding to 832 ± 51 pb.

Single top production in the Wt-channel [75], which constitutes the main single top contribution, was generated with Powheg Box v2 using the NNPDF3.0nlo PDF set. The overlap between $t\bar{t}$ and Wt production, arising due to NLO EW corrections to Wt, was treated within the diagram removal (DR) scheme [76] and the renormalisation and factorisation scales were set to $H_{\text{T}}/2$, where H_{T} denotes the scalar sum of the transverse momenta of all final-state particles in the event. The ME generator was interfaced with Pythia 8.307 [77] for the PS, hadronisation, and the UE modelling. The sample was normalised to the theory cross-sections for inclusive Wt, calculated at NLO accuracy in QCD with NNLL soft-gluon corrections and corresponding to 71.7 ± 3.8 pb [78].

Single top production in the s-channel [79] was generated with Powheg Box v2 at NLO in QCD using the five-flavour scheme and the NNPDF3.0nlo PDF set. Single top production in the t-channel was generated with Powheg Box v2 [80], using the four-flavour scheme for the NLO ME calculations together with the corresponding PDF NNPDF3.0 set. For this process, the top-quark decays were simulated using MadSpin [81], preserving all spin correlations. For both processes, the ME generator was also interfaced with Pythia 8.230. The inclusive cross-sections were corrected to the theory predictions at NLO in QCD with Hathor 2.1 [82, 83]. For the s-channel process, this cross-section corresponds to $6.35^{+0.23}_{-0.20}$ pb ($3.97^{+0.19}_{-0.17}$ pb) for single top (single anti-top) production [84], and for the t-channel process, this cross-section corresponds to $136.0^{+5.4}_{-4.6}$ pb ($81.0^{+4.1}_{-3.6}$ pb) [85] for single top (single anti-top) production.

The background from $t\bar{t} + V$ ($V = W, Z$) production was generated at NLO accuracy in QCD with MadGraph5_aMC@NLO 2.3.3 [86] with the NNPDF3.0nlo PDF set, interfaced with Pythia 8.210 for the PS, hadronisation, and UE. The samples were normalised to the theory cross-section calculated at NLO in QCD [87]. The background from $t\bar{t} + H$ production was generated at NLO accuracy in QCD with Powheg Box v2 with the NNPDF3.0nlo PDF set, interfaced with Pythia 8.230 for the PS, hadronisation, and UE. The samples were normalised to the theory cross-section calculated at NLO QCD and NLO EW accuracies [87].

The production of a single W boson in association with hadronic jets (W + jets) was simulated with Sherpa 2.2.11. The background from Z + jets production was simulated with Sherpa 2.2.11 in the 1-lepton channel and with Sherpa 2.2.1 in the 2-lepton channel. NLO ME calculations were used for up to two partons for all samples, and leading-order (LO) ME calculations for up to five (four) partons for the Sherpa 2.2.11 (Sherpa 2.2.1) samples. The MEs were calculated with the Comix [88] and OpenLoops [89–91] libraries. They were

JHEP10(2026)219

matched with the SHERPA PS [92] using the MEPS@NLO prescription [93–96] and the set of tuned parameters developed by the SHERPA authors. The NNPDF3.0NNLO set of PDFs was used for all V + jets samples. The W + jets and Z + jets samples were normalised to the theory cross-sections calculated at NLO accuracy in QCD [97]. An additional data-driven normalisation correction was derived for the W + jets background in the 1-lepton channel. Details can be found in section 8.1.

Diboson events with fully leptonic and semileptonic decays were simulated using SHERPA 2.2.1 and SHERPA 2.2.2 [98], respectively. The simulation includes off-shell effects and Higgs boson contributions, where appropriate. Events were simulated using ME calculations at NLO accuracy in QCD for up to one additional parton and at LO accuracy for up to three additional parton emissions. Samples for the loop-induced processes $gg \to VV$ were simulated using LO-accurate ME calculations for up to one additional parton emission. The ME calculations were matched and merged with the SHERPA PS based on the Catani-Seymour dipole factorisation [88, 92] using the MEPS@NLO prescription. The virtual QCD corrections were provided by the OPENLOOPS library. The NNPDF3.0NNLO set of PDFs was used, along with the dedicated set of tuned PS parameters developed by the SHERPA authors. The cross-sections from the generator were used for sample normalisation.

The fakes background in the 2-lepton channel is estimated using the single-lepton $t\bar{t}$ MC sample, the single top MC samples and the W + jets MC sample that contains two leptons. After requiring two reconstructed leptons, if at least one of the leptons is not matched to a prompt lepton at generator level, the event is considered to be part of the fakes background.

The production of each of the three signals decaying into $t\bar{t}$ was modelled at LO in QCD with the NNPDF2.3LO PDF set using MADGRAPH 2.9.3 for the Z'_{TC2} and g_{KK} signals, and MADGRAPH 2.2.3 for the G_{KK} signal. PYTHIA 8.245 was used to model the PS and hadronisation of the Z'_{TC2} and g_{KK} signals, and PYTHIA 8.210 was used for the G_{KK} signal. For the Z'_{TC2} signals, the generated values of the cross-section were scaled to the cross-section predictions obtained at NLO in QCD for the 1.2% width [99], whilst the cross-sections obtained with MADGRAPH were used directly for the g_{KK} and G_{KK} samples.

5 Object reconstruction

Common event-quality criteria and object definitions are applied for both analysis channels, including standard data-quality requirements to select data events with the detector in good operating condition [49]. In addition, in each analysis channel, dedicated event selection criteria, which are specific to the objects and kinematics of interest in those final states, are applied as described in section 6.

Events are required to have at least one reconstructed pp interaction vertex with a minimum of two associated tracks with $p_{\mathrm{T}} > 0.5$ GeV. The primary vertex matched to the hard-scatter of the interaction is defined as the vertex with the highest sum of squared transverse momenta of associated tracks [100]. A set of baseline quality criteria are applied to reject events with non-collision backgrounds or detector noise [101].

Two levels of object identification requirements are defined for charged leptons and jets: baseline and signal. Baseline leptons and jets are selected with looser identification criteria, and are used in computing the missing transverse momentum and in resolving possible

JHEP10(2026)219

reconstruction ambiguities. Signal leptons and jets are a subset of the baseline objects with tighter quality requirements, which are used to define the search regions. Isolation criteria are used to discriminate between prompt leptons and leptons arising from semileptonic heavy-flavour decays or jets mis-identified as leptons.

Jets are reconstructed from particle-flow objects [102] using the anti-k_t algorithm [103, 104] with a radius parameter $R = 0.4$. The particle-flow algorithm combines information about ID tracks and energy deposits in the calorimeters to form the input for jet reconstruction. A pile-up subtraction procedure [105] is applied along with a global sequential calibration to account for flavour dependencies. To suppress jets arising from pile-up, a jet-vertex-tagging (JVT) technique using a multivariate likelihood [106] is applied to jets with $p_{\mathrm{T}} < 60$ GeV and $|\eta| < 2.4$ to reject jets that do not orginate from the hard-scatter primary vertex. Baseline jets are selected by requiring $p_{\mathrm{T}} > 20$ GeV and $|\eta| < 4.5$. Signal jets are selected via the tighter requirements $p_{\mathrm{T}} > 30$ GeV and $|\eta| < 2.5$.

Jets with a larger radius parameter, $R = 1.0$, referred to as large-R jets in the following, are used as proxies for hadronically-decaying top quarks with a large Lorentz boost. They are reconstructed from three-dimensional topological clusters of energy deposits in the calorimeter using the anti-k_t algorithm. The topological clusters are calibrated to the hadronic energy scale with the local cluster weighting (LCW) [107] procedure to account for the non-compensating calorimeter response and the energy loss in dead material or due to out-of-cluster leakage of deposited energy. The large-R jets are trimmed [108] to reduce contributions from pile-up and soft interactions by reclustering the jet constituents into subjets, using the k_t algorithm [109–111] with a radius parameter $R = 0.2$, and discarding constituents belonging to subjets with p_{T} less than 5% of the p_{T} of the parent jet [112]. The four-momenta of large-R jets are reconstructed from the momentum vectors of the remaining subjets and calibrated using simulation [113]. The large-R jets used are required to have $p_{\mathrm{T}} > 350$ GeV and $|\eta| < 2.0$.

Large-R jets originating from a boosted hadronically-decaying top quark are identified using a multivariate classification algorithm based on a deep neural network (DNN) [30] that takes 13 jet moments, including the jet mass and p_{T}, as inputs for training. A DNN score between zero and one is obtained, with top-quark-initiated jets having values close to one and light-quark- and gluon-initiated jets having values close to zero. The top-tagging requirements used are optimised for "inclusive" jets containing some but not necessarily all of the decay products of the hadronically-decaying top quark. A large-R jet is considered "top-tagged" using a requirement on the DNN output score that corresponds to an identification efficiency of 80% for inclusive top-jets, evaluated in simulated SM $t\bar{t}$ events. The rejection factor for light-flavour quark and gluon jets varies as a function of the large-R jet p_{T}, from approximately 60 at 350 GeV to approximately 10 at 3000 GeV, where the rejection factor is defined as the reciprocal of the probability of mistakenly identifying a light-quark-initiated jet or a gluon-initiated jet as a top-quark-initiated jet. Scale factors are applied to all jets satisfying the top-tagging requirement in simulated events to correct for possible efficiency differences between simulated event samples and data [30].

Small-R jets in the range $|\eta| < 2.5$ are identified as likely to contain a b-hadron, henceforth called b-tagged, using the DL1r algorithm [114]. This algorithm is based on a multivariate classification technique with a DNN combining information from the impact parameters of

JHEP10(2026)219

tracks and topological properties of secondary and tertiary decay vertices reconstructed from the tracks associated with the jet. The b-tagged jets are selected using an operating point corresponding to an efficiency of 77% for identifying true b-jets in simulated SM $t\bar{t}$ events. This operating point corresponds to a rejection factor of 6 for c-jets and of 134 for light-flavour jets. Correction factors are applied to the simulated event samples to compensate for differences between data and simulation in the b-tagging efficiency for b-, c-, and light-flavour jets [115–117]. The correction for b-jets is derived from $t\bar{t}$ events with final states containing two leptons, and the corrections are consistent with unity within uncertainties at the level of a few percent over most of the jet p_{T} range. The corrections for c-jets and light-flavour jets are derived in semileptonic $t\bar{t}$ events and Z + jets events, respectively.

Muon candidates are reconstructed from matching tracks in the ID and MS, refined through a global fit that uses the hits from both subdetectors [118]. Baseline muons must have $p_{\mathrm{T}} > 10$ GeV and $|\eta| < 2.5$, and satisfy a set of medium identification criteria. Additionally, the longitudinal impact parameter is required to satisfy $|z_0 \sin\theta| < 0.5$ mm. Signal muons are required to have $p_{\mathrm{T}} > 25$ GeV and additionally satisfy the following requirement on the transverse impact parameter d_0 and its uncertainty σ_{d_0}: $|d_0/\sigma_{d_0}| < 3$. They are also required to be isolated using the requirement that the sum of the transverse momenta of the tracks within a variable-radius cone around the muon direction, excluding the muon track, be less than 6% of the transverse momentum of the muon [118]. The track isolation cone size is given by the minimum of $R = 10\ \mathrm{GeV}/p_{\mathrm{T}}^{\mu}$ and $R = 0.3$, where p_{T}^{μ} is the muon p_{T} [17].

Electron candidates are reconstructed from energy deposits in the electromagnetic calorimeter matched to a charged-particle track in the ID [119]. The track is required to be matched to the primary vertex by imposing the requirement $|z_0 \sin\theta| < 0.5$ mm. Electron candidates are required to be within $|\eta| < 2.47$, excluding the transition region between the barrel and endcap calorimeters ($1.37 < |\eta| < 1.52$). Baseline electrons are required to satisfy $p_{\mathrm{T}} > 10$ GeV and fulfil loose identification criteria, using a likelihood-based discriminant that combines information about tracks in the ID and energy deposits in the calorimeter system [119]. The number of hits in the innermost pixel layer is used to discriminate between electrons and converted photons. Signal electrons are required to also satisfy $p_{\mathrm{T}} > 25$ GeV and the tight likelihood identification criteria [119]. Additionally, signal electrons must fulfil $|d_0/\sigma(d_0)| < 5$. The same variable-cone isolation requirement as with muons is imposed on signal electrons, with the exception that the maximum cone radius is set to 0.2.

An overlap removal procedure is applied to resolve the reconstruction ambiguities between electrons, muons, and small-R jets. First, if an electron shares the same ID track with another electron, the electron with the lower transverse momentum is discarded. Electron candidates sharing the same inner-detector track as a muon are rejected, as they are likely mis-identified energy deposits from bremsstrahlung photons emitted by the muon. Next, the closest jet to an electron is rejected if it lies within $\Delta R = 0.2$ of the electron. Similarly, jets are rejected if they are within $\Delta R = 0.2$ of a muon if the jet has fewer than three associated tracks or the muon is matched to the jet through ghost association [120]. Next, to reduce the background contributions due to muons from heavy-flavour decays inside jets, muons are discarded if they are separated from the nearest jet by $\Delta R < 0.04 + 10\ \mathrm{GeV}/p_{\mathrm{T}}^{\mu}$. For electrons, an electron-in-jet subtraction method based on that employed in ref. [17] is used

JHEP10(2026)219

to suppress backgrounds from leptonic heavy-flavour decays inside jets, while maintaining a high reconstruction efficiency for electrons from highly collimated leptonic decays of boosted top quarks, which typically result in an electron close to a b-jet. If an electron is found within $\Delta R = 0.4$ of a jet, the four-momentum of the electron is subtracted from that of the jet, and the p_{T} of the electron-subtracted jet is calculated. A p_{T} threshold is defined using simulated $Z \to ee$ events and if the electron-subtracted jet has a p_{T} below this threshold, the jet is discarded and the electron is retained. If the electron-subtracted jet has a p_{T} above this threshold, the electron is discarded and the original jet is retained if the ΔR between the electron and the electron-subtracted jet is less than 0.2. Both the electron and the electron-subtracted jet are retained if the ΔR between them is greater than 0.2.

The missing transverse momentum $\vec{p}_{\mathrm{T}}^{\,\mathrm{miss}}$, with magnitude $E_{\mathrm{T}}^{\mathrm{miss}}$, is calculated as the negative vectorial sum of the transverse momenta of all baseline reconstructed objects (electrons, muons, small-R jets and photons [119]) and a soft term. The soft term includes all tracks associated with the primary vertex but not matched to any reconstructed physics object. Tracks not associated with the primary vertex are not considered in the $E_{\mathrm{T}}^{\mathrm{miss}}$ calculation, improving the $E_{\mathrm{T}}^{\mathrm{miss}}$ resolution by suppressing the effect of pile-up [121].

6 Event selection and categorisation

Events satisfying the single-electron and single-muon trigger requirements outlined in section 4, and the data-quality requirements described in section 5, are classified as belonging to the 1- or 2-lepton channels based on the number of signal electrons or muons they contain. The lepton requirements applied in this context are designed to ensure orthogonality between the two channels. Events in the 1-lepton channel are further classified into orthogonal event categories based on whether their detector signature is compatible with the presence of either a merged or resolved hadronic top-quark decay, and based on the number of associated b-jets. Angular requirements are used to define orthogonal signal and validation regions in both the 1- and 2-lepton channels. The latter have a similar background composition to the corresponding signal regions but are depleted in the expected signal processes. They serve to validate the modelling of the dominant background from SM $t\bar{t}$ production.

6.1 Event selection and categorisation in the 1-lepton channel

Events are required to contain exactly one signal electron or muon with a minimum $p_{\mathrm{T}}^{\ell} > 28$ GeV. This threshold is chosen to ensure that events are selected from the trigger efficiency plateau. The electron or muon is also required to be matched, within $\Delta R < 0.15$, to the respective trigger object. Events with a second signal electron or muon (with $p_{\mathrm{T}} > 25$ GeV, see section 5) are vetoed. Regions are not split according to the flavour of the selected lepton because it was found that such a splitting would not increase the sensitivity of the analysis.

The detector signature of a $t\bar{t}$ decay in the 1-lepton channel involves the presence of a substantial amount of missing transverse momentum from the leptonically-decaying W boson. To suppress background from the fakes that can cause small amounts of $E_{\mathrm{T}}^{\mathrm{miss}}$ via leptonic decays in heavy-flavour jets or mis-measured jet energies, the requirement $E_{\mathrm{T}}^{\mathrm{miss}} > 20$ GeV is imposed. Additionally, events are required to fulfil $E_{\mathrm{T}}^{\mathrm{miss}} + m_{\mathrm{T}}^{W} > 60$ GeV, where the

JHEP10(2026)219

transverse mass of the selected lepton and the $\vec{p}_{\mathrm{T}}^{\,\mathrm{miss}}$, referred to as the W transverse mass, or $m_{\mathrm{T}}^{\mathrm{W}}$, is defined as:

$$m_{\mathrm{T}}^{\mathrm{W}} = \sqrt{2p_{\mathrm{T}}^{\ell}E_{\mathrm{T}}^{\mathrm{miss}}(1-\cos\Delta\phi(p_{\mathrm{T}}^{\ell},\vec{p}_{\mathrm{T}}^{\,\mathrm{miss}}))}\,.$$

All events must contain at least one b-tagged small-R jet.

Events are further categorised based on their detector signature as containing either a merged hadronic top-quark decay ("merged category"), reconstructed as a single large-R jet, or a resolved hadronic top-quark decay ("resolved category"), resulting in three individual (small-R) jets. To obtain orthogonal signal regions, only events that do not meet the requirements for the merged-topology selection are considered for the resolved-topology selection. The preference for the merged- over the resolved-topology selection is based on its superior $m_{t\bar{t}}$ resolution (see section 7.1).

Events in the merged category must contain at least one small-R jet with a distance $\Delta R < 2.0$ to the selected lepton. If only one jet is found, it is identified as the b-jet candidate from the leptonic top-quark decay. If more than one jet is found within $\Delta R < 2.0$ from the selected lepton, the b-jet candidate is chosen as the jet with the highest p_{T} among all b-tagged candidate jets. If none of the candidate jets is b-tagged, the jet with the highest p_{T} is chosen instead. In addition, exactly one top-tagged large-R jet must be present in the event with a distance $\Delta R > 1.5$ to the lepton and to the selected b-jet candidate from the leptonic top-quark decay.

Only events failing the merged selection are considered for the resolved-topology selection. A fully resolved hadronic top-quark decay is expected to result in three small-R jets, one of which is a b-jet, in addition to a b-jet from the leptonic top-quark decay. Hence, events with a resolved decay topology are required to contain at least four selected small-R jets. The $t\bar{t}$ system is then reconstructed using a χ^2 algorithm, defined in section 7.1.1. Only well-reconstructed events, defined via the requirement $\log_{10}(\chi^2) < 0.9$, are kept for further analysis. This requirement has an efficiency of around 60% for SM $t\bar{t}$ events. All selection criteria are summarised in table 2.

In figure 2, the selection efficiency times acceptance for the $\ell+$jets final state is shown for the resolved, merged, and the combined resolved+merged categories, separately for the three benchmark scenarios described in section 2. It is given as a function of $m_{t\bar{t}}^{\mathrm{beforeFSR}}$, which is defined using the invariant mass of the top and anti-top quarks at parton level, before final-state radiation (FSR), and allows access to the invariant mass of the partonic system immediately from the resonance decay. The product of the acceptance times efficiency is defined as the ratio of events satisfying the signal region requirements to the total number of generated events. For reference, the branching ratio for $t\bar{t}$ to $e+$jets or $\mu+$jets final states is about 17% for each lepton flavour, taking into account leptonic τ-lepton decays [122]. The efficiency times acceptance is dominated by the merged topology selection for $t\bar{t}$ invariant mass values $m_{t\bar{t}} > 1000$ GeV, while the resolved topology selection covers the region down to the kinematic threshold of the analysis at 400 GeV. The selection efficiency times acceptance has a comparable $m_{t\bar{t}}$ dependence for all three benchmark models with small differences arising due to differences between the spin of the intermediate resonance, which leads to differences in the angular distributions of the $t\bar{t}$ decay products. The values vary from around

JHEP10(2026)219

Selection	Criteria
Common selection	
Event cleaning	All detector components with acceptable conditions
Single-lepton trigger	Single-electron or single-muon trigger
Exactly one lepton	Exactly one e or μ with $p_{\mathrm{T}} > 28$ GeV
	Veto second e or μ with $p_{\mathrm{T}} > 25$ GeV
$E_{\mathrm{T}}^{\mathrm{miss}}$	$E_{\mathrm{T}}^{\mathrm{miss}} > 20$ GeV
$E_{\mathrm{T}}^{\mathrm{miss}} + m_{\mathrm{T}}^{\mathrm{W}}$	$E_{\mathrm{T}}^{\mathrm{miss}} + m_{\mathrm{T}}^{W} > 60$ GeV
b-tagging	≥ 1 b-tagged small-R jet
Merged topology selection	
Large-R jet	≥ 1 large-R jet with $p_{\mathrm{T}} > 350$ GeV
Candidate top-jet (hadronic decay)	$= 1$ large-R jet passing top-tagging requirements
Candidate b-jet (leptonic decay)	≥ 1 small-R jet with $\Delta R(\ell, \text{jet}) < 2.0$
No overlap between objects	$\Delta R(\text{candidate b-jet}, \ell) < 2.0$
	$\Delta R(\text{candidate top-jet, candidate b-jet}) > 1.5$
	$\Delta R(\text{candidate top-jet}, \ell) > 1.5$
Resolved topology selection	
Veto events passing merged selection	
Small-R jets	≥ 4 small-R jets with $p_{\mathrm{T}} > 25$ GeV
Well-reconstructed $t\bar{t}$ system	$\log_{10}(\chi^2) < 0.9$

Table 2. Summary of the event selection criteria for the merged and resolved categories in the 1-lepton channel.

3% for the lowest mass signals up to around 12% for signals with masses between about 1 and 1.5 TeV. They are consistent within a few % between the different signal hypotheses.

To further increase the search sensitivity, events passing the resolved topology selection are divided into separate sub-categories based on whether one or both of the reconstructed top quarks have an associated b-tagged jet. The matching of b-tagged jets to the leptonic or hadronic top quark is performed by checking whether the small-R jet assigned as the b-candidate jet to the leptonic side or one of the small-R jets used for the reconstruction of the hadronic decay (based on the result of the χ^2 minimisation) is b-tagged. The *Resolved* $2b$ category contains events in which both top-quark candidates have associated b-tagged jets, while the *Resolved* $1b$ category contains events in which only the leptonically- or hadronically-decaying top-quark candidate has an associated b-tagged jet. No b-tagging categorisation is used for the merged topology as it provides minimal improvement in sensitivity.

The three 1-lepton categories (Merged, Resolved $2b$, and Resolved $1b$) are further subdivided into orthogonal signal and validation regions based on the absolute value of the pseudorapidity difference between the selected lepton and the hadronic top quark, $\left|\Delta\eta_{\ell,t^{\mathrm{had}}}\right|$.

JHEP10(2026)219

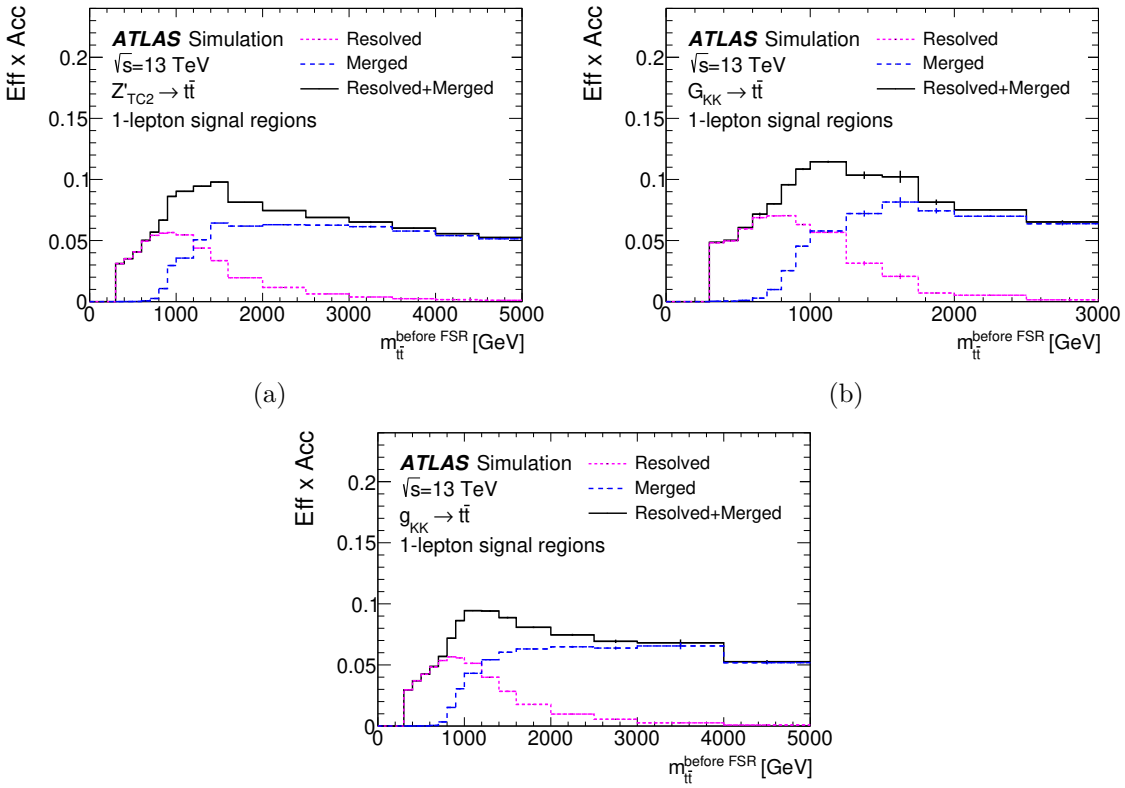


Figure 2. Selection efficiency times acceptance (Eff x Acc) for the ℓ + jets final state as a function of the $t\bar{t}$ invariant mass at the parton level before the emission of FSR, for the (a) Z'_{TC2}, (b) G_{KK}, and (c) g_{KK} signals. The selections in the resolved topology only (short-dashed magenta), the merged topology only (dashed blue) and the combined resolved+merged topology (solid black) are shown. The error bars correspond to the statistical uncertainty. All $t\bar{t}$ decay modes are considered.

The pseudorapidity difference (between top-quark pairs or between particular decay products of each of them) is mostly sensitive to the different production mechanisms for SM $t\bar{t}$ with respect to a $t\bar{t}$-resonance production process. Indeed, in SM $t\bar{t}$ production, which proceed predominantly via gluon-initiated t-channel diagrams, top quarks are preferentially produced along the incoming parton directions. On the other hand, for $t\bar{t}$ resonances the primary diagrams are s-channel ones (quark- or gluon-initiated, depending on the type of resonance), with a consequently more isotropic distribution. Spin-parity properties of the resonance can modify such pseudorapidity distributions, especially if the difference is taken between top-quark decay products such as charged leptons, but the separation power versus SM $t\bar{t}$ stays mostly the same for all the considered signals. This makes $\left|\Delta\eta_{\ell,t^{\mathrm{had}}}\right|$ particularly useful to split between signal and validation regions, with validation regions having similar background composition as their corresponding signal regions, but being depleted in any of the signal processes considered. The separation power of these pseudorapidity variables grows with $m_{t\bar{t}}$, with less and less partonic energy left for boosting the $t\bar{t}$ system along the z-direction and consequently narrowing the pseudorapidity distribution of the $t\bar{t}$ system.

JHEP10(2026)219

$m_{t\bar{t}}$ range [GeV]	Resolved signal region requirement on $\left\|\Delta\eta_{\ell,t^{\text{had}}}\right\|$
$m_{t\bar{t}} < 640$	< 1.5
$640 \leq m_{t\bar{t}} < 800$	< 2.0
$800 \leq m_{t\bar{t}} < 1280$	< 2.5
$1280 \leq m_{t\bar{t}} < 1700$	< 3.0
$m_{t\bar{t}} \geq 1700$	< 3.5

$m_{t\bar{t}}$ [GeV]	Merged signal region requirement on $\left\|\Delta\eta_{\ell,t^{\text{had}}}\right\|$
$m_{t\bar{t}} < 1040$	< 1.0
$1040 \leq m_{t\bar{t}} < 1850$	< 1.5
$1850 \leq m_{t\bar{t}} < 2500$	< 2.0
$2500 \leq m_{t\bar{t}} < 3500$	< 2.5
$m_{t\bar{t}} \geq 3500$	< 3.0

Table 3. Requirement on $\left|\Delta\eta_{\ell,t^{\text{had}}}\right|$ used to define the signal regions for the resolved and merged decay topologies of the 1-lepton channel as a function of $m_{t\bar{t}}$. Values larger than those listed in the table correspond instead to the validation regions.

These validation regions serve to validate the modelling of the dominant background from SM $t\bar{t}$ production before the hypothesis testing in data. The $\left|\Delta\eta_{\ell,t^{\text{had}}}\right|$ values chosen to define the signal and validation regions depend on the $m_{t\bar{t}}$ range. This $m_{t\bar{t}}$-dependent $\left|\Delta\eta_{\ell,t^{\text{had}}}\right|$ requirement is motivated by both statistical and kinematic considerations: it is relaxed at high $m_{t\bar{t}}$ to retain sufficient expected event yields in the signal regions, while accounting for the increasing correlation between $\left|\Delta\eta_{\ell,t^{\text{had}}}\right|$ and $m_{t\bar{t}}$, particularly for the SM $t\bar{t}$ background, as discussed above. The values are summarised in table 3 and figure 3(a) shows the distribution of $\left|\Delta\eta_{\ell,t^{\text{had}}}\right|$, inclusive in $m_{t\bar{t}}$. Very good agreement is observed between the data and the simulated backgounds already pre-fit.

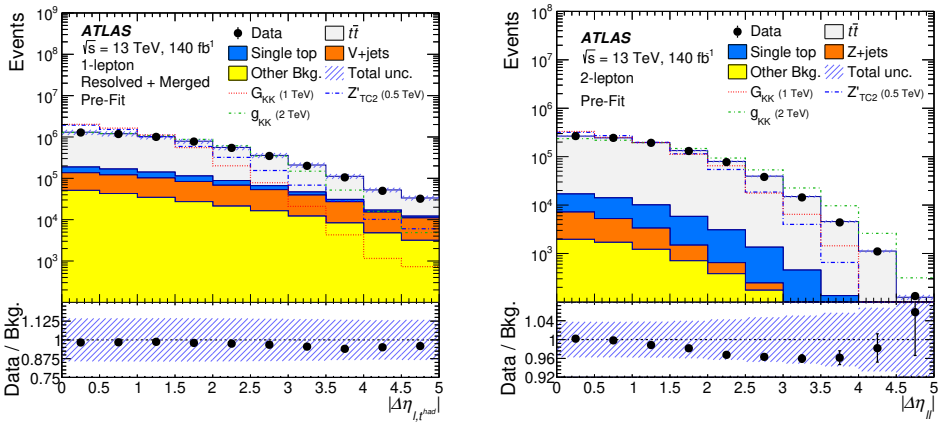
The highest SM $t\bar{t}$ contribution (94.9%) is found in the Resolved 2b region due to the requirement of two b-tagged jets. In the Resolved 1b and Merged signal regions, the SM $t\bar{t}$ production contributes to 79.2% and 88.9%, respectively, of the total SM background.

Additional control and validation regions enriched in hadronic jets falsely identified as leptons are defined for the data-driven estimate of the fakes background via the matrix method [123]. These are obtained by inverting the $E_{\text{T}}^{\text{miss}}$ and/or m_{T}^{W} requirements of the signal regions and additionally loosening the lepton identification and isolation requirements. Details are given in section 8.2.

6.2 Event selection and categorisation in the 2-lepton channel

Candidate events for the 2-lepton channel are required to have exactly two signal leptons and at least two reconstructed jets. At least one of these leptons is required to have $p_{\text{T}} > 28$ GeV

JHEP10(2026)219



(a) (b)

Figure 3. Distribution of (a) the reconstructed $|\Delta\eta_{\ell,t^{\mathrm{had}}}|$ in the 1-lepton channel and (b) the reconstructed $|\Delta\eta_{\ell\ell}|$ in the 2-lepton channel. The distributions and the uncertainty band are obtained before the final fit to the data (pre-fit). "V + jets" refers to the Z + jets and W + jets backgrounds, whilst "Other Bkg." combines the $t\bar{t}+V$, $t\bar{t}+H$, diboson and fakes backgrounds together. A 0.5 TeV Z'_{TC2} signal (blue dashed and dotted line), a 1 TeV G_{KK} signal (red dotted line) and a 2 TeV g_{KK} signal (green short-dashed and dotted line) are overlaid for illustration purposes, normalised to the total background. The lower panels show the ratio of the data to the total SM background prediction. The error bands include both the statistical and systematic uncertainties.

and to match, within $\Delta R < 0.15$, the lepton of the same flavour reconstructed by the trigger algorithm. Additionally, at least one of the jets is required to be b-tagged. Depending on the flavour of the charged leptons, three channels are defined: ee, $\mu\mu$ and $e\mu$. Events satisfying these requirements are then further classified into signal and validation regions.

Events are required to contain two leptons with opposite-sign electric charge (OS). In the ee and $\mu\mu$ channels, to further suppress the background from Z/γ^* + jets production, the dilepton invariant mass, $m_{\ell\ell}$, is required to be greater than 15 GeV and not within the range 81–101 GeV (excluding the Z-boson pole). The missing transverse momentum is also required to be larger than 45 GeV. Additionally, events must meet the requirement that the invariant masses of the lepton–b-jet pairs, $m_{\ell b}$, be smaller than 150 GeV for at least one of the two possible b-jet to lepton assignments. In this context, the two b-jets are either taken as the two b-tagged jets with the largest p_{T} or, if only one jet in the event is b-tagged, the b-tagged jet and the jet with the highest p_{T} among the jets that are not b-tagged. This requirement is meant to veto events where at least one of the lepton–b-jet pairs does not originate from a top-quark decay. It effectively suppresses events from Wt production and $t\bar{t}$ events in which at least one of the selected b-jets does not originate from a top-quark decay but, for example, from initial-state radiation (ISR). It has a 64% efficiency for SM $t\bar{t}$ events with both top quarks decaying leptonically, and a 68% efficiency for signal events with a resonance mass of 1000 GeV. The event selection requirements are summarised in table 4 and the relative contribution of SM $t\bar{t}$ production to the total SM background amounts to 94.7%.

Five orthogonal regions based on the absolute value of the azimuthal angle between the two leptons, $|\Delta\phi_{\ell\ell}|$, divided by π are defined: [0, 0.50], (0.50, 0.80], (0.80, 0.90], (0.90, 0.95],

JHEP10(2026)219

Selection	Criteria
Event cleaning	All detector components with acceptable conditions
Single-lepton trigger	Single-electron or single-muon trigger
Exactly two leptons	Exactly two (ee, $\mu\mu$, or $e\mu$) with $p_{\mathrm{T}} > 25$ GeV Leading lepton with $p_{\mathrm{T}} > 28$ GeV
Small-R jets	≥ 2 jets with $p_{\mathrm{T}} > 25$ GeV
b-tagging	≥ 1 b-tagged jet
Opposite-sign leptons	e^+e^-, $\mu^+\mu^-$, $e^+\mu^-$, or $e^-\mu^+$
$E_{\mathrm{T}}^{\mathrm{miss}}$	$E_{\mathrm{T}}^{\mathrm{miss}} > 45$ GeV (ee and $\mu\mu$ channels only)
Dilepton invariant mass	$15 < m_{\ell\ell} < 81$ GeV or $m_{\ell\ell} > 101$ GeV (ee and $\mu\mu$ channels only)
Lepton-plus-b-jet invariant mass	$\min(m_{\ell b}) < 150$ GeV

Table 4. Summary of the event selection criteria for the signal regions in the 2-lepton channel.

$m_{\ell\ell bb}$ range [GeV]	Signal region requirement on $\lvert\Delta\eta_{\ell\ell}\rvert$
< 450	< 1.0
450–1000	< 1.5
1000–1500	< 2.0
1500–2500	< 2.5
> 2500	none

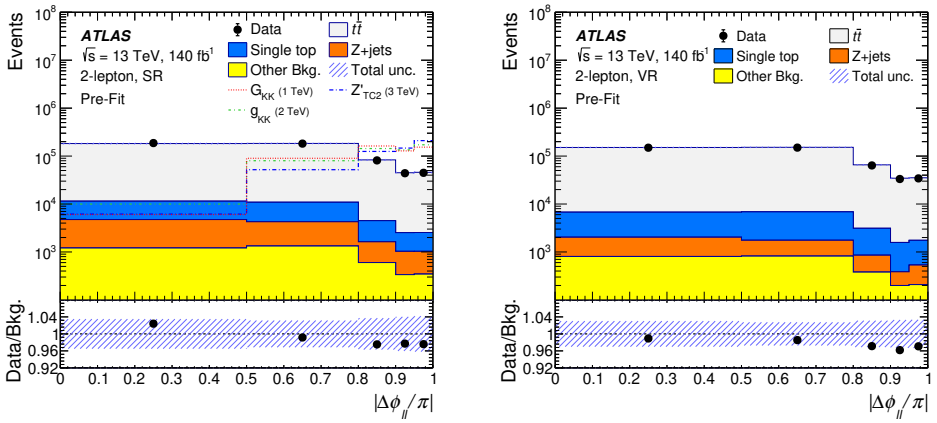
Table 5. Requirement on $|\Delta\eta_{\ell\ell}|$ used to define the signal regions as a function of $m_{\ell\ell bb}$. Values larger than those listed in the table correspond instead to the validation regions.

and (0.95, 1.00]. The $|\Delta\phi_{\ell\ell}|$ distribution is shaped by both the kinematics of the $t\bar{t}$ system and the spin correlations of the top-quark pair. Increasing $m_{t\bar{t}}$ leads to more boosted top quarks and hence larger values of $|\Delta\phi_{\ell\ell}|$. On the other hand, at fixed $m_{t\bar{t}}$, spin-correlation effects in SM $t\bar{t}$ production, together with the fact that charged leptons are emitted mostly along the spin directions of their parent top or antitop quark in the respective rest frame, tend to favour configurations where charged leptons have smaller opening angles in the laboratory frame. Instead, heavy spin-1 or spin-2 resonances, due to the different possible spin configurations, produce on average charged-lepton pairs with larger opening angles. The exact $\frac{|\Delta\phi_{\ell\ell}|}{\pi}$ values used to define the five regions have been chosen to optimise the sensitivity of the 2-lepton channel to spin-1 resonances, while ensuring that each region contains enough data.

In analogy to the 1-lepton channel, events in these five regions are further divided into orthogonal signal and validation regions based on the absolute pseudorapidity difference between the two selected leptons, $|\Delta\eta_{\ell\ell}|$. The $|\Delta\eta_{\ell\ell}|$ values chosen to define the signal and validation regions depend on the $m_{\ell\ell bb}$ range and are summarised in table 5. Figure 3(b) shows the distribution of $|\Delta\eta_{\ell\ell}|$, inclusive in $m_{\ell\ell bb}$. Very good agreement is observed between the data and the simulated backgrounds already pre-fit.

The pre-fit distribution of $\frac{|\Delta\phi_{\ell\ell}|}{\pi}$ in the 2-lepton channel is shown in figure 4, separately for the signal and validation regions. Each $\frac{|\Delta\phi_{\ell\ell}|}{\pi}$ bin corresponds to a signal or validation

JHEP10(2026)219



(a) (b)

Figure 4. Distribution of the reconstructed $\frac{|\Delta\phi_{\ell\ell}|}{\pi}$ in (a) the signal regions and (b) the validation regions of the 2-lepton channel. Each bin corresponds to one of the signal or validation regions. The distributions and the uncertainty band are obtained before the final fit to the data (pre-fit). "Other Bkg." combines the $t\bar{t}+V$, $t\bar{t}+H$, diboson and fakes backgrounds together. In (a), a 3 TeV Z'_{TC2} signal (blue dashed and dotted line), a 1 TeV G_{KK} signal (red dotted line) and a 2 TeV g_{KK} signal (green short-dashed and dotted line) are overlaid for illustration purposes, normalised to the total background. The lower panels show the ratio of the data to the total SM background prediction. The error bands include both the statistical and systematic uncertainties.

region, respectively. Excellent agreement is observed between the data and the SM yields already pre-fit, in both regions.

In addition to the signal and validation regions defined above, an orthogonal region is used to correct the MC-based modelling of the $Z+$jets background component. A control region enriched in $Z+$jets events, CR_Z, is defined by requiring events to satisfy the common selection requirements and additionally contain two same-flavour leptons with opposite charge and with an invariant mass consistent with leptons arising from a Z boson decay, $81 < m_{\ell\ell} < 101$ GeV.

7 Observables

The primary observable used to separate signal from background is the invariant mass of the $t\bar{t}$ system, $m_{t\bar{t}}$. Additionally, angular variables sensitive to the $t\bar{t}$ spin correlations are used in both the 1- and 2-lepton channels to define validation regions for the SM $t\bar{t}$ background and, in the case of the 2-lepton channel, to increase the sensitivity of the signal regions. The angular variables provide additional discrimination power between the signal process, in which the $t\bar{t}$ system is produced via the s-channel diagram, and the background from SM $t\bar{t}$ production, which mostly proceeds via the t-channel diagram.

7.1 Observables in the 1-lepton channel

The calculation of $m_{t\bar{t}}$ requires the correct identification and reconstruction of all $t\bar{t}$ decay products, including the four-momentum of the neutrino from the leptonic decay of one of the two top quarks. In both the resolved and the merged event topologies, the transverse momentum of the neutrino is taken to be the transverse missing momentum in the event, $\vec{p}_{\mathrm{T}}^{\,\mathrm{miss}}$.

JHEP10(2026)219

The four-momentum component longitudinal to the beam axis, p_z^ν, is calculated from the kinematic constraint that the squared sum of the neutrino and charged lepton four-momenta must yield the squared mass of the W boson [17]. If the resulting equation has exactly one real solution, it is taken as the neutrino longitudinal momentum. If it has no real solutions, the $\vec{p}_{\mathrm{T}}^{\,\mathrm{miss}}$ vector is rescaled and rotated in the transverse plane by the minimal amount required to obtain exactly one real solution [20]. This procedure is based on the assumption that the lack of a real solution is caused by a mis-measurement of the transverse missing momentum. If two real solutions are found, in the resolved topology selection, the choice is made with a χ^2 algorithm, while in the merged topology selection the solution with the smallest absolute value of p_z^ν is chosen [20].

7.1.1 Resolved topology

A χ^2 minimisation approach is used to select the four jets from the $t\bar{t}$ decay from all selected small-R jets and assign them to the leptonically- and hadronically-decaying top quarks, identically to what is done in ref. [25]. All possible jet permutations are tested, and the one with the lowest χ^2 is used; if there are two solutions for the neutrino longitudinal momentum, the one that yields the lowest χ^2 is kept. Any b-tagged jet can only be assigned to either of the b-quarks produced by the decay of a top quark, reducing the number of permutations to test. The experimental resolution of $m_{t\bar{t}}$ in the resolved signal region is around 12% for $m_{t\bar{t}}^{\mathrm{afterFSR}} = 400$ GeV and 10% for $m_{t\bar{t}}^{\mathrm{afterFSR}} = 1000$ GeV.

7.1.2 Merged topology

For the merged topology, the hadronically-decaying top quark can be straightforwardly identified with the top-tagged large-R jet that passes the requirements in section 5. The leptonically-decaying top quark is reconstructed from the selected jet identified with the b-jet from the leptonic top-quark decay, the selected lepton, and the reconstructed neutrino (section 6.1). The $m_{t\bar{t}}$ resolution for events in the merged signal region is around 10% for $m_{t\bar{t}} > 600$ GeV.

In figure 5, the distributions of the reconstructed $t\bar{t}$ invariant mass are shown for various representative resonance masses in the three benchmark models described in section 2. At low resonance masses, the $m_{t\bar{t}}$ distributions show a clear peak at the resonance mass. At larger resonance masses, a tail towards masses lower than the generated mass is visible, which arises from off-shell production of the signal and the growth of low-x partons in the proton PDF (where x stands for the Bjorken-x of the proton) [17].

7.2 Observables in the 2-lepton channel

The invariant mass of the $t\bar{t}$ system cannot be unambiguously reconstructed in the 2-lepton channel due to the presence of the two neutrinos from the two leptonically-decaying top quarks. Therefore, instead of the $t\bar{t}$ invariant mass, the invariant mass of the two selected b-jets and the two charged leptons, $m_{\ell\ell bb}$, is used as the discriminating variable.

Figure 6 shows the distributions of the reconstructed $m_{\ell\ell bb}$ discriminant for the same representative signal masses as shown in the 1-lepton channel. The same trend of low-mass

JHEP10(2026)219

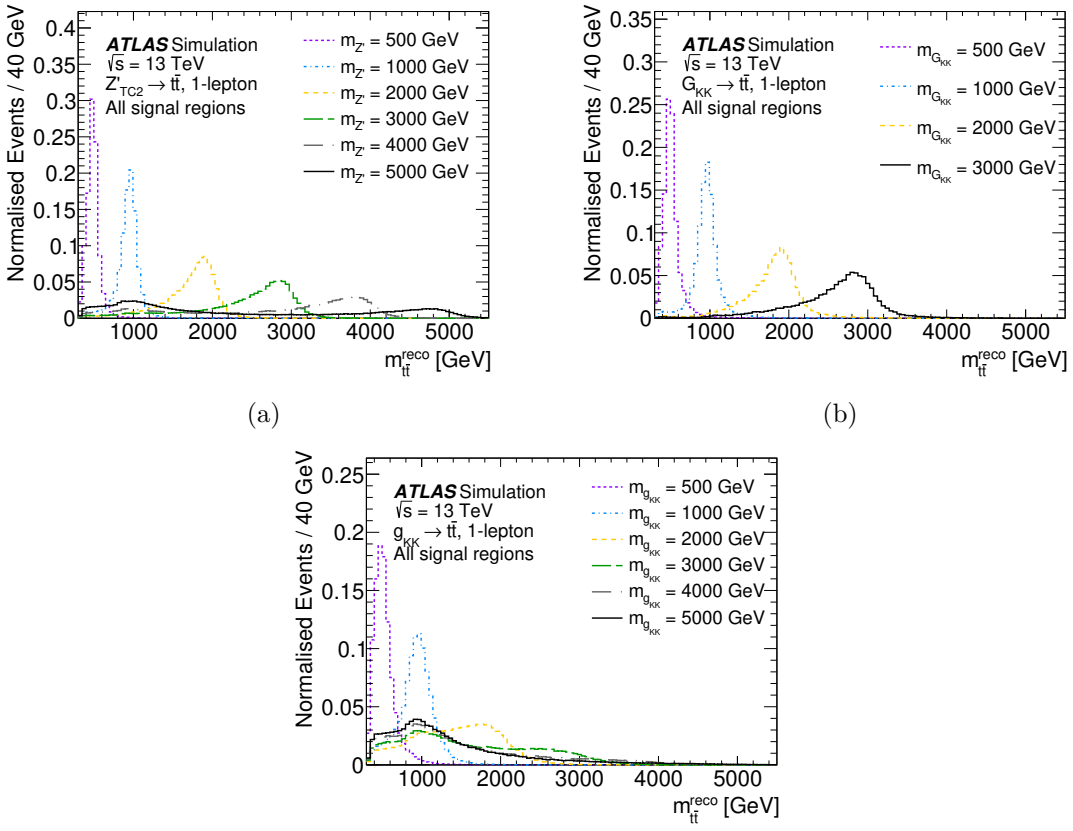


Figure 5. Signal distributions in $m_{t\bar{t}}$ after the signal region selection of the 1-lepton channel for the (a) Z'_{TC2}, (b) G_{KK}, and (c) g_{KK} signals for various representative values of the resonance mass. Events from the Resolved 1b, Resolved 2b, and Merged signal regions are included.

tails for the high-mass signals that were seen in the $m_{t\bar{t}}$ distributions are also visible in the $m_{\ell\ell bb}$ distributions.

8 Data-driven estimation of background contributions

8.1 W + jets background in the 1-lepton channel

Scale factors derived from data are applied before the final analysis to correct the normalisation of the W + jets background in the Sherpa MC simulation samples, to account for possible mis-modelling of the cross-section times acceptance. The scale factors are determined by comparing the measured W boson charge asymmetry in data with that predicted by the simulation. Given that pp collisions at the LHC result in a charge-asymmetric initial state, the total number of W+jets events in data in a given signal region, $N_{W^+}+N_{W^-}$, can be written as

$$N_{W^+} + N_{W^-} = \frac{N^{\mathrm{MC}}_{W^+} + N^{\mathrm{MC}}_{W^-}}{N^{\mathrm{MC}}_{W^+} - N^{\mathrm{MC}}_{W^-}} (D_{\mathrm{corr}+} - D_{\mathrm{corr}-}) \,, \tag{8.1}$$

where $N^{\mathrm{MC}}_{W^\pm}$ denotes the number of W + jets events with a positively- or negatively-charged lepton obtained from the Sherpa MC simulation. $D_{\mathrm{corr}+(-)}$ is the number of observed data

JHEP10(2026)219

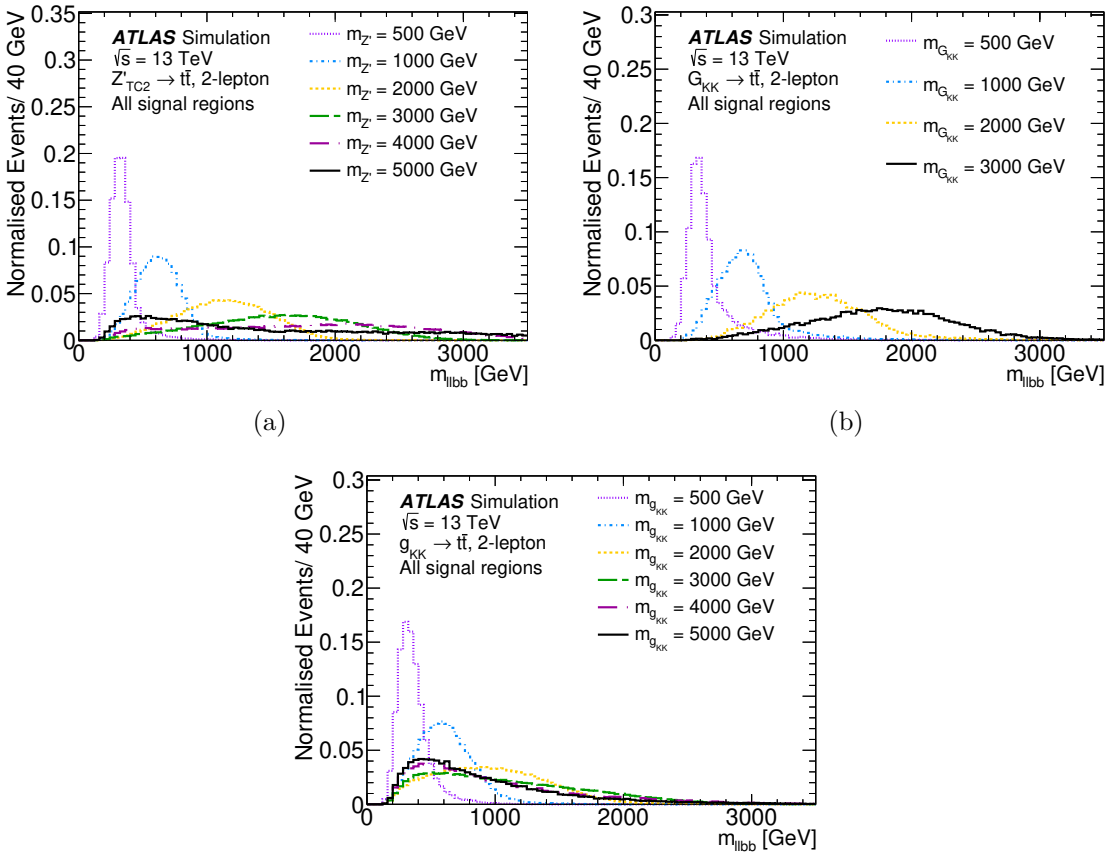


Figure 6. Signal distributions in $m_{\ell\ell bb}$ after the signal region selection of the 2-lepton channel for the (a) Z'_{TC2}, (b) G_{KK}, and (c) g_{KK} signals for various representative values of the resonance mass. Events from the five signal regions are combined.

events with a positively-charged (negatively-charged) lepton. This method relies on the fact that the charge asymmetry obtained in MC simulation is in excellent agreement with the value measured in data [124]. Contributions to $D_{\mathrm{corr}+(-)}$ from charge-asymmetric processes such as single-top, WZ, and $t\bar{t}+W$ production are estimated from MC simulation and are subtracted from the data samples. Contributions from charge-symmetric processes such as $t\bar{t}$ production and the signal process itself cancel out in the difference on the right-hand side of eq. (8.1). The final scale factor, $C_A = 1.125 \pm 0.031$, is then calculated as the ratio of $N_{W^+} + N_{W^-}$ evaluated from data to that predicted from the SHERPA MC simulation. The scale factor is evaluated for the combined $e+$jets and $\mu+$jets events channels in the merged and resolved regions combined; it was verified that the scale factors evaluated from the $e+$jets and $\mu+$jets channels separately are consistent.

The scale factors obtained in the method described above are applied to the single, combined template for the $W+$jets background. A 50% uncertainty is assigned to the normalisation after the C_A correction to account for additional theory uncertainties related to the $W+$jets sample, discussed further in section 10.1.3. Furthermore, the fraction of

JHEP10(2026)219

W + HF in the W + jets nominal template is varied by ±50%, with this variation applied as an additional systematic uncertainty to cover any residual mis-modelling arising from the relative flavour contributions [20].

8.2 Fakes background in the 1-lepton channel

The fakes background in the 1-lepton channel consists of events with a non-prompt lepton or a jet mis-reconstructed as a lepton that satisfies the lepton identification and isolation criteria applied in this search (referred to as *tight* lepton requirements in the following). In the μ+jets channel, muons arising from semileptonic decays of hadrons constitute the main source of this background. In the e + jets channel, additional fakes arise from events containing jets with a large electromagnetic component, for example from $\pi^0 \to \gamma\gamma$ decays, or photons mis-identified as isolated electrons. The normalisation, $t\bar{t}$ invariant mass shape, statistical and systematic uncertainties associated with the fakes background are estimated from data using the *matrix method*. The matrix method used in this search is based on the one used in previous ATLAS $t\bar{t}$ resonance searches and measurements [17, 20] and is the same as that employed in ref. [25].

The number of events with leptons satisfying loose lepton identification and isolation criteria [119], N_L, is defined as

$$N_{\mathrm{L}} = N_{\mathrm{prompt}} + N_{\mathrm{fakes}}\,, \tag{8.2}$$

where N_{prompt} denotes the number of events with prompt leptons, and N_{fakes} denotes the number of events with non-prompt leptons and other sources mis-identified as leptons. The number of events with leptons satisfying the tight lepton identification criteria applied in the signal regions, N_T, can be written as

$$N_{\mathrm{T}} = \epsilon \times N_{\mathrm{prompt}} + f \times N_{\mathrm{fakes}}\,, \tag{8.3}$$

where the *real rate*, ϵ, is an estimator for the probability of a prompt lepton passing the loose lepton identification criteria to also pass the tight critieria, and the *fake rate*, f, is an estimator for the probability that a lepton from other sources passing the loose criteria also passes the tight criteria. The fake rate is estimated from a control region, defined by applying the same selection criteria as the resolved signal region, but with the missing transverse momentum and transverse mass requirements inverted. The veto on events passing the merged topology selection criteria is also not imposed to define this control region, to increase the available data. Contributions from processes leading to prompt leptons are subtracted from the data in this fakes-enriched control region using their predictions from MC simulation. The real rate is determined using SM $t\bar{t}$ MC samples. Solving eqs. (8.2) and (8.3) simultaneously for N_{prompt} and N_{fakes} yields the fakes contribution in the given signal region. The fakes estimate is performed separately for the e + jets and μ + jets events.

A smoothing procedure is applied to the fakes background templates in both the resolved and the merged signal regions to mitigate large statistical fluctuations due to the limited data. In the resolved region, a parabolic smoothing algorithm is applied, whereby the input distribution histogram is rebinned to achieve a smooth behaviour. The limited amount of data has a larger effect in the high-$m_{t\bar{t}}$ tails, and the parabolic smoothing used in the resolved regions was observed to be too agressive for the merged topology, removing all entries in

JHEP10(2026)219

the tail of the distribution. Therefore, a custom smoothing procedure, applied separately for the $e+\text{jets}$ and $\mu+\text{jets}$ channels, and separately in the signal and validation regions, was designed and implemented for the fakes background in the 1-lepton merged regions. The algorithm uses an analytic function fit to the unbinned templates to smooth the binned template, with care taken to ensure there is continuity in the function when considering the $m_{t\bar{t}}$-dependent $\left|\Delta\eta\left(\ell, t^{\text{had}}\right)\right|$ requirement. The systematic uncertainty assigned to this smoothing procedure is described in section 10.1.3.

The fakes modelling before applying the smoothing is validated in separate dedicated validation regions, where only one of the $E_{\text{T}}^{\text{miss}}$ or $E_{\text{T}}^{\text{miss}}+m_{\text{T}}^{\text{W}}$ requirements is inverted. These validation regions contain a background composition that is more similar to that in the signal region, while still having an enhanced fakes contribution. Based on the modelling performance observed in these validation regions, a conservative 50% normalisation uncertainty that is decorrelated across signal regions is assigned to the fakes background, in addition to the uncertainties related to the estimate and smoothing procedures.

8.3 $Z+\text{jets}$ background in the 2-lepton channel

Data-driven corrections are applied to the Sherpa MC simulation samples for the $Z+\text{jets}$ background in the 2-lepton channel before the final fit to correct the overall normalisation of this background component and the modelling of relevant kinematic variables. The corrections are derived in the $Z+\text{jets}$ enriched CR_Z, where disagreement in the modelling of the background prediction obtained with the Sherpa MC simulated samples is observed compared with data for two kinematic variables in particular: the transverse momentum of the dilepton system, $p_{\text{T}}^{\ell\ell}$, and the invariant mass $m_{\ell\ell bb}$. In both cases, the mis-modelling exhibits a linear trend, with good agreement observed for small values of these variables and a linear increase in the difference between data and MC prediction towards higher values. As a result, a reweighting procedure in $m_{\ell\ell bb}$ is used to correct the Sherpa MC samples for the $Z+\text{jets}$ background to the data in CR_Z. Each simulated event is assigned a multiplicative correction weight based on its value of $m_{\ell\ell bb}$:

$$w = a \cdot (1 - b \cdot m_{\ell\ell bb})\,. \tag{8.4}$$

The correction factors a and b are derived from a maximum-likelihood fit to the $m_{\ell\ell bb}$ distributions, taking into account only the statistical uncertainty in the MC predictions. The following values are obtained for the correction factors:

$$a = 1.190 \pm 0.003\,, \quad b = (-1.7 \pm 0.1) \cdot 10^{-4}\ \text{GeV}^{-1}\,.$$

Good agreement between the data and the SM expectation is observed for all relevant kinematic variables after applying the reweighting correction. To cover the residual non-closure seen in the $Z+\text{jets}$ control region after requiring 2 b-jets, two uncertainties are introduced. The first is a flat 30% normalisation uncertainty, and the second is estimated by varying the slope of eq. (8.4) by 30% of its best-fit value and obtaining the reweighted $m_{\ell\ell bb}$ distribution in this case. The difference between the nominal and the varied reweighted $m_{\ell\ell bb}$ distributions is taken as the systematic uncertainty.

JHEP10(2026)219

9 Statistical analysis

The compatibility of the data with the SM prediction is quantified by a binned profile-likelihood fit [125, 126] of the expected $m_{t\bar{t}}$ (1-lepton channel) and $m_{\ell\ell bb}$ (2-lepton channel) distributions to the observed distributions. The fit is performed simultaneously in the three signal regions of the 1-lepton channel and the five signal regions of the 2-lepton channel. The shape of the binned $m_{t\bar{t}}$ or $m_{\ell\ell bb}$ distributions is parameterised in terms of the signal strength, μ, interpreted as the ratio of the observed and predicted number of signal events. The SM $t\bar{t}$ normalisation is a free parameter in the fit, while the other simulated background processes are normalised to their theory predictions, with uncertainties as described in section 10.

Systematic uncertainties, described in section 10, are taken into account as nuisance parameters (NPs) constrained by Gaussian distributions. The Beeston-Barlow "lite" technique [127] is used to incorporate uncertainties due to the limited data available for the MC samples used in the analysis, referred to as *MC statistics*, where one additional NP with a Poissonian constraint is added per bin of the discriminant distribution to the likelihood function. The statistical uncertainty originating from the fakes background estimate is also accounted for in these same bin-by-bin NPs, see section 10.1.3 below. The combination of the MC statistical uncertainty and the fakes background uncertainty is referred to as *background statistical uncertainties* in the remainder of this paper.

10 Systematic uncertainties

The modelling of signal and background events is affected by various experimental uncertainties related to the reconstruction, identification, and calibration of object and event properties. In addition, uncertainties related to the theory modelling of the simulated backgrounds, most importantly SM $t\bar{t}$ production, are taken into account. The largest sources of systematic uncertainties in the analysis vary depending on the mass and width of the signal hypothesis being tested, but overall are related to the modelling of the SM $t\bar{t}$ and the 1-lepton fakes background processes, followed by uncertainties in the jet energy scale and resolution. Table 6 in section 11 summarises the main sources of uncertainty for three signal hypotheses and their impact on the observed signal strengths.

10.1 Modelling uncertainties

10.1.1 Uncertainties in the modelling of the SM $t\bar{t}$ background

Modelling uncertainties are considered relating to the background from SM $t\bar{t}$ production, which is estimated by using MC simulation at NLO+PS precision, and corrected to NNLO-QCD+NLO-EW calculations (see section 4). The background prediction for this process is hence subject to uncertainties in the higher-order calculations and uncertainties related to the reweighting procedure, collectively grouped together as $t\bar{t}$ NNLO uncertainties in table 6, and uncertainties due to modelling choices made in the NLO+PS simulation. As mentioned earlier, the impact of including a potential quasi-bound state consistent with that observed by CMS was found to be negligible.

The uncertainties in the higher-order calculations are assessed by variations of the renormalisation and factorisation scales, the PDF set, and the EW contribution, which is not

JHEP10(2026)219

present in the NLO+PS prediction. The scale uncertainties are estimated separately for the (anti)top-quark p_{T} and $m_{t\bar{t}}$ distributions by varying the renormalisation and factorisation scales independently up and down by a factor of two, yielding four independent scale uncertainty components. The uncertainty in the PDF set is taken as the envelope of the intra-PDF uncertainties of the LUXQED PDF set [128], which is used to obtain the NNLO-QCD+NLO-EW predictions. The uncertainty in the EW contribution is estimated by comparing the nominal spectra with those obtained with the NNPDF3.0QED PDF set [64, 129], which has been found to yield a significantly different prediction for the EW contributions due to a different treatment of the photon PDF compared to the nominal LUXQED PDF set [67].

Two uncertainties are assigned to the iterative reweighting method. Possible biases due to the order in which the reweighting is applied on the $m_{t\bar{t}}$ and (anti)top-quark p_{T} distributions is estimated by comparing the nominal reweighted sample with an alternative sample in which the reweighting is applied in a different order. The second uncertainty is derived to account for differences between the definitions of the parton-level top-quark: in the higher-order calculations, it includes at most two real emissions, whereas for the NLO MC generator, any number of real emissions can be included. To account for this, an alternative MC sample is created with the same generators and settings as the nominal NLO MC sample, but without decaying the top quarks and forbidding PS emissions after the first one. The nominal NLO sample is then reweighted to match the parton-level distributions of this modified sample, with the exact same procedure as the reweighting to the higher-order predictions. The difference between this reweighted sample and the un-reweighted sample is taken as the uncertainty in the observables at detector level.

Uncertainties due to the modelling choices made for the NLO+PS MC simulation are estimated by comparing the nominal SM $t\bar{t}$ prediction to alternative predictions, obtained by either varying parameters within the nominal generators or with alternative MC generators. The alternative MC samples are reweighted to the respective higher-order predictions if the uncertainties they represent do not affect the parton-level variables used for the reweighting, namely $m_{t\bar{t}}$ and the (anti)top-quark p_{T}. The following uncertainties in this group are:

- the uncertainty related to the ME-PS matching, estimated by comparing the predictions obtained with the nominal sample with those obtained from an alternative sample generated with the same generator settings as the nominal sample but setting the $p_{\mathrm{T}}^{\mathrm{hard}}$ parameter[4] in Pythia to 1 instead of 0 [130];

- the uncertainty related to the choice of the h_{damp} parameter, estimated by comparing the predictions of the nominal sample with those obtained with an alternative sample with the h_{damp} parameter increased by a factor of $1.5m_{\mathrm{top}}$ compared with its nominal value;

- variations in the ISR ME calculation, which are estimated by varying the factorisation and renormalisation scales independently up and down by a factor of two; and,

[4]The $p_{\mathrm{T}}^{\mathrm{hard}}$ parameter regulates the definition of the vetoed region of the showering to avoid holes or overlaps in the phase space filled by Powheg and Pythia.

JHEP10(2026)219

- variations in the FSR, assessed by varying the renormalisation scale for final-state PS emissions up and down by a factor of two.

For the cases of the ME-PS matching and the h_{damp} uncertainties, the resulting one-sided uncertainties are symmetrised to obtain effective *up* and *down* variations.

The uncertainty associated with variations of the renormalisation scale in the ISR PS is obtained via the corresponding systematic variation in the A14 tune. This variation does not have an explicit higher-order prediction so the nominal reweighting is applied instead, since the uncertainty also does not affect the parton-level variables used for the reweighting.

Finally, several modelling uncertainties are not reweighted at all and compared with the unreweighted nominal sample. These include:

- the uncertainty related to the choice of the PS and hadronisation model, which is estimated by comparing the nominal predictions with those obtained from a sample generated at NLO in QCD with POWHEG BOX v2 with the same PDF set and h_{damp} value as in the nominal sample but interfaced with HERWIG 7.13 [131–133], using the HERWIG 7.1 default set of tuned parameters [132, 133];

- the uncertainty related to the $t\bar{t}$ lineshape, estimated by comparing the predictions obtained with the nominal sample to those obtained with an alternative sample generated with the same setup as the nominal sample but using MADSPIN to decay the top quarks; and,

- the uncertainty related to the choice of m_{top}, estimated by comparing the nominal sample with $m_{\text{top}} = 172.5$ GeV to two alternative samples with m_{top} values of 171.0 GeV and 174.0 GeV, respectively, and multiplying the difference by 0.2. This yields an uncertainty of ± 0.3 GeV, corresponding ot the current world-average uncertainty in the top-quark mass [134].

Again, for both the PS uncertainty and the lineshape uncertainty, the resulting one-sided uncertainties are symmetrised to obtain effective *up* and *down* variations.

10.1.2 Uncertainties in the modelling of the signal

Theory uncertainties relating to the scale and PDF+α_s variations are taken into account for the Z'_{TC2} signal processes. The impact of uncertainties related to the modelling of the signals on the acceptance times efficiency was assessed and found to be negligible compared with the uncertainties from instrumental sources.

10.1.3 Uncertainties in the modelling of the non-$t\bar{t}$ backgrounds

The largest background contributions from processes other than SM $t\bar{t}$ production arise from single-top quark production and, in the 1-lepton channel, from both W + jets and fakes.

The main uncertainty in the modelling of single-top quark production is determined from a comparison of the diagram removal scheme and the alternative diagram subtraction scheme [65, 76] for the treatment of interference effects and overlap between SM $t\bar{t}$ and Wt production. It is estimated by comparing the nominal Wt samples, generated with the

JHEP10(2026)219

diagram removal scheme, to a set of alternative samples obtained with the diagram subtraction scheme, using the same generator settings as in the nominal single-top samples. As in the case of the SM $t\bar{t}$ background, an uncertainty related to the choice of the PS and hadronisation model is estimated for the Wt background component by comparing the nominal prediction to that obtained with the same ME generator settings but interfaced with Herwig 7.16, using the Herwig 7.1 default set of tuned parameters [132, 133] and the MMHT2014lo PDF set [135]. The uncertainty related to the ME-PS matching is estimated by comparing the predictions obtained with the nominal sample to those obtained from an alternative sample generated with the same generator settings as the nominal sample but setting the $p_{\mathrm{T}}^{\mathrm{hard}}$ parameter in Pythia to 1 instead of 0. Modelling uncertainties related to the choice of the renormalisation and factorisation scales, the levels of ISR and FSR, and the choice of PDF set have also been evaluated but are found to be negligible. The theory uncertainties in the cross-sections for Wt-, t-, and s-channel production are applied as pure normalisation uncertainties in the respective components. They are estimated by summing in quadrature the scale and the PDF+α_s uncertainties in the nominal cross-sections, and amount to $\pm 5.4\%$ for Wt production [78], $^{+4.3\%}_{-3.7\%}$ for t-channel production [85], and $^{+4.4\%}_{-4.1\%}$ for s-channel production.

For the $W+$jets production in the 1-lepton channel, a $\pm 50\%$ normalisation uncertainty is assigned, and uncertainties related to the choice of scales and PDF set are taken into account as shape-only uncertainties for the MC modelling. To account for any residual mis-modelling of the flavour fractions in the $W+$jets background after applying the correction (see section 8.1), the heavy-flavour fraction of the template is varied up and down by 50%, consistent with the corrections to the $W+$jets template in ref. [20]. In the 2-lepton channel, no separate uncertainty is assigned to the background from $W+$jets production as it is included in the fakes background component, which has a 30% uncertainty applied to cover the disagreement observed between data and the MC simulation in a fake-enriched control region.[5]

The systematic uncertainty applied to the $Z+$jets background in the 2-lepton channel is related to the data-driven reweighting described in section 8.3. It consists of two components, one affecting the shape and the other affecting the normalisation of this background component. In the 1-lepton channel, where $Z+$jets production constitutes an even smaller background component, a 30% normalisation uncertainty is applied, which covers both the $\pm 5\%$ uncertainty in the $Z+$jets production cross-section and acceptance uncertainties related to possible mis-modellings of higher jet multiplicities.

The uncertainty assigned to the data-driven estimate of the fakes background in the 1-lepton channel consists of three components:

- a 50% normalisation uncertainty that is applied separately to the $e+$jets and $\mu+$jets contributions of the fakes estimate;
- an uncertainty related to the statistical uncertainty in the original Matrix Method estimate, before smoothing; and,
- an additional systematic uncertainty regulating the shape of the tail of the distribution in the merged regions, obtained from the smoothing procedure.

[5]The fake-enriched control region is defined by requiring two signal leptons with the same-sign electric charge and either $e\mu$ or $\mu\mu$ events, and that $m_{\mathrm{T}}^{\mathrm{W}} < 100$ GeV for at least one of the W bosons in the event.

JHEP10(2026)219

The dominant uncertainty in the fakes estimate is due to the limited data available for the data-driven estimate.

In the case of the remaining small backgrounds, only normalisation uncertainties are applied. For the backgrounds originating from $t\bar{t}+Z$, $t\bar{t}+W$, and $t\bar{t}+H$ production, the uncertainties in the respective higher-order cross-sections are taken into account. They amount to $^{+10\%}_{-12\%}$, $^{+13\%}_{-12\%}$, and $^{+6.8\%}_{-9.8\%}$, respectively. A 50% normalisation uncertainty is applied to the diboson background to take into account any possible mis-modelling in the production of additional jets [136] and heavy-flavour jets [137].

10.2 Experimental uncertainties

The dominant experimental uncertainties affecting the $m_{t\bar{t}}$ and $m_{\ell\ell bb}$ spectra are the uncertainties in the jet energy scale (JES) and resolution (JER) of the small-R jets, for which there are 30 and 13 uncorrelated NPs included in the fit, respectively. Jet mass scale (JMS) uncertainties are also included for small-R jets but do not have a large impact. The small-R jet uncertainties are evaluated from a combination of simulations, test-beam data, and in situ measurements [105]. Additional contributions from jet flavour composition, punch-through, single-particle response, calorimeter response to different jet flavours and pile-up are also taken into account. Additionally, an uncertainty is assigned to the efficiency of the JVT requirement on jets [106]. For large-R jets, uncertainties in the JES, JER and JMS are derived in similar ways to small-R jets, using a combination of simulation, test-beam data, and in situ measurements [113]. Uncertainties related to jet mass resolution (JMR) are also included for large-R jets [113].

Further experimental uncertainties in the correction factors for the b-tagging efficiencies [115], as well as the rates of mis-tagging c–[116] and light-flavour jets [117], derived from looking at dedicated flavour-enriched samples in data, are applied to the simulated event samples. An additional b-tagging efficiency uncertainty is applied for high-momentum jets ($p_T > 400$ GeV) to account for uncertainties in the modelling of the track reconstruction in high-p_{T} environments [138]. Uncertainties are applied to large-R jets that satisfy the top-tagging requirements described in section 5. They are derived from a combination of measurements and account for background efficiency, signal efficiency, high-p_{T} extrapolation and inefficiency uncertainties. Correlations with the JES and b-tagging uncertainties are taken into account [139].

Smaller experimental uncertainties are related to the efficiencies of the lepton identification, isolation, and reconstruction, as well as the lepton energy scale and resolution [118, 119] and to the scale and resolution of the track soft-term in the $E_{\mathrm{T}}^{\mathrm{miss}}$ calculation [121]. Variations in the reweighting applied to simulated samples to match the expected mean number of interactions observed in each bunch crossing in data are included. They cover the uncertainty in the ratio between the predicted and measured inelastic cross-section. A constant 0.83% normalisation uncertainty is applied to all signal and background samples, except for fakes and $W+$jets that are estimated from data, accounting for the uncertainty in the integrated luminosity.

JHEP10(2026)219

10.3 Uncertainty correlation scheme

All experimental uncertainties are treated as fully correlated across samples and the signal regions of the 1- and 2-lepton channels in the final profile-likelihood fit (section 9). The modelling uncertainties are treated as uncorrelated between all background samples, but in general correlated across signal regions. However, the uncertainties in the SM $t\bar{t}$ background related to the modelling of the PS and hadronisation, the PS-ME matching, the lineshape, the FSR and the choice of the h_{damp} parameter are treated as uncorrelated between all 3+5 signal regions of the 1- and 2-lepton channels, and separated into their shape and acceptance components. These uncertainties are obtained by comparing the nominal sample to an alternative SM $t\bar{t}$ sample in each case (*two-point systematic uncertainties*), an approach that typically yields large pre-fit uncertainties that are often highly constrained in a profile-likelihood fit. Keeping these uncertainties uncorrelated between all signal regions is chosen to prevent constraints propagating across regions, thus minimising the overall constraints on these NPs. Additionally, the uncertainties in the SM $t\bar{t}$ background related to the choice of renormalisation and factorisation scales cannot be assumed to be fully correlated across different kinematic regimes, and are therefore treated as uncorrelated between the resolved and merged signal regions of the 1-lepton channel and between the 1- and 2-lepton channels, although they are treated as correlated across the different b-tagging bins of the 1-lepton channel and the different angular bins of the 2-lepton channel.

The uncertainty in the nomalisation factor assigned to the fakes background in the 1-lepton channel is uncorrelated across all three signal regions, and between the $e+$jets and $\mu+$jets channels. The normalisation factor and $W+$HF shape factor assigned to the $W+$jets background in the 1-lepton channel are also treated as uncorrelated across the three signal regions. All other modelling NPs are treated as correlated across all signal regions.

11 Results

The data are confirmed to be consistent with the background-only hypothesis through a fit of the observed data to the SM prediction with $\mu = 0$ in the eight signal regions, where only the NPs are allowed to vary. The $m_{t\bar{t}}$ distributions in the three signal regions of the 1-lepton channel and the $m_{\ell\ell bb}$ distributions in the five signal regions of the 2-lepton channel after the fit to the full 140 fb^{-1} data sample are shown in figures 7 and 8, respectively. Good compatibility of the observed $m_{t\bar{t}}$ and $m_{\ell\ell bb}$ spectra with the post-fit expected spectra is seen in all signal regions, with a goodness-of-fit probability of 95% obtained from a saturated model test [140].

Good modelling of the SM background as a function of $m_{t\bar{t}}$ or $m_{\ell\ell bb}$ was validated by applying the post-fit model parameters and constraints from the signal regions in the corresponding validation regions. The results are shown in figures 9 and 10 for the 1-lepton and 2-lepton channels, respectively. The correlations of the systematic uncertainties described in section 10.3 are maintained, and systematic uncertainties are also correlated between the corresponding signal and validation regions.

11.1 Uncertainty impact

The relative importance of the different categories of systematic uncertainties is quantified via their post-fit impact on the observed signal strength for three representative signal hypotheses.

JHEP10(2026)219

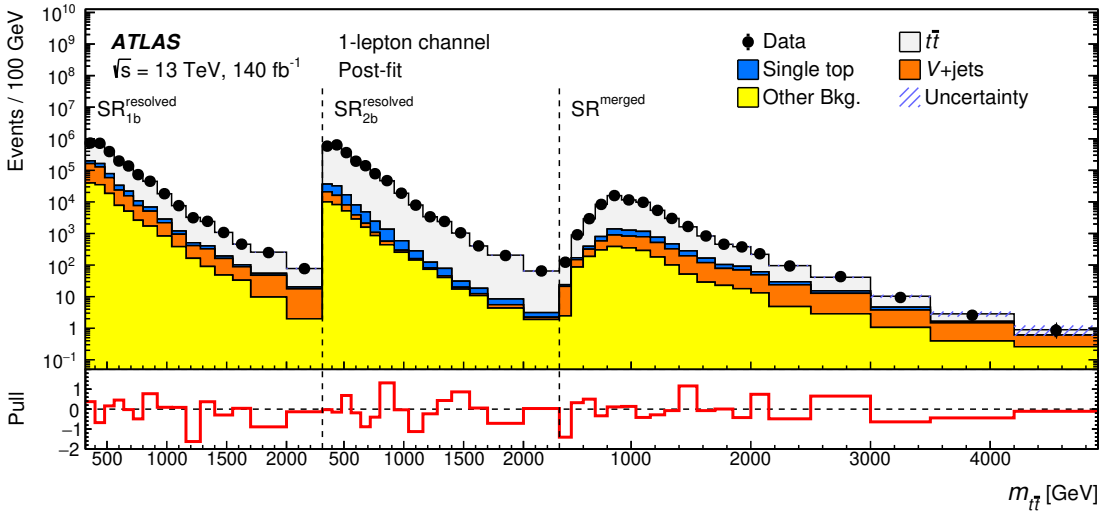


Figure 7. Post-fit distributions of the reconstructed $m_{t\bar{t}}$ for the three signal regions of the 1-lepton channel, after performing the profile-likelihood fit under the background-only hypothesis in the 3+5 signal regions of the 1-lepton and 2-lepton channels, respectively. The overflow is added to the final bins. The lower panel shows the pulls from the fit (red line), where the pull in each bin is defined as $(n_{\text{obs}} - n_{\text{pred}})/\sqrt{n_{\text{obs}}}$, and n_{obs} and n_{pred} refer to the number of observed events in data and the number of predicted events, respectively. "V + jets" refers to the Z + jets and W + jets backgrounds, whilst "Other Bkg." combines the $t\bar{t}+V$, $t\bar{t}+H$, diboson, and fakes backgrounds together.

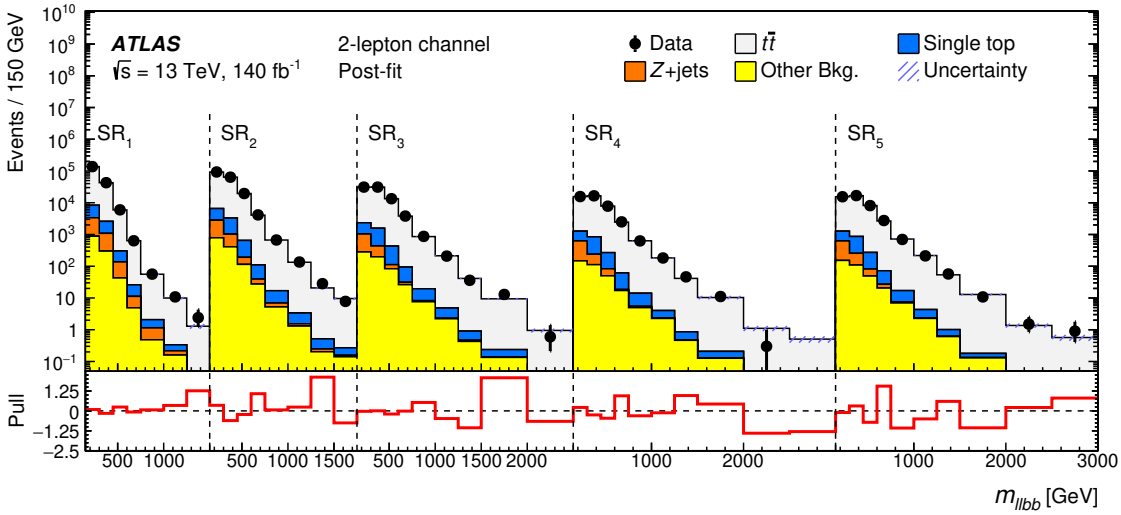


Figure 8. Post-fit distributions of the reconstructed $m_{\ell\ell bb}$ for the five signal regions of the 2-lepton channel, after performing the profile-likelihood fit under the background-only hypothesis in the 3+5 signal regions of the 1-lepton and 2-lepton channels, respectively. The overflow is added to the final bins. The lower panel shows the pulls from the fit (red line), where the pull in each bin is defined as $(n_{\text{obs}} - n_{\text{pred}})/\sqrt{n_{\text{obs}}}$, and n_{obs} and n_{pred} refer to the number of observed events in data and the number of predicted events, respectively. "Other Bkg." combines the $t\bar{t}+V$, $t\bar{t}+H$, diboson, and fakes backgrounds together.

JHEP10(2026)219

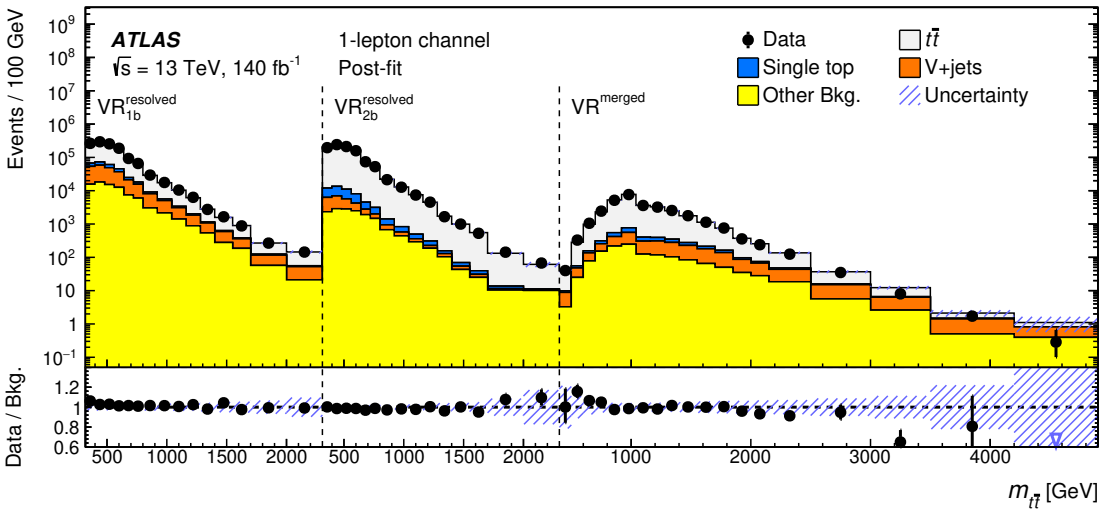


Figure 9. Distributions of the reconstructed $m_{t\bar{t}}$ in the three validation regions of the 1-lepton channel, projected from the results of the profile-likelihood fit under the background-only hypothesis in the 3+5 signal regions of the 1-lepton and 2-lepton channels, respectively. The overflow is added to the final bins. In the lower panel, the ratio of the data and the post-fit background in the validation region is shown (data points), as well as the total uncertainty (shaded band). The arrow indicates when the ratio is outside of the range shown. "V + jets" refers to the Z + jets and W + jets backgrounds, whilst "Other Bkg." combines the $t\bar{t}+V$, $t\bar{t}+H$, diboson, and fakes backgrounds together.

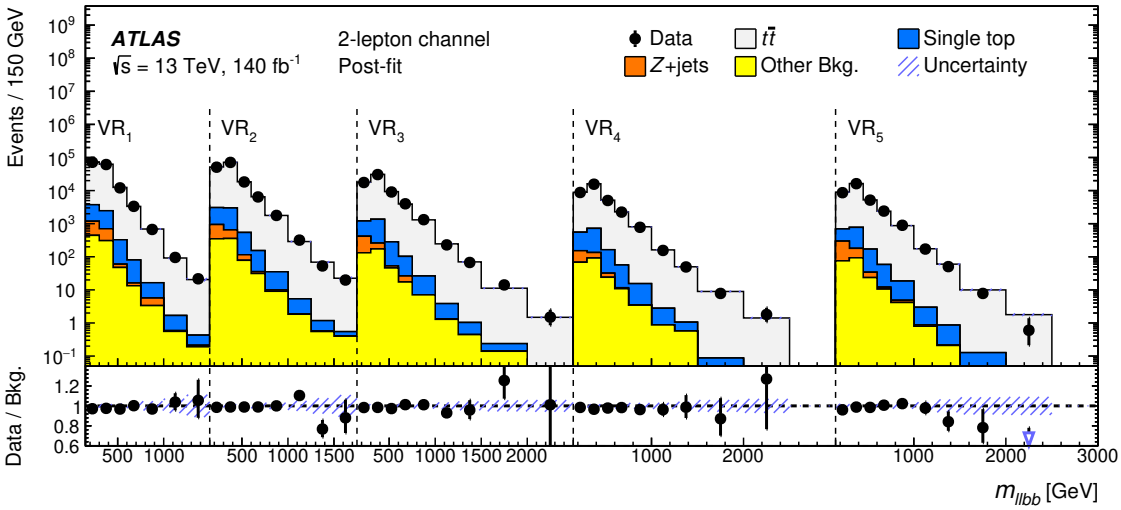


Figure 10. Distributions of the reconstructed $m_{\ell\ell bb}$ in the five validation regions of the 2-lepton channel, projected from the results of the profile-likelihood fit under the background-only hypothesis in the 3+5 signal regions of the 1-lepton and 2-lepton channels, respectively. The overflow is added to the final bins. In the lower panel, the ratio of the data and the post-fit background in the validation region is shown (data points), as well as the total uncertainty (shaded band). The arrow indicates when the ratio is outside of the range shown. "Other Bkg." combines the $t\bar{t}+V$, $t\bar{t}+H$, diboson and fakes backgrounds together.

JHEP10(2026)219

The results are shown for one narrow, low-mass Z'_{TC2} signal and one wide, low-mass g_{KK} signal, both of which are fully contained in the resolved signal regions, and one narrow, high-mass Z'_{TC2} signal, which is contained mostly in the merged signal region. The G_{KK} signals show the same trends as the Z'_{TC2}, due to the similar widths and similar reconstructed $m_{t\bar{t}}$ shapes; therefore, the discussion below on the Z'_{TC2} uncertainties also applies to the G_{KK} signals.

The impact of each NP on the signal strength is evaluated from the covariance matrix of the fit, and the impact of a group of NPs is obtained by summing in quadrature the impacts of all NPs in the respective category. Similarly, the total systematic uncertainty is obtained by summing in quadrature the impacts of all relevant NP groups. The statistical uncertainty is calculated by subtracting in quadrature the total systematic uncertainty from the total uncertainty in the signal strength. Table 6 summarises the impacts, where the fractional contribution to the total uncertainty in the observed signal strength of each category is given. The observed signal strength and the corresponding absolute uncertainty are shown in the top row.

Of the systematic uncertainties, the dominant impact on the post-fit result depends on the signal hypothesis being tested; however, the $t\bar{t}$ background modelling uncertainties usually have relatively large impacts for all mass points. The largest experimental systematic uncertainties are those related to the jet energy scale and jet energy resolution of the small-R jets for the low-mass signals and to top-tagging for the high-mass signals, followed by flavour-tagging related systematic uncertainties. Besides the systematic uncertainties, the NPs related to the statistical uncertainty from the fakes background, included in "Modelling: statistical uncertainty" in table 6, are also important, and for some mass points, these are among the parameters with the highest impact. For the highest mass regions, this is directly due to limited data. On the other hand, for the low-mass, narrow signals, the NPs related to the statistical uncertainty in the fakes are highly-correlated with the parameter of interest. This is because these NPs are completely uncorrelated across bins, and the width of the narrow signals is similar to the bin-width used. The total uncertainty in this analysis is still predominantly statistically dominated for the narrow resonances; however, for the wide resonances, the systematic uncertainties are comparable or even larger than the statistical uncertainties.

11.2 Constraints on selected benchmark models

No significant excesses are observed across the entire $m_{t\bar{t}}$ or $m_{\ell\ell bb}$ spectra; therefore, upper limits at the 95% confidence level (CL) are derived on the production cross-section times branching ratio to $t\bar{t}$ for the resonances predicted in the benchmark scenarios described in section 2. The upper limits are calculated using the CL_s frequentist formalism [141] and the approximate limits for intermediate masses are interpolated between the tested mass hypotheses. For the G_{KK} signal, the detector resolution is finer than the grid spacing, so the interpolation is only for display purposes.

The observed and expected exclusion limits are shown in figure 11 for the Z'_{TC2}, g_{KK} and G_{KK} signal hypotheses. The observed limits are in good agreement with the expected limits. Upper limits on the cross-section are extracted to be 3.6 pb, 1.8 pb, and 6.4 pb for a 500 GeV Z'_{TC2}, G_{KK}, and g_{KK} signal, respectively. The results in this paper are the best limits on the cross-section times branching fraction to $t\bar{t}$ for the Z'_{TC2} signal for $m_{t\bar{t}} < 1.5$ TeV, and the best

JHEP10(2026)219

	$m_{Z'_{\mathrm{TC2}}} = 500\,\mathrm{GeV}$ $\mu = 0.019 \pm 0.027$	$m_{Z'_{\mathrm{TC2}}} = 3\,\mathrm{TeV}$ $\mu = 0.06 \pm 0.31$	$m_{g_{\mathrm{KK}}} = 1\,\mathrm{TeV}$ $\mu = 0.002 \pm 0.018$
Uncertainty component	Fractional contribution [%]		
Experimental	**27**	**21**	**37**
Small-R jets	25	12	31
Large-R jets	1.6	3.8	5.8
Flavour tagging	10	6.2	8.9
Top-tagging	2.8	15	13
Leptons	4.1	4.8	11
Other	3.9	2.6	6.9
Modelling: SM $t\bar{t}$	**26**	**48**	**46**
$t\bar{t}$ NNLO	11	7.9	13
$t\bar{t}$ lineshape	14	19	15
$t\bar{t}$ ME-PS ($p_{\mathrm{T}}^{\mathrm{hard}}$)	11	6.8	17
$t\bar{t}$ ME-PS (h_{damp})	9.5	10	14
$t\bar{t}$ ISR& FSR	9.7	13	29
$t\bar{t}$ PS	8.2	40	20
Modelling: signal	**1.0**	**0.78**	–
Modelling: other	**21**	**20**	**31**
Fakes	17	5.1	10
W + jets	9.0	18	6.8
Z + jets	1.9	0.31	3.1
Other	9.2	3.0	28
Modelling: statistical uncertainty	**48**	**49**	**33**
Total systematic uncertainty	**65**	**74**	**74**
Total statistical uncertainty	**76**	**67**	**67**

Table 6. Post-fit fractional contributions of different uncertainty categories to the total uncertainty in the observed signal strength, μ, as determined in the combined fit to the 1- and 2-lepton channels for three representative signal hypotheses: a 500 GeV Z'_{TC2} signal, a 3 TeV Z'_{TC2} signal, and a 500 GeV g_{KK} signal. The observed value of μ and the corresponding absolute uncertainty are also shown. The details of how the impact of each NP on the signal strength is evaluated, as well as how the total systematic and statistical uncertainties are calculated, are given in the text. "Modelling: statistical uncertainty" refers to the contribution from the statistical uncertainties of the MC simulated samples and the data-driven background estimate for the 1-lepton fakes background. "Modelling: signal" refers to the theory uncertainties on the Z'_{TC2} signal; these uncertainties are not considered for the G_{KK} and g_{KK} signals. The individual components do not necessarily add up in quadrature to the total due to rounding.

JHEP10(2026)219

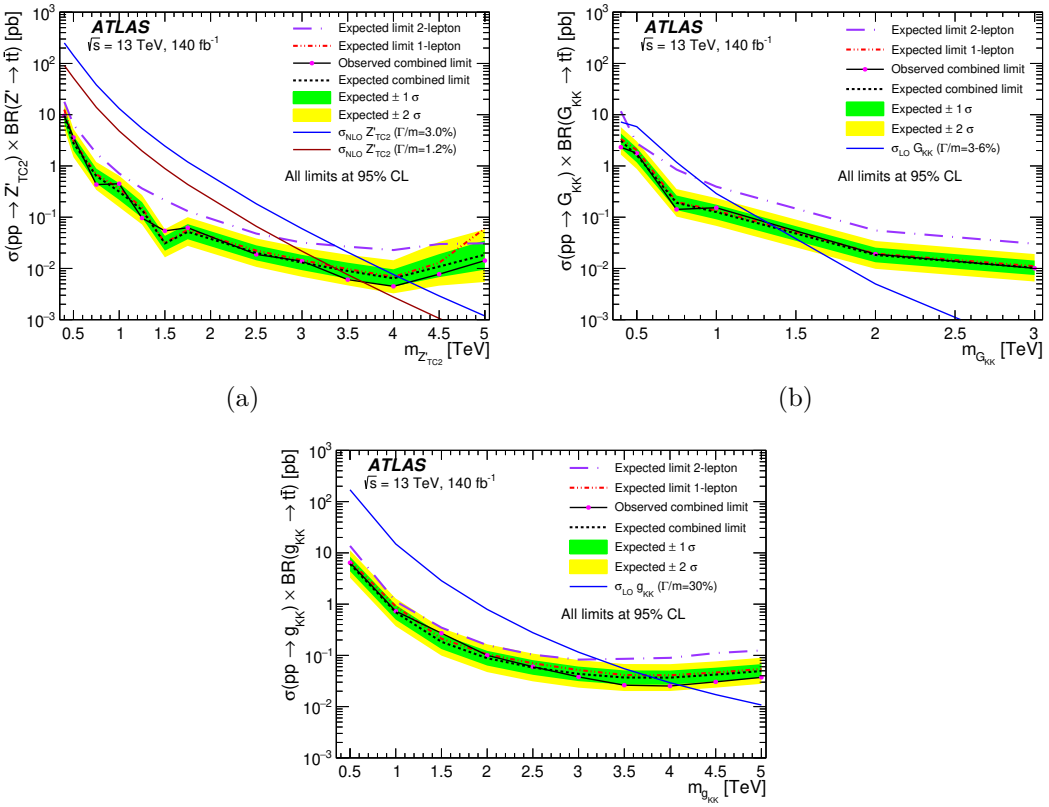


Figure 11. Observed (pink data points) and expected (black dashed line) upper limits on the signal cross-section times branching ratio to $t\bar{t}$ for the (a) Z'_{TC2}, (b) G_{KK}, and (c) g_{KK} signals at 95% CL. Approximate limits for intermediate masses are interpolated between the tested mass hypotheses. For the G_{KK} signal in (b), the detector resolution is finer than the grid spacing, so the interpolation is only for display purposes. The theory predictions for the production cross-section times branching ratio at the corresponding masses are also shown in (a) for a Z'_{TC2} with a width of 3% (blue line) and a Z'_{TC2} with a width of 1.2% (dark red line), in (b) a G_{KK} with a width ranging from 3%–6%, and in (c) a g_{KK} with a width of 30%. Also shown is the relative contribution of the 1-lepton (red dashed and dotted line) and 2-lepton (purple long-dashed and dotted line) channels to the expected combination limits.

across the full $m_{t\bar{t}}$ range considered for the G_{KK} and g_{KK} signals to date. Z'_{TC2} signals with a width of 3% (1.2%) and g_{KK} signals are excluded up to masses of 4.2 TeV (3.65 TeV) and 4.1 TeV, respectively, while the G_{KK} is excluded up to 1.3 TeV. The g_{KK} mass exclusions set the strongest limits on this benchmark model to date. The Z'_{TC2} mass exclusions significantly increase the previously excluded ATLAS limits in the 1-lepton channel on 36 fb^{-1} of data; however, the ATLAS search in fully hadronic final states still provide the most stringent mass limits on these models [24]. The mass limit on the G_{KK} signal is the most stringent limit to date in the $t\bar{t}$ decay channel, although complementary searches in diboson final states do provide stronger mass exclusions.

JHEP10(2026)219

12 Conclusion

The search presented in this paper targets heavy resonances decaying into top-antitop-quark pairs using final states with exactly one or two leptons. The analysis is performed using 140 fb^{-1} of proton-proton collision data recorded by the ATLAS detector at the LHC at a centre-of-mass energy of $\sqrt{s} = 13$ TeV. The search covers resonance masses in the range of 0.4 TeV to 5.0 TeV and considers both narrow and broad resonances, relative to the detector resolution.

No significant deviation from the Standard Model background expectation is observed across the probed invariant mass spectrum. As a result, upper limits are set on the production cross-section times branching fraction for three benchmark scenarios. For $m_{t\bar{t}} < 1.5$ TeV, the search sets the most stringent constraints to date on narrow $t\bar{t}$ resonances, excluding, for instance, values of the production cross-section times branching fraction greater than 3.6 pb for a Z'_{TC2} with a mass of 500 GeV.

The Z'_{TC2} signal with a relative width of 3% (1.2%) is excluded for masses below 4.2 TeV (3.65 TeV). These limits are slightly weaker than those obtained in the ATLAS analysis targeting fully-hadronic final states, which excluded masses up to 4.7 TeV using the same data, yet the present results offer complementary sensitivity in alternative $t\bar{t}$ decay channels.

Furthermore, the analysis yields the strongest exclusions to date for the g_{KK} signal with a relative width of 30%, excluding those with a mass below 4.1 TeV. The constraints on G_{KK} signals are the strongest to date in the studied decay channels, ruling out masses below 1.3 TeV and significantly extending the reach of previously published results in the $t\bar{t}$ decay channel.

Overall, the results reported in this study enhance existing exclusion limits across a broad range of models predicting heavy resonances decaying into top-quark pairs.

Acknowledgments

We thank CERN for the very successful operation of the LHC and its injectors, as well as the support staff at CERN and at our institutions worldwide without whom ATLAS could not be operated efficiently.

The crucial computing support from all WLCG partners is acknowledged gratefully, in particular from CERN, the ATLAS Tier-1 facilities at TRIUMF/SFU (Canada), NDGF (Denmark, Norway, Sweden), CC-IN2P3 (France), KIT/GridKA (Germany), INFN-CNAF (Italy), NL-T1 (Netherlands), PIC (Spain), RAL (U.K.) and BNL (U.S.A.), the Tier-2 facilities worldwide and large non-WLCG resource providers. Major contributors of computing resources are listed in ref. [142].

We gratefully acknowledge the support of ANPCyT, Argentina; YerPhI, Armenia; ARC, Australia; BMWFW and FWF, Austria; ANAS, Azerbaijan; CNPq and FAPESP, Brazil; NSERC, NRC and CFI, Canada; CERN; ANID, Chile; CAS, MOST and NSFC, China; Minciencias, Colombia; MEYS CR, Czech Republic; DNRF and DNSRC, Denmark; IN2P3-CNRS and CEA-DRF/IRFU, France; SRNSFG, Georgia; BMFTR, HGF and MPG, Germany; GSRI, Greece; RGC and Hong Kong SAR, China; ICHEP and Academy of Sciences and Humanities, Israel; INFN, Italy; MEXT and JSPS, Japan; CNRST, Morocco; NWO, Netherlands; RCN, Norway; MNiSW, Poland; FCT, Portugal; MNE/IFA, Romania; MSTDI,

JHEP10(2026)219

Serbia; MSSR, Slovakia; ARIS and MVZI, Slovenia; DSI/NRF, South Africa; MICIU/AEI, Spain; SRC and Wallenberg Foundation, Sweden; SERI, SNSF and Cantons of Bern and Geneva, Switzerland; NSTC, Taipei; TENMAK, Türkiye; STFC/UKRI, United Kingdom; DOE and NSF, United States of America.

Individual groups and members have received support from BCKDF, CANARIE, CRC and DRAC, Canada; CERN-CZ, FORTE and PRIMUS, Czech Republic; COST, ERC, ERDF, Horizon 2020 and Marie Skłodowska-Curie Actions, European Union; Investissements d'Avenir Labex, Investissements d'Avenir Idex and ANR, France; DFG and AvH Foundation, Germany; Herakleitos, Thales and Aristeia programmes co-financed by EU-ESF and the Greek NSRF, Greece; BSF-NSF and MINERVA, Israel; NCN and NAWA, Poland; La Caixa Banking Foundation, CERCA and AGAUR programs from Generalitat de Catalunya and PROMETEO and GenT Programmes Generalitat Valenciana, Spain; Göran Gustafssons Stiftelse, Sweden; The Royal Society and Leverhulme Trust, United Kingdom; Eric and Wendy Schmidt Fund for Strategic Innovation, United States of America.

In addition, individual members wish to acknowledge support from Chile: Agencia Nacional de Investigación y Desarrollo (ANID FONDECYT reg. 1230987, FONDECYT 1230812, FONDECYT 1240864, Fondecyt 3240661, Fondecyt Regular 1240721); China: Chinese Ministry of Science and Technology (MOST-2023YFA1605700, MOST-2023YFA1609300), National Natural Science Foundation of China (NSFC — 12175119, NSFC 12275265); Czech Republic: Czech Science Foundation (GACR — 24-11373S), Ministry of Education Youth and Sports (ERC-CZ-LL2327, FORTE CZ.02.01.01/00/22_008/0004632), PRIMUS Research Programme (PRIMUS/21/SCI/017); EU: H2020 European Research Council (ERC — 101002463); European Union: European Research Council (BARD No. 101116429, ERC — 948254, ERC 101089007), European Regional Development Fund (HE COFUND GA No.101081355, ERDF), European Union, Future Artificial Intelligence Research (FAIR-NextGenerationEU PE00000013), Marie Sklodowska-Curie Actions (ERC Horizon-2020, GA 956086, GAP-101168829); France: Agence Nationale de la Recherche (ANR-21-CE31-0013, ANR-21-CE31-0022, ANR-22-EDIR-0002, ANR-24-CE31-0504-01); Germany: Deutsche Forschungsgemeinschaft (DFG — 469666862, DFG — CR 312/5-2); China: Research Grants Council (GRF); Italy: Ministero dell'Università e della Ricerca (NextGenEU 153D23001490006 M4C2.1.1, NextGenEU I53D23000820006 M4C2.1.1, NextGenEU I53D23001490006 M4C2.1.1, SOE2024_0000023); Japan: Japan Society for the Promotion of Science (JSPS KAKENHI JP25H0063, JSPS KAKENHI JP22H01227, JSPS KAKENHI JP22H04944, JSPS KAKENHI JP22KK0227, JSPS KAKENHI JP24K23939, JSPS KAKENHI JP24KK0251, JSPS KAKENHI JP25H00650, JSPS KAKENHI JP25H01291, JSPS KAKENHI JP25K01011, JSPS KAKENHI JP25K01023); Norway: Research Council of Norway (RCN-314472); Poland: Ministry of Science and Higher Education (IDUB AGH, POB8, D4 no 9722), Polish National Science Centre (NCN 2021/42/E/ST2/00350, NCN OPUS 2023/51/B/ST2/02507, NCN OPUS nr 2022/47/B/ST2/03059, NCN UMO-2019/34/E/ST2/00393, UMO-2022/47/O/ST2/00148, UMO-2023/49/B/ST2/04085, UMO-2023/51/B/ST2/00920, UMO-2024/53/N/ST2/00869); Portugal: Foundation for Science and Technology (FCT); Spain: Agència de Gestió d'Ajuts Universitaris i de Recerca. (AGAUR — 2023 BP 00141), Generalitat Valenciana (ASFAE/2022/008), Ministry of Science and

Innovation (RYC2019-028510-I, RYC2020-030254-I, RYC2021-031273-I, RYC2022-038164-I), Ministerio de Ciencia, Innovación y Universidades/Agencia Estatal de Investigación (EU NextGenerationEU (PRTR-C17.I1), PID2022-142604OB-C22); Sweden: Carl Trygger Foundation (Carl Trygger Foundation CTS 22:2312), Swedish Research Council (Swedish Research Council 2023-04654, VR 2021-03651, VR 2022-03845, VR 2022-04683, VR 2023-03403, VR 2024-05451), Knut and Alice Wallenberg Foundation (KAW 2018.0458, KAW 2022.0358, KAW 2023.0366); Switzerland: Swiss National Science Foundation (SNSF — PCEFP2_194658); United Kingdom: The Binks Trust, Royal Society (NIF-R1-231091); United States of America: U.S. Department of Energy (ECA DE-AC02-76SF00515), Neubauer Family Foundation.

Data Availability Statement. This article has no associated data or the data will not be deposited.

Code Availability Statement. This article has no associated code or the code will not be deposited.

Open Access. This article is distributed under the terms of the Creative Commons Attribution License (CC-BY4.0), which permits any use, distribution and reproduction in any medium, provided the original author(s) and source are credited.

References

[1] G. 't Hooft, *Naturalness, chiral symmetry, and spontaneous chiral symmetry breaking*, *NATO Sci. Ser. B* **59** (1980) 135 [INSPIRE].

[2] M.J.G. Veltman, *The infrared-ultraviolet connection*, *Acta Phys. Polon. B* **12** (1981) 437 [INSPIRE].

[3] C.T. Hill and S.J. Parke, *Top production: sensitivity to new physics*, *Phys. Rev. D* **49** (1994) 4454 [hep-ph/9312324] [INSPIRE].

[4] C.T. Hill, *Topcolor assisted technicolor*, *Phys. Lett. B* **345** (1995) 483 [hep-ph/9411426] [INSPIRE].

[5] R.M. Harris, C.T. Hill and S.J. Parke, *Cross-section for topcolor Z'_t decaying to $t\bar{t}$*, hep-ph/9911288 [INSPIRE].

[6] R.M. Harris and S. Jain, *Cross sections for leptophobic topcolor Z' decaying to top-antitop*, *Eur. Phys. J. C* **72** (2012) 2072 [arXiv:1112.4928] [INSPIRE].

[7] L. Randall and R. Sundrum, *A large mass hierarchy from a small extra dimension*, *Phys. Rev. Lett.* **83** (1999) 3370 [hep-ph/9905221] [INSPIRE].

[8] B. Lillie, L. Randall and L.-T. Wang, *The bulk RS KK-gluon at the LHC*, *JHEP* **09** (2007) 074 [hep-ph/0701166] [INSPIRE].

[9] L. Evans and P. Bryant, *LHC machine*, 2008 *JINST* **3** S08001 [INSPIRE].

[10] ATLAS collaboration, *A search for $t\bar{t}$ resonances with the ATLAS detector in 2.05 fb^{-1} of proton-proton collisions at $\sqrt{s} = 7$ TeV*, *Eur. Phys. J. C* **72** (2012) 2083 [arXiv:1205.5371] [INSPIRE].

JHEP10(2026)219

[11] ATLAS collaboration, *A search for $t\bar{t}$ resonances in lepton+jets events with highly boosted top quarks collected in pp collisions at $\sqrt{s} = 7$ TeV with the ATLAS detector*, *JHEP* **09** (2012) 041 [arXiv:1207.2409] [INSPIRE].

[12] ATLAS collaboration, *Search for $t\bar{t}$ resonances in the lepton plus jets final state with ATLAS using 4.7fb^{-1} of pp collisions at $\sqrt{s} = 7$ TeV*, *Phys. Rev. D* **88** (2013) 012004 [arXiv:1305.2756] [INSPIRE].

[13] CMS collaboration, *Search for anomalous $t\bar{t}$ production in the highly-boosted all-hadronic final state*, *JHEP* **09** (2012) 029 [*Erratum ibid.* **03** (2014) 132] [arXiv:1204.2488] [INSPIRE].

[14] CMS collaboration, *Search for Z' resonances decaying to $t\bar{t}$ in dilepton + jets final states in pp collisions at $\sqrt{s} = 7$ TeV*, *Phys. Rev. D* **87** (2013) 072002 [arXiv:1211.3338] [INSPIRE].

[15] CMS collaboration, *Search for resonant $t\bar{t}$ production in lepton+jets events in pp collisions at $\sqrt{s} = 7$ TeV*, *JHEP* **12** (2012) 015 [arXiv:1209.4397] [INSPIRE].

[16] CMS collaboration, *Searches for new physics using the $t\bar{t}$ invariant mass distribution in pp collisions at $\sqrt{s} = 8$ TeV*, *Phys. Rev. Lett.* **111** (2013) 211804 [*Erratum ibid.* **112** (2014) 119903] [arXiv:1309.2030] [INSPIRE].

[17] ATLAS collaboration, *A search for $t\bar{t}$ resonances using lepton-plus-jets events in proton-proton collisions at $\sqrt{s} = 8$ TeV with the ATLAS detector*, *JHEP* **08** (2015) 148 [arXiv:1505.07018] [INSPIRE].

[18] CMS collaboration, *Search for resonant $t\bar{t}$ production in proton-proton collisions at $\sqrt{s} = 8$ TeV*, *Phys. Rev. D* **93** (2016) 012001 [arXiv:1506.03062] [INSPIRE].

[19] ATLAS collaboration, *Search for heavy Higgs bosons A/H decaying to a top quark pair in pp collisions at $\sqrt{s} = 8$ TeV with the ATLAS detector*, *Phys. Rev. Lett.* **119** (2017) 191803 [arXiv:1707.06025] [INSPIRE].

[20] ATLAS collaboration, *Search for heavy particles decaying into top-quark pairs using lepton-plus-jets events in proton–proton collisions at $\sqrt{s} = 13$ TeV with the ATLAS detector*, *Eur. Phys. J. C* **78** (2018) 565 [arXiv:1804.10823] [INSPIRE].

[21] ATLAS collaboration, *Search for heavy particles decaying into a top-quark pair in the fully hadronic final state in pp collisions at $\sqrt{s} = 13$ TeV with the ATLAS detector*, *Phys. Rev. D* **99** (2019) 092004 [arXiv:1902.10077] [INSPIRE].

[22] CMS collaboration, *Search for $t\bar{t}$ resonances in highly boosted lepton+jets and fully hadronic final states in proton-proton collisions at $\sqrt{s} = 13$ TeV*, *JHEP* **07** (2017) 001 [arXiv:1704.03366] [INSPIRE].

[23] CMS collaboration, *Search for resonant $t\bar{t}$ production in proton-proton collisions at $\sqrt{s} = 13$ TeV*, *JHEP* **04** (2019) 031 [arXiv:1810.05905] [INSPIRE].

[24] ATLAS collaboration, *Search for $t\bar{t}$ resonances in fully hadronic final states in pp collisions at $\sqrt{s} = 13$ TeV with the ATLAS detector*, *JHEP* **10** (2020) 061 [arXiv:2005.05138] [INSPIRE].

[25] ATLAS collaboration, *Search for heavy neutral Higgs bosons decaying into a top quark pair in 140fb^{-1} of proton-proton collision data at $\sqrt{s} = 13$ TeV with the ATLAS detector*, *JHEP* **08** (2024) 013 [arXiv:2404.18986] [INSPIRE].

[26] CMS collaboration, *Search for heavy pseudoscalar and scalar bosons decaying to a top quark pair in proton–proton collisions at $\sqrt{s} = 13$ TeV*, *Rept. Prog. Phys.* **88** (2025) 127801 [arXiv:2507.05119] [INSPIRE].

JHEP10(2026)219

[27] CMS collaboration, *Observation of a pseudoscalar excess at the top quark pair production threshold*, *Rept. Prog. Phys.* **88** (2025) 087801 [arXiv:2503.22382] [INSPIRE].

[28] ATLAS collaboration, *Observation of quantum entanglement with top quarks at the ATLAS detector*, *Nature* **633** (2024) 542 [arXiv:2311.07288] [INSPIRE].

[29] CMS collaboration, *Observation of quantum entanglement in top quark pair production in proton–proton collisions at* $\sqrt{s} = 13$ *TeV*, *Rept. Prog. Phys.* **87** (2024) 117801 [arXiv:2406.03976] [INSPIRE].

[30] ATLAS collaboration, *Performance of top-quark and W-boson tagging with ATLAS in Run 2 of the LHC*, *Eur. Phys. J. C* **79** (2019) 375 [arXiv:1808.07858] [INSPIRE].

[31] ATLAS collaboration, *Search for new resonances in mass distributions of jet pairs using* $139\,fb^{-1}$ *of pp collisions at* $\sqrt{s} = 13$ *TeV with the ATLAS detector*, *JHEP* **03** (2020) 145 [arXiv:1910.08447] [INSPIRE].

[32] ATLAS collaboration, *Search for heavy particles in the b-tagged dijet mass distribution with additional b-tagged jets in proton-proton collisions at* $\sqrt{s} = 13$ *TeV with the ATLAS experiment*, *Phys. Rev. D* **105** (2022) 012001 [arXiv:2108.09059] [INSPIRE].

[33] ATLAS collaboration, *Search for low-mass resonances decaying into two jets and produced in association with a photon or a jet at* $\sqrt{s} = 13$ *TeV with the ATLAS detector*, *Phys. Rev. D* **110** (2024) 032002 [*Erratum ibid.* **113** (2026) 119901] [arXiv:2403.08547] [INSPIRE].

[34] CMS collaboration, *Search for high mass dijet resonances with a new background prediction method in proton-proton collisions at* $\sqrt{s} = 13$ *TeV*, *JHEP* **05** (2020) 033 [arXiv:1911.03947] [INSPIRE].

[35] ATLAS collaboration, *Constraints on simplified dark matter models involving an s-channel mediator with the ATLAS detector in pp collisions at* $\sqrt{s} = 13$ *TeV*, *Eur. Phys. J. C* **84** (2024) 1102 [arXiv:2404.15930] [INSPIRE].

[36] K. Agashe, H. Davoudiasl, G. Perez and A. Soni, *Warped gravitons at the LHC and beyond*, *Phys. Rev. D* **76** (2007) 036006 [hep-ph/0701186] [INSPIRE].

[37] A.L. Fitzpatrick, J. Kaplan, L. Randall and L.-T. Wang, *Searching for the Kaluza-Klein graviton in bulk RS models*, *JHEP* **09** (2007) 013 [hep-ph/0701150] [INSPIRE].

[38] ATLAS collaboration, *Combination of searches for heavy resonances decaying into bosonic and leptonic final states using* $36\,fb^{-1}$ *of proton-proton collision data at* $\sqrt{s} = 13$ *TeV with the ATLAS detector*, *Phys. Rev. D* **98** (2018) 052008 [arXiv:1808.02380] [INSPIRE].

[39] CMS collaboration, *Search for ZZ resonances in the* $2\ell 2\nu$ *final state in proton-proton collisions at 13 TeV*, *JHEP* **03** (2018) 003 [arXiv:1711.04370] [INSPIRE].

[40] S. Ask et al., *Identifying the colour of TeV-scale resonances*, *JHEP* **01** (2012) 018 [arXiv:1108.2396] [INSPIRE].

[41] K. Agashe et al., *LHC signals from warped extra dimensions*, *Phys. Rev. D* **77** (2008) 015003 [hep-ph/0612015] [INSPIRE].

[42] ATLAS collaboration, *The ATLAS experiment at the CERN Large Hadron Collider*, 2008 *JINST* **3** S08003 [INSPIRE].

[43] ATLAS collaboration, *ATLAS Insertable B-Layer: technical design report*, https://cds.cern.ch/record/1291633 (2010).

[44] ATLAS IBL collaboration, *Production and integration of the ATLAS Insertable B-Layer*, 2018 *JINST* **13** T05008 [arXiv:1803.00844] [INSPIRE].

JHEP10(2026)219

[45] G. Avoni et al., *The new LUCID-2 detector for luminosity measurement and monitoring in ATLAS*, 2018 *JINST* **13** P07017 [INSPIRE].

[46] ATLAS collaboration, *Operation of the ATLAS trigger system in run 2*, 2020 *JINST* **15** P10004 [arXiv:2007.12539] [INSPIRE].

[47] ATLAS collaboration, *The ATLAS simulation infrastructure*, *Eur. Phys. J. C* **70** (2010) 823 [arXiv:1005.4568] [INSPIRE].

[48] ATLAS collaboration, *Luminosity determination in pp collisions at* $\sqrt{s} = 13$ *TeV using the ATLAS detector at the LHC*, *Eur. Phys. J. C* **83** (2023) 982 [arXiv:2212.09379] [INSPIRE].

[49] ATLAS collaboration, *ATLAS data quality operations and performance for 2015–2018 data-taking*, 2020 *JINST* **15** P04003 [arXiv:1911.04632] [INSPIRE].

[50] ATLAS collaboration, *Performance of the ATLAS muon triggers in run 2*, 2020 *JINST* **15** P09015 [arXiv:2004.13447] [INSPIRE].

[51] ATLAS collaboration, *Performance of electron and photon triggers in ATLAS during LHC run 2*, *Eur. Phys. J. C* **80** (2020) 47 [arXiv:1909.00761] [INSPIRE].

[52] T. Sjöstrand, S. Mrenna and P.Z. Skands, *A brief introduction to PYTHIA 8.1*, *Comput. Phys. Commun.* **178** (2008) 852 [arXiv:0710.3820] [INSPIRE].

[53] ATLAS collaboration, *ATLAS Pythia 8 tunes to 7 TeV data*, ATL-PHYS-PUB-2014-021 (2014) [INSPIRE].

[54] R.D. Ball et al., *Parton distributions with LHC data*, *Nucl. Phys. B* **867** (2013) 244 [arXiv:1207.1303] [INSPIRE].

[55] SHERPA collaboration, *Event generation with Sherpa 2.2*, *SciPost Phys.* **7** (2019) 034 [arXiv:1905.09127] [INSPIRE].

[56] D.J. Lange, *The EvtGen particle decay simulation package*, *Nucl. Instrum. Meth. A* **462** (2001) 152 [INSPIRE].

[57] GEANT4 collaboration, *GEANT4 — a simulation toolkit*, *Nucl. Instrum. Meth. A* **506** (2003) 250 [INSPIRE].

[58] ATLAS collaboration, *The Pythia 8 A3 tune description of ATLAS minimum bias and inelastic measurements incorporating the Donnachie-Landshoff diffractive model*, ATL-PHYS-PUB-2016-017 (2016) [INSPIRE].

[59] P. Nason, *A new method for combining NLO QCD with shower Monte Carlo algorithms*, *JHEP* **11** (2004) 040 [hep-ph/0409146] [INSPIRE].

[60] S. Frixione, P. Nason and G. Ridolfi, *A positive-weight next-to-leading-order Monte Carlo for heavy flavour hadroproduction*, *JHEP* **09** (2007) 126 [arXiv:0707.3088] [INSPIRE].

[61] S. Frixione, P. Nason and C. Oleari, *Matching NLO QCD computations with parton shower simulations: the POWHEG method*, *JHEP* **11** (2007) 070 [arXiv:0709.2092] [INSPIRE].

[62] S. Alioli, P. Nason, C. Oleari and E. Re, *A general framework for implementing NLO calculations in shower Monte Carlo programs: the POWHEG BOX*, *JHEP* **06** (2010) 043 [arXiv:1002.2581] [INSPIRE].

[63] J.M. Campbell, R.K. Ellis, P. Nason and E. Re, *Top-pair production and decay at NLO matched with parton showers*, *JHEP* **04** (2015) 114 [arXiv:1412.1828] [INSPIRE].

[64] NNPDF collaboration, *Parton distributions for the LHC run II*, *JHEP* **04** (2015) 040 [arXiv:1410.8849] [INSPIRE].

JHEP10(2026)219

[65] ATLAS collaboration, *Studies on top-quark Monte Carlo modelling for Top2016*, ATL-PHYS-PUB-2016-020 (2016) [INSPIRE].

[66] T. Sjöstrand et al., *An introduction to PYTHIA 8.2*, *Comput. Phys. Commun.* **191** (2015) 159 [arXiv:1410.3012] [INSPIRE].

[67] M. Czakon et al., *Top-pair production at the LHC through NNLO QCD and NLO EW*, *JHEP* **10** (2017) 186 [arXiv:1705.04105] [INSPIRE].

[68] M. Beneke, P. Falgari, S. Klein and C. Schwinn, *Hadronic top-quark pair production with NNLL threshold resummation*, *Nucl. Phys. B* **855** (2012) 695 [arXiv:1109.1536] [INSPIRE].

[69] M. Cacciari et al., *Top-pair production at hadron colliders with next-to-next-to-leading logarithmic soft-gluon resummation*, *Phys. Lett. B* **710** (2012) 612 [arXiv:1111.5869] [INSPIRE].

[70] P. Bärnreuther, M. Czakon and A. Mitov, *Percent level precision physics at the Tevatron: first genuine NNLO QCD corrections to $q\bar{q} \to t\bar{t} + X$*, *Phys. Rev. Lett.* **109** (2012) 132001 [arXiv:1204.5201] [INSPIRE].

[71] M. Czakon and A. Mitov, *NNLO corrections to top-pair production at hadron colliders: the all-fermionic scattering channels*, *JHEP* **12** (2012) 054 [arXiv:1207.0236] [INSPIRE].

[72] M. Czakon and A. Mitov, *NNLO corrections to top pair production at hadron colliders: the quark-gluon reaction*, *JHEP* **01** (2013) 080 [arXiv:1210.6832] [INSPIRE].

[73] M. Czakon, P. Fiedler and A. Mitov, *Total top-quark pair-production cross section at hadron colliders through $O(\alpha_S^4)$*, *Phys. Rev. Lett.* **110** (2013) 252004 [arXiv:1303.6254] [INSPIRE].

[74] M. Czakon and A. Mitov, *Top++: a program for the calculation of the top-pair cross-section at hadron colliders*, *Comput. Phys. Commun.* **185** (2014) 2930 [arXiv:1112.5675] [INSPIRE].

[75] E. Re, *Single-top Wt-channel production matched with parton showers using the POWHEG method*, *Eur. Phys. J. C* **71** (2011) 1547 [arXiv:1009.2450] [INSPIRE].

[76] S. Frixione et al., *Single-top hadroproduction in association with a W boson*, *JHEP* **07** (2008) 029 [arXiv:0805.3067] [INSPIRE].

[77] C. Bierlich et al., *A comprehensive guide to the physics and usage of PYTHIA 8.3*, *SciPost Phys. Codeb.* **2022** (2022) 8 [arXiv:2203.11601] [INSPIRE].

[78] N. Kidonakis, *Two-loop soft anomalous dimensions for single top quark associated production with a W^- or H^-*, *Phys. Rev. D* **82** (2010) 054018 [arXiv:1005.4451] [INSPIRE].

[79] S. Alioli, P. Nason, C. Oleari and E. Re, *NLO single-top production matched with shower in POWHEG: s- and t-channel contributions*, *JHEP* **09** (2009) 111 [*Erratum ibid.* **02** (2010) 011] [arXiv:0907.4076] [INSPIRE].

[80] R. Frederix, E. Re and P. Torrielli, *Single-top t-channel hadroproduction in the four-flavour scheme with POWHEG and aMC@NLO*, *JHEP* **09** (2012) 130 [arXiv:1207.5391] [INSPIRE].

[81] P. Artoisenet, R. Frederix, O. Mattelaer and R. Rietkerk, *Automatic spin-entangled decays of heavy resonances in Monte Carlo simulations*, *JHEP* **03** (2013) 015 [arXiv:1212.3460] [INSPIRE].

[82] M. Aliev et al., *HATHOR: HAdronic Top and Heavy quarks crOss section calculatoR*, *Comput. Phys. Commun.* **182** (2011) 1034 [arXiv:1007.1327] [INSPIRE].

[83] P. Kant et al., *HatHor for single top-quark production: updated predictions and uncertainty estimates for single top-quark production in hadronic collisions*, *Comput. Phys. Commun.* **191** (2015) 74 [arXiv:1406.4403] [INSPIRE].

JHEP10(2026)219

[84] N. Kidonakis, *NNLL resummation for s-channel single top quark production*, *Phys. Rev. D* **81** (2010) 054028 [arXiv:1001.5034] [INSPIRE].

[85] N. Kidonakis, *Next-to-next-to-leading-order collinear and soft gluon corrections for t-channel single top quark production*, *Phys. Rev. D* **83** (2011) 091503 [arXiv:1103.2792] [INSPIRE].

[86] J. Alwall et al., *The automated computation of tree-level and next-to-leading order differential cross sections, and their matching to parton shower simulations*, *JHEP* **07** (2014) 079 [arXiv:1405.0301] [INSPIRE].

[87] LHC Higgs Cross Section Working Group collaboration, *Handbook of LHC Higgs cross sections: 4. Deciphering the nature of the Higgs sector*, arXiv:1610.07922 [DOI:10.23731/CYRM-2017-002] [INSPIRE].

[88] T. Gleisberg and S. Höche, *Comix, a new matrix element generator*, *JHEP* **12** (2008) 039 [arXiv:0808.3674] [INSPIRE].

[89] F. Buccioni et al., *OpenLoops 2*, *Eur. Phys. J. C* **79** (2019) 866 [arXiv:1907.13071] [INSPIRE].

[90] F. Cascioli, P. Maierhöfer and S. Pozzorini, *Scattering amplitudes with OpenLoops*, *Phys. Rev. Lett.* **108** (2012) 111601 [arXiv:1111.5206] [INSPIRE].

[91] A. Denner, S. Dittmaier and L. Hofer, *COLLIER: a fortran-based Complex One-Loop LIbrary in Extended Regularizations*, *Comput. Phys. Commun.* **212** (2017) 220 [arXiv:1604.06792] [INSPIRE].

[92] S. Schumann and F. Krauss, *A parton shower algorithm based on Catani-Seymour dipole factorisation*, *JHEP* **03** (2008) 038 [arXiv:0709.1027] [INSPIRE].

[93] S. Höche, F. Krauss, M. Schönherr and F. Siegert, *A critical appraisal of NLO+PS matching methods*, *JHEP* **09** (2012) 049 [arXiv:1111.1220] [INSPIRE].

[94] S. Höche, F. Krauss, M. Schönherr and F. Siegert, *QCD matrix elements + parton showers: the NLO case*, *JHEP* **04** (2013) 027 [arXiv:1207.5030] [INSPIRE].

[95] S. Catani, F. Krauss, R. Kuhn and B.R. Webber, *QCD matrix elements + parton showers*, *JHEP* **11** (2001) 063 [hep-ph/0109231] [INSPIRE].

[96] S. Höche, F. Krauss, S. Schumann and F. Siegert, *QCD matrix elements and truncated showers*, *JHEP* **05** (2009) 053 [arXiv:0903.1219] [INSPIRE].

[97] S. Catani et al., *Vector boson production at hadron colliders: a fully exclusive QCD calculation at NNLO*, *Phys. Rev. Lett.* **103** (2009) 082001 [arXiv:0903.2120] [INSPIRE].

[98] ATLAS collaboration, *Multi-boson simulation for 13 TeV ATLAS analyses*, ATL-PHYS-PUB-2017-005 (2017) [INSPIRE].

[99] R. Bonciani et al., *Electroweak top-quark pair production at the LHC with Z' bosons to NLO QCD in POWHEG*, *JHEP* **02** (2016) 141 [arXiv:1511.08185] [INSPIRE].

[100] ATLAS collaboration, *Vertex reconstruction performance of the ATLAS detector at $\sqrt{s} = 13$ TeV*, ATL-PHYS-PUB-2015-026 (2015) [INSPIRE].

[101] ATLAS collaboration, *Selection of jets produced in 13 TeV proton-proton collisions with the ATLAS detector*, ATLAS-CONF-2015-029 (2015) [INSPIRE].

[102] ATLAS collaboration, *Jet reconstruction and performance using particle flow with the ATLAS detector*, *Eur. Phys. J. C* **77** (2017) 466 [arXiv:1703.10485] [INSPIRE].

[103] M. Cacciari, G.P. Salam and G. Soyez, *The anti-k_t jet clustering algorithm*, *JHEP* **04** (2008) 063 [arXiv:0802.1189] [INSPIRE].

JHEP10(2026)219

[104] M. Cacciari, G.P. Salam and G. Soyez, *FastJet user manual*, *Eur. Phys. J. C* **72** (2012) 1896 [arXiv:1111.6097] [INSPIRE].

[105] ATLAS collaboration, *Jet energy scale and resolution measured in proton–proton collisions at $\sqrt{s} = 13$ TeV with the ATLAS detector*, *Eur. Phys. J. C* **81** (2021) 689 [arXiv:2007.02645] [INSPIRE].

[106] ATLAS collaboration, *Performance of pile-up mitigation techniques for jets in pp collisions at $\sqrt{s} = 8$ TeV using the ATLAS detector*, *Eur. Phys. J. C* **76** (2016) 581 [arXiv:1510.03823] [INSPIRE].

[107] ATLAS collaboration, *Topological cell clustering in the ATLAS calorimeters and its performance in LHC run 1*, *Eur. Phys. J. C* **77** (2017) 490 [arXiv:1603.02934] [INSPIRE].

[108] D. Krohn, J. Thaler and L.-T. Wang, *Jet trimming*, *JHEP* **02** (2010) 084 [arXiv:0912.1342] [INSPIRE].

[109] S. Catani et al., *New clustering algorithm for multi-jet cross-sections in e^+e^- annihilation*, *Phys. Lett. B* **269** (1991) 432 [INSPIRE].

[110] S.D. Ellis and D.E. Soper, *Successive combination jet algorithm for hadron collisions*, *Phys. Rev. D* **48** (1993) 3160 [hep-ph/9305266] [INSPIRE].

[111] S. Catani, Y.L. Dokshitzer, M.H. Seymour and B.R. Webber, *Longitudinally invariant K_t clustering algorithms for hadron hadron collisions*, *Nucl. Phys. B* **406** (1993) 187 [INSPIRE].

[112] ATLAS collaboration, *Optimisation of large-radius jet reconstruction for the ATLAS detector in 13 TeV proton–proton collisions*, *Eur. Phys. J. C* **81** (2021) 334 [arXiv:2009.04986] [INSPIRE].

[113] ATLAS collaboration, *In situ calibration of large-radius jet energy and mass in 13 TeV proton–proton collisions with the ATLAS detector*, *Eur. Phys. J. C* **79** (2019) 135 [arXiv:1807.09477] [INSPIRE].

[114] ATLAS collaboration, *ATLAS flavour-tagging algorithms for the LHC run 2 pp collision dataset*, *Eur. Phys. J. C* **83** (2023) 681 [arXiv:2211.16345] [INSPIRE].

[115] ATLAS collaboration, *ATLAS b-jet identification performance and efficiency measurement with $t\bar{t}$ events in pp collisions at $\sqrt{s} = 13$ TeV*, *Eur. Phys. J. C* **79** (2019) 970 [arXiv:1907.05120] [INSPIRE].

[116] ATLAS collaboration, *Measurement of the c-jet mistagging efficiency in $t\bar{t}$ events using pp collision data at $\sqrt{s} = 13$ TeV collected with the ATLAS detector*, *Eur. Phys. J. C* **82** (2022) 95 [arXiv:2109.10627] [INSPIRE].

[117] ATLAS collaboration, *Calibration of the light-flavour jet mistagging efficiency of the b-tagging algorithms with Z+jets events using 139 fb^{-1} of ATLAS proton–proton collision data at $\sqrt{s} = 13$ TeV*, *Eur. Phys. J. C* **83** (2023) 728 [arXiv:2301.06319] [INSPIRE].

[118] ATLAS collaboration, *Muon reconstruction and identification efficiency in ATLAS using the full Run 2 pp collision data set at $\sqrt{s} = 13$ TeV*, *Eur. Phys. J. C* **81** (2021) 578 [arXiv:2012.00578] [INSPIRE].

[119] ATLAS collaboration, *Electron and photon performance measurements with the ATLAS detector using the 2015–2017 LHC proton-proton collision data*, 2019 *JINST* **14** P12006 [arXiv:1908.00005] [INSPIRE].

[120] M. Cacciari, G.P. Salam and G. Soyez, *The catchment area of jets*, *JHEP* **04** (2008) 005 [arXiv:0802.1188] [INSPIRE].

JHEP10(2026)219

[121] ATLAS collaboration, *The performance of missing transverse momentum reconstruction and its significance with the ATLAS detector using 140 fb^{-1} of $\sqrt{s} = 13$ TeV pp collisions*, *Eur. Phys. J. C* **85** (2025) 606 [arXiv:2402.05858] [INSPIRE].

[122] PARTICLE DATA GROUP collaboration, *Review of particle physics*, *PTEP* **2022** (2022) 083C01 [INSPIRE].

[123] ATLAS collaboration, *Tools for estimating fake/non-prompt lepton backgrounds with the ATLAS detector at the LHC*, 2023 *JINST* **18** T11004 [arXiv:2211.16178] [INSPIRE].

[124] ATLAS collaboration, *Measurement of the cross-section and charge asymmetry of W bosons produced in proton–proton collisions at $\sqrt{s} = 8$ TeV with the ATLAS detector*, *Eur. Phys. J. C* **79** (2019) 760 [arXiv:1904.05631] [INSPIRE].

[125] G. Cowan, K. Cranmer, E. Gross and O. Vitells, *Asymptotic formulae for likelihood-based tests of new physics*, *Eur. Phys. J. C* **71** (2011) 1554 [*Erratum ibid.* **73** (2013) 2501] [arXiv:1007.1727] [INSPIRE].

[126] ROOT collaboration, *HistFactory: a tool for creating statistical models for use with RooFit and RooStats*, CERN-OPEN-2012-016 (2012) [INSPIRE].

[127] R.J. Barlow and C. Beeston, *Fitting using finite Monte Carlo samples*, *Comput. Phys. Commun.* **77** (1993) 219 [INSPIRE].

[128] A. Manohar, P. Nason, G.P. Salam and G. Zanderighi, *How bright is the proton? A precise determination of the photon parton distribution function*, *Phys. Rev. Lett.* **117** (2016) 242002 [arXiv:1607.04266] [INSPIRE].

[129] NNPDF collaboration, *Parton distributions with QED corrections*, *Nucl. Phys. B* **877** (2013) 290 [arXiv:1308.0598] [INSPIRE].

[130] ATLAS collaboration, *Studies on the improvement of the matching uncertainty definition in top-quark processes simulated with Powheg+Pythia 8*, ATL-PHYS-PUB-2023-029 (2023) [INSPIRE].

[131] M. Bähr et al., *Herwig++ physics and manual*, *Eur. Phys. J. C* **58** (2008) 639 [arXiv:0803.0883] [INSPIRE].

[132] J. Bellm et al., *Herwig 7.0/Herwig++ 3.0 release note*, *Eur. Phys. J. C* **76** (2016) 196 [arXiv:1512.01178] [INSPIRE].

[133] J. Bellm et al., *Herwig 7.1 release note*, arXiv:1705.06919 [INSPIRE].

[134] ATLAS and CMS collaborations, *Combination of measurements of the top quark mass from data collected by the ATLAS and CMS experiments at $\sqrt{s} = 7$ and 8 TeV*, *Phys. Rev. Lett.* **132** (2024) 261902 [arXiv:2402.08713] [INSPIRE].

[135] L.A. Harland-Lang, A.D. Martin, P. Motylinski and R.S. Thorne, *Parton distributions in the LHC era: MMHT 2014 PDFs*, *Eur. Phys. J. C* **75** (2015) 204 [arXiv:1412.3989] [INSPIRE].

[136] J. Alwall et al., *Comparative study of various algorithms for the merging of parton showers and matrix elements in hadronic collisions*, *Eur. Phys. J. C* **53** (2008) 473 [arXiv:0706.2569] [INSPIRE].

[137] ATLAS collaboration, *Search for the standard model Higgs boson produced in association with top quarks and decaying into a $b\bar{b}$ pair in pp collisions at $\sqrt{s} = 13$ TeV with the ATLAS detector*, *Phys. Rev. D* **97** (2018) 072016 [arXiv:1712.08895] [INSPIRE].

[138] ATLAS collaboration, *Simulation-based extrapolation of b-tagging calibrations towards high transverse momenta in the ATLAS experiment*, ATL-PHYS-PUB-2021-003 (2021) [INSPIRE].

JHEP10(2026)219

[139] ATLAS collaboration, *Boosted hadronic vector boson and top quark tagging with ATLAS using Run 2 data*, ATL-PHYS-PUB-2020-017 (2020) [INSPIRE].

[140] R.D. Cousins, *Generalization of chisquare goodness-of-fit test for binned data using saturated models, with application to histograms*, https://www.physics.ucla.edu/~cousins/stats/cousins_saturated.pdf (2013).

[141] A.L. Read, *Presentation of search results: the CL_s technique*, *J. Phys. G* **28** (2002) 2693 [INSPIRE].

[142] ATLAS collaboration, *ATLAS computing acknowledgements*, https://cds.cern.ch/record/2952666 (2026).

JHEP10(2026)219

The ATLAS collaboration

G. Aad[103], E. Aakvaag[17], B. Abbott[121], S. Abdelhameed[84b], K. Abeling[55], N.J. Abicht[49], S.H. Abidi[30], M. Aboelela[45], A. Aboulhorma[36e], H. Abramowicz[155], B.S. Acharya[69a,69b,a], A. Ackermann[63a], C. Adam Bourdarios[4], L. Adamczyk[86a], S.V. Addepalli[147], M. J. Addison[102], J. Adelman[117], A. Adiguzel[22c], T. Adye[135], A.A. Affolder[137], Y. Afik[40], M.N. Agaras[13], A. Aggarwal[101], C. Agheorghiesei[28c], F. Ahmadov[39,b], S. Ahuja[96], S. Ahuja[167], X. Ai[141b], G. Aielli[76a,76b], A. Aikot[167], M. Ait Tamlihat[36e], B. Aitbenchikh[36a], T.P.A. Åkesson[99], D. Akiyama[172], N.N. Akolkar[25], S. Aktas[170], G.L. Alberghi[24b], J. Albert[169], U. Alberti[20], P. Albicocco[53], G.L. Albouy[60], S. Alderweireldt[52], Z.L. Alegria[122], M. Aleksa[37], I.N. Aleksandrov[39], C. Alexa[28b], T. Alexopoulos[10], F. Alfonsi[24b], M. Algren[56], M. Alhroob[171], B. Ali[133], H. M. J. Ali[92,c], S. Ali[32], S.W. Alibocus[93], M. Aliev[34c], G. Alimonti[71a], W. Alkakhi[55], C. Allaire[66], B.M.M. Allbrooke[150], D. R. Allen[122], J. S. Allen[102], J.F. Allen[52], A. Aloisio[72a,72b], F. Alonso[91], C. Alpigiani[140], Z.M.K. Alsolami[92], A. Alvarez Fernandez[101], M. Alves Cardoso[56], M.G. Alviggi[72a,72b], M. Aly[102], Y. Amaral Coutinho[82b], A. Ambler[105], C. Amelung[37], M. Amerl[102], C.G. Ames[110], T. Amezza[128], B. Amini[54], K. Amirie[159], A. Amirkhanov[39], S.P. Amor Dos Santos[131a], D. Amperiadou[156], S. An[83], C. Anastopoulos[143], T. Andeen[11], J.K. Anders[93], A. C. Anderson[59], A. Andreazza[71a,71b], S. Angelidakis[9], A. Angerami[42], A.V. Anisenkov[39], A. Annovi[74a], C. Antel[37], E. Antipov[149], M. Antonelli[53], F. Anulli[75a], M. Aoki[83], T. Aoki[157], M.A. Aparo[13], L. Aperio Bella[48], M. Apicella[31], C. Appelt[155], A. Apyan[27], M. Arampatzi[10], S. J. Arbiol Val[87], C. Arcangeletti[53], A.T.H. Arce[51], J-F. Arguin[109], S. Argyropoulos[156], J.-H. Arling[48], O. Arnaez[4], H. Arnold[149], G. Artoni[75a,75b], H. Asada[112], K. Asai[119], S. Asatryan[177], N.A. Asbah[37], R. A. Ashby Pickering[171], A. M. Aslam[96], K. Assamagan[30], R. Astalos[29a], K. S. V. Astrand[99], S. Atashi[163], R.J. Atkin[34a], H. Atmani[36f], P.A. Atmasiddha[129], K. Augsten[133], A.D. Auriol[41], V.A. Austrup[102], A.S. Avad[95], G. Avolio[37], K. Axiotis[56], A. Azzam[13], D. Babal[29b], H. Bachacou[136], K. Bachas[156,d], A. Bachiu[35], E. Bachmann[50], M. J. Backes[63a], A. Badea[40], T.M. Baer[107], P. Bagnaia[75a,75b], M. Bahmani[19], D. Bahner[54], K. Bai[124], J.T. Baines[135], L. Baines[95], O.K. Baker[176], E. Bakos[16], D. Bakshi Gupta[8], L.E. Balabram Filho[82b], V. Balakrishnan[121], R. Balasubramanian[4], E.M. Baldin[38], P. Balek[86a], E. Ballabene[24b,24a], F. Balli[136], L.M. Baltes[63a], W.K. Balunas[33], J. Balz[101], I. Bamwidhi[84c], E. Banas[87], M. Bandieramonte[130], A. Bandyopadhyay[25], S. Bansal[25], L. Barak[155], M. Barakat[48], W.M. Barbe[41], E.L. Barberio[106], D. Barberis[18b], M. Barbero[103], M. Z. Barel[116], T. Barillari[111], M-S. Barisits[37], T. Barklow[147], P. Baron[134], D.A. Baron Moreno[102], A. Baroncelli[62], A.J. Barr[127], J.D. Barr[97], F. Barreiro[100], J. Barreiro Guimarães da Costa[14], M.G. Barros Teixeira[131a], S. Barsov[38], F. Bartels[63a], R. Bartoldus[147], A.E. Barton[92], P. Bartos[29a], M. Baselga[49], S. Bashiri[87], A. Bassalat[66,e], M.J. Basso[160a], S. Bataju[45], R. Bate[168], R.L. Bates[59], S. Batlamous[100], M. Battaglia[137], D. Battulga[19], M. Bauce[75a,75b], L. Bauckhage[48], P. Bauer[25], L. T. Bayer[48], L.T. Bazzano Hurrell[31], J.B. Beacham[111], T. Beau[128], J.Y. Beaucamp[91], P.H. Beauchemin[162], P. Bechtle[25], H.P. Beck[20,f], K. Becker[171], A.J. Beddall[81], V.A. Bednyakov[39], C.P. Bee[149], L.J. Beemster[16], M. Begalli[82d], M. Begel[30], J.K. Behr[48],

JHEP10(2026)219

J.F. Beirer[37], F. Beisiegel[25], M. Belfkir[84c], G. Bella[155], L. Bellagamba[24b], A. Bellerive[35], C.D. Bellgraph[68], P. Bellos[21], K. Beloborodov[38], I. Benaoumeur[21], D. Benchekroun[36a], F. Bendebba[36a], Y. Benhammou[155], K.C. Benkendorfer[61], L. Beresford[48], M. Beretta[53], E. Bergeaas Kuutmann[165], N. Berger[4], B. Bergmann[133], J. Beringer[18a], G. Bernardi[5], C. Bernius[147], F.U. Bernlochner[25], A. Berrocal Guardia[13], T. Berry[96], P. Berta[134], A. Berti[131a], R. Bertrand[103], S. Bethke[111], A. Betti[75a,75b], A.J. Bevan[95], L. Bezio[56], N.K. Bhalla[54], S. Bharthuar[111], S. Bhatta[149], P. Bhattarai[147], Z.M. Bhatti[118], K. D. Bhide[54], V.S. Bhopatkar[122], R.M. Bianchi[130], G. Bianco[24b,24a], O. Biebel[110], M. Biglietti[77a], P. Bijl[54], C. S. Billingsley[45], Y. Bimgdi[36f], M. Bindi[55], A. Bingham[175], A. Bingul[22b], C. Bini[75a,75b], G.A. Bird[33], M. Birman[173], M. Biros[134], S. Biryukov[150], T. Bisanz[49], E. Bisceglie[24b,24a], J.P. Biswal[135], D. Biswas[145], I. Bloch[48], A. Blue[59], U. Blumenschein[95], V.S. Bobrovnikov[39], L. Boccardo[57b,57a], M. Boehler[54], B. Boehm[170], D. Bogavac[13], A.G. Bogdanchikov[38], L. S. Boggia[128], V. Boisvert[96], P. Bokan[165], T. Bold[86a], M. Bomben[5], M. Bona[95], M. Boonekamp[136], A.G. Borbély[59], I.S. Bordulev[38], G. Borissov[92], D. Bortoletto[127], D. Boscherini[24b], M. Bosman[13], K. Bouaouda[36a], N. Bouchhar[167], L. Boudet[4], J. Boudreau[130], E.V. Bouhova-Thacker[92], D. Boumediene[41], R. Bouquet[57b,57a], A. Boveia[120], J. Boyd[37], D. Boye[30], I.R. Boyko[39], L. Bozianu[56], J. Bracinik[21], N. Brahimi[4], G. Brandt[175], O. Brandt[33], B. Brau[104], R. Brener[173], L. Brenner[116], R. Brenner[165], S. Bressler[173], G. Brianti[116], D. Britton[59], D. Britzger[111], I. Brock[25], R. Brock[108], G. Brooijmans[42], A.J. Brooks[68], E. M. Brooks[160b], E. Brost[30], L.M. Brown[169,160a], L.E. Bruce[61], T.L. Bruckler[127], P.A. Bruckman de Renstrom[87], B. Brüers[48], A. Bruni[24b], G. Bruni[24b], D. Brunner[47a,47b], M. Bruschi[24b], N. Bruscino[75a,75b], T. Buanes[17], Q. Buat[140], D. Buchin[111], A.G. Buckley[59], J. Bucko[134], O. Bulekov[81], B.A. Bullard[147], S. Burdin[93], C.D. Burgard[49], A.M. Burger[90], B. Burghgrave[8], O. Burlayenko[54], J. Burleson[166], J.C. Burzynski[146], V. Büscher[101], P.J. Bussey[59], O. But[25], J.M. Butler[26], C.M. Buttar[59], J.M. Butterworth[97], P. Butti[37], W. Buttinger[135], C.J. Buxo Vazquez[108], A.R. Buzykaev[39], S. Cabrera Urbán[167], L. Cadamuro[66], H. Cai[37], Y. Cai[24b,113c,24a], Y. Cai[113a], V.M.M. Cairo[37], O. Cakir[3a], N. Calace[37], P. Calafiura[18a], G. Calderini[128], P. Calfayan[35], L. Calic[99], G. Callea[59], L.P. Caloba[82b], D. Calvet[41], S. Calvet[41], R. Camacho Toro[128], S. Camarda[37], D. Camarero Munoz[27], P. Camarri[76a,76b], C. Camincher[37], M. Campanelli[97], A. Camplani[43], V. Canale[72a,72b], A.C. Canbay[3a], E. Canonero[96], J. Cantero[167], Y. Cao[166], F. Capocasa[27], M. Capua[44b,44a], A. Carbone[71a,71b], R. Cardarelli[76a], J.C.J. Cardenas[8], M. P. Cardiff[27], G. Carducci[44b,44a], T. Carli[37], G. Carlino[72a], J.I. Carlotto[13], B.T. Carlson[130,g], E.M. Carlson[169], L. Carminati[71a,71b], A. Carnelli[4], M. Carnesale[37], S. Caron[115], E. Carquin[138g], I.B. Carr[106], S. Carrà[73a,73b], G. Carratta[24b,24a], C. Carrion Martinez[167], A.M. Carroll[124], M.P. Casado[13,h], P. Casolaro[72a,72b], M. Caspar[48], W.R. Castiglioni[40], F.L. Castillo[4], L. Castillo Garcia[13], V. Castillo Gimenez[167], N.F. Castro[131a,131e], A. Catinaccio[37], J.R. Catmore[126], T. Cavaliere[4], V. Cavaliere[30], L.J. Caviedes Betancourt[23b], E. Celebi[81], S. Cella[37], V. Cepaitis[56], K. Cerny[123], A.S. Cerqueira[82a], A. Cerri[74a,i], L. Cerrito[76a,76b], F. Cerutti[18a], B. Cervato[71a,71b], A. Cervelli[24b], G. Cesarini[53], S.A. Cetin[81], P.M. Chabrillat[128], R. Chakkappai[66], S. Chakraborty[171], A. Chambers[61], J. Chan[18a],

JHEP10(2026)219

W.Y. Chan[157], J.D. Chapman[33], E. Chapon[136], B. Chargeishvili[153b], D.G. Charlton[21], C. Chauhan[134], Y. Che[113a], S. Chekanov[6], G.A. Chelkov[39,j], B. Chen[169], H. Chen[30], J. Chen[142a], J. Chen[146], M. Chen[127], S. Chen[88], S.J. Chen[113a], X. Chen[142a], X. Chen[15,k], Z. Chen[62], C.L. Cheng[174], H.C. Cheng[64a], S. Cheong[147], A. Cheplakov[39], E. Cherepanova[116], E. Cheu[7], K. Cheung[65], L. Chevalier[136], V. Chiarella[53], G. Chiarelli[74a], G. Chiodini[70a], A.S. Chisholm[21], A. Chitan[28b], M. Chitishvili[167], M.V. Chizhov[39,l], K. Choi[11], Y. Chou[140], E.Y.S. Chow[115], K.L. Chu[173], M.C. Chu[64a], Z. Chubinidze[53], J. Chudoba[132], J.J. Chwastowski[87], D. Cieri[111], K.M. Ciesla[86a], V. Cindro[94], A. Ciocio[18a], F. Cirotto[72a,72b], Z.H. Citron[173], M. Citterio[71a], D.A. Ciubotaru[28b], A. Clark[56], P.J. Clark[52], N. Clarke Hall[97], C. Clarry[159], S.E. Clawson[48], C. Clement[47a,47b], L. Clissa[24b,24a], Y. Coadou[103], M. Cobal[69a,69c], A. Coccaro[57b], R.F. Coelho Barrue[131a], R. Coelho Lopes De Sa[104], S. Coelli[71a], M.M. Cohen[129], L. S. Colangeli[159], B. Cole[42], P. Collado Soto[100], J. Collot[60], M.R. Coluccia[70a], P. Conde Muiño[131a,131g], M.P. Connell[34c], S.H. Connell[34c], E.I. Conroy[127], M. Contreras Cossio[11], F. Conventi[72a,m], A.M. Cooper-Sarkar[127], L. Corazzina[75a,75b], F. A. Corchia[24b,24a], A. Cordeiro Oudot Choi[140], L.D. Corpe[41], M. Corradi[75a,75b], F. Corriveau[105,n], A. Cortes-Gonzalez[157], M.J. Costa[167], F. Costanza[4], D. Costanzo[143], J. Couthures[4], G. Cowan[96], K. Cranmer[174], L. Cremer[49], D. Cremonini[24b,24a], S. Crépé-Renaudin[60], F. Crescioli[128], T. Cresta[73a,73b], M. Cristinziani[145], M. Cristoforetti[78a,78b], E. Critelli[97], G. Crosetti[44b,44a], A. Cueto[100], H. Cui[97], Z. Cui[7], B.M. Cunnett[150], W.R. Cunningham[59], F. Curcio[167], J. R. Curran[52], G. D'amen[30], V. D'Amico[110], M. D'Andrea[57b,57a], G. D'anniballe[74a,74b], S. D'Auria[71a,71b], A. D'Avanzo[72a,72b], L. D'Eramo[41], A. D'Onofrio[72a,72b], M. D'Onofrio[93], M. D'uffizi[102], M.J. Da Cunha Sargedas De Sousa[57b,57a], J.V. Da Fonseca Pinto[82b], C. Da Via[102], W. Dabrowski[86a], T. Dado[37], S. Dahbi[152], T. Dai[107], D. Dal Santo[20], C. Dallapiccola[104], M. Dam[43], J.R. Dandoy[35], D. Dannheim[37], M. Danninger[146], V. Dao[149], G. Darbo[57b], S.J. Das[30], F. Dattola[48], T. Davidek[134], J. Davidson[171], I. Dawson[95], K. De[8], C. De Almeida Rossi[159], R. De Asmundis[72a], N. De Biase[48], S. De Castro[24b,24a], N. De Groot[115], P. de Jong[116], H. De la Torre[117], A. De Maria[113a], A. De Salvo[75a], U. De Sanctis[76a,76b], F. De Santis[70a,70b], A. De Santo[150], J.B. De Vivie De Regie[60], J. Debevc[94], D.V. Dedovich[39], J. Degens[93], A.M. Deiana[45], J. Del Peso[100], L. Delagrange[128], F. Deliot[136], C.M. Delitzsch[49], A. Dell'Acqua[37], L. Dell'Asta[71a,71b], M. Della Pietra[72a,72b], D. Della Volpe[56], M. Delmastro[4], C.C. Delogu[57b,57a], P.A. Delsart[60], S. Demers[176], M. Demichev[39], S.P. Denisov[38], H. Denizli[22a,o], M.G. Depala[93], D. Derendarz[87], F. Derue[128], P. Dervan[93,†], A. M. Desai[1], K. Desch[25], F.A. Di Bello[74a,74b], A. Di Ciaccio[76a,76b], L. Di Ciaccio[4], A. Di Domenico[75a,75b], C. Di Donato[72a,72b], A. Di Girolamo[37], G. Di Gregorio[66], A. Di Luca[78a,78b], B. Di Micco[77a,77b], R. Di Nardo[77a,77b], K.F. Di Petrillo[40], M. Diamantopoulou[35], F.A. Dias[116], M.A. Diaz[138a,138b], A. R. Didenko[39], M. Didenko[167], S.D. Diefenbacher[18a], E.B. Diehl[107], S. Díez Cornell[48], C. Diez Pardos[145], C. Dimitriadi[148], A. Dimitrievska[21], A. Dimri[149], Y. Ding[62], J. Dingfelder[25], T. Dingley[127], I-M. Dinu[28b], S.J. Dittmeier[63b], F. Dittus[37], M. Divisek[134], B. Dixit[93], F. Djama[103], T. Djobava[153b], C. Doglioni[102,99], A. Dohnalova[29a], Z. Dolezal[134], K. Domijan[86a], K.M. Dona[40], M. Donadelli[82d],

JHEP10(2026)219

B. Dong[108], J. Donini[41], J. Dopke[135], A. Doria[72a], N. Dos Santos Fernandes[131a], I.A. Dos Santos Luz[82e], P. Dougan[45], M.T. Dova[91], A.T. Doyle[59], M.P. Drescher[55], E. Dreyer[173], I. Drivas-koulouris[10], M. Drnevich[118], D. Du[62], T.A. du Pree[116], Z. Duan[113a], M. Dubau[4], F. Dubinin[39], M. Dubovsky[29a], E. Duchovni[173], G. Duckeck[110], P. K. Duckett[97], O.A. Ducu[28b], D. Duda[52], A. Dudarev[37], M.M. Dudek[87], E. R. Duden[27], L. Duflot[66], M. Dührssen[37], I. Duminica[28g], A.E. Dumitriu[28b], M. Dunford[63a], A. Duperrin[103], H. Duran Yildiz[3a], A. Durglishvili[153b], G.I. Dyckes[18a], M. Dyndal[86a], B.S. Dziedzic[37], Z.O. Earnshaw[150], G.H. Eberwein[127], B. Eckerova[29a], S. Eggebrecht[55], E. Egidio Purcino De Souza[82e], G. Eigen[17], K. Einsweiler[18a], T. Ekelof[165], P.A. Ekman[99], S. El Farkh[36b], Y. El Ghazali[62], H. El Jarrari[105], A. El Moussaouy[36a], D. Elitez[37], M. Ellert[165], F. Ellinghaus[175], T.A. Elliot[96], J. Elmsheuser[30], M. Elsawy[84b], M. Elsing[37], D. Emeliyanov[135], Y. Enari[83], S. Epari[109], D. Ernani Martins Neto[87], F. Ernst[37], M. Escalier[66], C. Escobar[167], E. Etzion[155], G. Evans[131a,131b], H. Evans[68], L.S. Evans[48], A. Ezhilov[38], S. Ezzarqtouni[36a], F. Fabbri[24b,24a], L. Fabbri[24b,24a], G. Facini[97], V. Fadeyev[137], R.M. Fakhrutdinov[38], D. Fakoudis[101], S. Falciano[75a], L.F. Falda Ulhoa Coelho[27], F. Fallavollita[111], G. Falsetti[44b,44a], J. Faltova[134], C. Fan[166], K. Y. Fan[64b], Y. Fan[14], Y. Fang[14,113c], M. Fanti[71a,71b], M. Faraj[69a,69c], Z. Farazpay[98], A. Farbin[8], A. Farilla[77a], K. Farman[152], J. N. Farr[176], M. S. Farrington[61], S.M. Farrington[135,52], F. Fassi[36e], D. Fassouliotis[9], L. Fayard[66], P. Federic[134], P. Federicova[132], O.L. Fedin[38,j], M. Feickert[174], L. Feligioni[103], D.E. Fellers[18a], C. Feng[141a], Y. Feng[14], Z. Feng[116], B. Fernandez Barbadillo[92], P. Fernandez Martinez[67], M.J.V. Fernoux[103], J. Ferrando[92], A. Ferrari[165], P. Ferrari[116,115], R. Ferrari[73a], D. Ferrere[56], C. Ferretti[107], M. P. Fewell[1], D. Fiacco[75a,75b], F. Fiedler[101], P. Fiedler[133], S. Filimonov[39], M.S. Filip[28b,p], A. Filipčič[94], E.K. Filmer[160a], F. Filthaut[115], M.C.N. Fiolhais[131a,131c,q], L. Fiorini[167], W.C. Fisher[108], T. Fitschen[102], P. M. Fitzhugh[136], I. Fleck[145], P. Fleischmann[107], T. Flick[175], M. Flores[34d,r], L.R. Flores Castillo[64a], M. Foll[126], F.M. Follega[78a,78b], N. Fomin[33], J.H. Foo[159], A. Formica[136], A.C. Forti[102], E. Fortin[37], A.W. Fortman[18a], L. Foster[18a], L. Fountas[9], H. Fox[92], P. Francavilla[74a,74b], S. Francescato[61], S. Franchellucci[56], M. Franchini[24b,24a], S. Franchino[63a], D. Francis[37], L. Franco[48], L. Franconi[48], M. Franklin[61], G. Frattari[27], Y.Y. Frid[155], J. Friend[59], N. Fritzsche[37], A. Froch[56], D. Froidevaux[37], J.A. Frost[135], Y. Fu[108], S. Fuenzalida Garrido[138g], M. Fujimoto[149], K. Y. Fung[64a], E. Furtado De Simas Filho[82e], M. Furukawa[157], M. Fuste Costa[48], J. Fuster[167], A. Gaa[55], A. Gabrielli[24b,24a], A. Gabrielli[159], P. Gadow[37], G. Gagliardi[57b,57a], L.G. Gagnon[18a], S. Gaid[84d], S. Galantzan[155], J. Gallagher[1], E.J. Gallas[127], A.L. Gallen[165], B.J. Gallop[135], K.K. Gan[120], Y. Gao[52], A. Garabaglu[140], F.M. Garay Walls[138a,138b], C. García[167], A. Garcia Alonso[116], A.G. Garcia Caffaro[176], J.E. García Navarro[167], M. A. Garcia Ruiz[23b], M. Garcia-Sciveres[18a], G.L. Gardner[129], R.W. Gardner[40], N. Garelli[162], R.B. Garg[147], J.M. Gargan[33], C.A. Garner[159], C.M. Garvey[34a], V. K. Gassmann[162], G. Gaudio[73a], V. Gautam[13], P. Gauzzi[75a,75b], J. Gavranovic[94], I.L. Gavrilenko[131a], A. Gavrilyuk[38], C. Gay[168], G. Gaycken[124], A. Gekow[120], C. Gemme[57b], M.H. Genest[60], A. D. Gentry[114], S. George[96], T. Geralis[46], A. A. Gerwin[121], P. Gessinger-Befurt[37], M. Ghani[171], K. Ghorbanian[95], A. Ghosal[145], A. Ghosh[163], A. Ghosh[7], B. Giacobbe[24b],

JHEP10(2026)219

S. Giagu[75a,75b], T. Giani[116], A. Giannini[62], S.M. Gibson[96], D.T. Gil[86b], A.K. Gilbert[86a], B.J. Gilbert[42], D. Gillberg[35], G. Gilles[116], D.M. Gingrich[2,s], M.P. Giordani[69a,69c], P.F. Giraud[136], G. Giugliarelli[69a,69c], D. Giugni[71a], F. Giuli[76a,76b], I. Gkialas[9,t], L.K. Gladilin[38], C. Glasman[100], M. Glazewska[20], R. M. Gleason[163], G. Glemža[48], M. Glisic[124], I. Gnesi[44b], Y. Go[30], M. Goblirsch-Kolb[37], B. Gocke[49], D. Godin[109], B. Gokturk[22a], S. Goldfarb[106], T. Golling[56], M.G.D. Gololo[34c], A. Golub[140], D. Golubkov[38], J.P. Gombas[108], A. Gomes[131a,131b], G. Gomes Da Silva[145], A.J. Gomez Delegido[37], R. Gonçalo[131a], A. Gongadze[153c], F. Gonnella[21], J.L. Gonski[147], R.Y. González Andana[52], S. González de la Hoz[167], M. V. Gonzalez Rodrigues[48], R. Gonzalez Suarez[165], S. Gonzalez-Sevilla[56], L. Goossens[37], B. Gorini[37], E. Gorini[70a,70b], A. Gorišek[94], T.C. Gosart[129], A.T. Goshaw[51], M.I. Gostkin[39], S. Goswami[122], C.A. Gottardo[37], S. A. Gotz[110], M. Gouighri[36b], A.G. Goussiou[140], N. Govender[34c], R. P. Grabarczyk[127], I. Grabowska-Bold[86a], K. Graham[35], E. Gramstad[126], S. Grancagnolo[70a,70b], C.M. Grant[1], P.M. Gravila[28f], F.G. Gravili[70a,70b], H.M. Gray[18a], M. Greco[111], M. J. Green[1], C. Grefe[25], A. S. Grefsrud[17], I.M. Gregor[48], K.T. Greif[163], P. Grenier[147], S.G. Grewe[111], K. Grimm[32], S. Grinstein[13,u], E. Gross[173], J. Grosse-Knetter[55], L.H. Grossman[18b], L. Guan[107], G. Guerrieri[37], R. Guevara[126], R. Gugel[101], J.A.M. Guhit[107], A. Guida[19], E. Guilloton[171], S. Guindon[37], F. Guo[14,113c], J. Guo[142a], L. Guo[48], L. Guo[113b,v], Y. Guo[107], Y. Guo[42], A. Gupta[49], R. Gupta[130], S. Gupta[27], S. Gurbuz[25], S.S. Gurdasani[48], G. Gustavino[75a,75b], P. Gutierrez[121], L.F. Gutierrez Zagazeta[129], M. Gutsche[50], C. Gutschow[97], C. Gwenlan[127], C.B. Gwilliam[93], E.S. Haaland[126], A. Haas[118], M. Habedank[59], C. Haber[18a], H.K. Hadavand[8], A. Haddad[41], A. Hadef[50], A.I. Hagan[92], J. J. Hahn[145], E.H. Haines[97], M. Haleem[170], J. Haley[122], G.D. Hallewell[103], J.A. Hallford[48], K. Hamano[169], H. Hamdaoui[165], M. Hamer[25], S. E. D. Hammoud[66], E.J. Hampshire[96], L. Han[113a], L. Han[62], S. Han[14], K. Hanagaki[83], M. Hance[137], D.A. Hangal[42], H. Hanif[146], M.D. Hank[129], J.B. Hansen[43], P.H. Hansen[43], T. Harenberg[175], S. Harkusha[177], M.L. Harris[104], Y.T. Harris[25], J. Harrison[13], P.F. Harrison[171], M. L. E. Hart[97], N.M. Hartman[111], N.M. Hartmann[110], R. Z. Hasan[96,135], Y. Hasegawa[144], D. Hashimoto[112], F. Haslbeck[127], S. Hassan[17], R. Hauser[108], M. Haviernik[134], C.M. Hawkes[21], R.J. Hawkings[37], Y. Hayashi[157], D. Hayden[108], R.L. Hayes[116], C.P. Hays[127], J.M. Hays[95], H.S. Hayward[93], M. He[14,113c], Y. He[48], Y. He[97], N.B. Heatley[95], V. Hedberg[99], J. Heilman[35], S. Heim[48], T. Heim[18a], J.J. Heinrich[124], L. Heinrich[111], J. Hejbal[132], M. Helbig[50], A. Held[174], S. Hellesund[17], C.M. Helling[168], H. Herde[99], Y. Hernández Jiménez[149], L.M. Herrmann[25], G. Herten[54], R. Hertenberger[110], L. Hervas[37], M.E. Hesping[101], N.P. Hessey[160a], J. Hessler[111], M. Hidaoui[36b], N. Hidic[134], E. Hill[159], T. S. Hillersoy[17], S.J. Hillier[21], J.R. Hinds[108], F. Hinterkeuser[25], M. Hirose[125], S. Hirose[161], D. Hirschbuehl[175], T.G. Hitchings[102], B. Hiti[94], J. Hobbs[149], R. Hobincu[28e], N. Hod[173], A.M. Hodges[166], M.C. Hodgkinson[143], B.H. Hodkinson[127], A. Hoecker[37], D. D. Hofer[107], J. Hofer[167], J. Hofner[101], M. Holzbock[37], L.B.A.H. Hommels[33], V. Homsak[127], J. J. Hong[68], T.M. Hong[130], B.H. Hooberman[166], W.H. Hopkins[6], M. C. Hoppesch[166], Y. Horii[112], M. E. Horstmann[111], S. Hou[152], M. R. Housenga[166], J. Howarth[59], J. Hoya[6], M. Hrabovsky[123], T. Hryn'ova[4], P.J. Hsu[65],

JHEP10(2026)219

S.-C. Hsu[140], T. Hsu[66], M. Hu[18a], Q. Hu[62], S. Huang[33], X. Huang[14,113c], Y. Huang[134], Y. Huang[113b], Y. Huang[14], Z. Huang[66], Z. Hubacek[133], F. Huegging[25], T.B. Huffman[127], M. Hufnagel Maranha De Faria[82a], C. A. Hugli[48], M. Huhtinen[37], S.K. Huiberts[126], R. Hulsken[105], C. E. Hultquist[18a], D.L. Humphreys[104], N. Huseynov[12], J. Huston[108], B. Huth[37], J. Huth[61], L. Huth[48], R. Hyneman[7], G. Iacobucci[56], G. Iakovidis[30], L. Iconomidou-Fayard[66], J. P. Iddon[37], P. Iengo[72a,72b], Y. Iiyama[157], T. Iizawa[157], Y. Ikegami[83], D. Iliadis[156], N. Ilic[159], H. Imam[36a], G. Inacio Goncalves[82d], S. A. Infante Cabanas[138c], T. Ingebretsen Carlson[47a,47b], J. M. Inglis[95], G. Introzzi[73a,73b], M. Iodice[77a], V. Ippolito[75a,75b], R. K. Irwin[93], M. Ishino[157], W. Islam[174], C. Issever[19], S. Istin[22a,w], K. Itabashi[125], H. Ito[172], R. Iuppa[78a,78b], A. Ivina[173], S. Izumiyama[112], V. Izzo[72a], P. Jacka[133], P. Jackson[1], P. R. Jacobson[51], P. Jain[48], K. Jakobs[54], T. Jakoubek[173], J. Jamieson[59], W. Jang[157], S. Jankovych[116], M. Javurkova[104], P. Jawahar[102], L. Jeanty[124], J. Jejelava[153a,x], P. Jenni[54,y], C.E. Jessiman[35], H. Jia[168], J. Jia[149], X. Jia[111,113c], Z. Jia[113a], C. Jiang[52], Q. Jiang[64b], S. Jiggins[48], M. Jimenez Ortega[167], J. Jimenez Pena[13], S. Jin[113a], A. Jinaru[28b], O. Jinnouchi[139], P. Johansson[143], K.A. Johns[7], J.W. Johnson[137], F. A. Jolly[48], D.M. Jones[150], E. Jones[48], K.S. Jones[8], P. Jones[33], R.W.L. Jones[92], T.J. Jones[93], H.L. Joos[55], R. Joshi[120], J. Jovicevic[16], X. Ju[18a], J.J. Junggeburth[37], T. Junkermann[63a], A. Juste Rozas[13,u], M.K. Juzek[87], S. Kabana[138f], A. Kaczmarska[87], S. A. Kadir[147], M. Kado[111], H. Kagan[120], M. Kagan[147], A. Kahn[129], C. Kahra[101], T. Kaji[157], E. Kajomovitz[154], N. Kakati[173], N. Kakoty[13], S. Kandel[8], N. Kanellos[10], N.J. Kang[137], D. Kar[34j,†], E. Karentzos[25], K. Karki[8], O. Karkout[116], S.N. Karpov[39], Z.M. Karpova[39], V. Kartvelishvili[92,153b], A.N. Karyukhin[38], E. Kasimi[156], J. Katzy[48], S. Kaur[35], K. Kawade[144], M.P. Kawale[121], C. Kawamoto[88], E.F. Kay[37], S. Kazakos[108], K. Kazakova[103], V.F. Kazanin[38], J.M. Keaveney[34a], R. Keeler[169], G.V. Kehris[61], J.S. Keller[35], J. M. Kelly[169], J.J. Kempster[150], O. Kepka[132], J. Kerr[160b], B.P. Kerridge[135], B.P. Kerševan[94], L. Keszeghova[29a], R. A. Khan[130], A. Khanov[122], A.G. Kharlamov[38], T. Kharlamova[38], M. Kholodenko[131a], T.J. Khoo[19], G. Khoriauli[170], Y. Khoulaki[36a], Y.A.R. Khwaira[128], D. Kim[6], D.W. Kim[18b], Y.K. Kim[40], N. Kimura[97], M.K. Kingston[55], C. Kirfel[25], F. Kirfel[25], J. Kirk[135], A.E. Kiryunin[111], S. Kita[161], O. Kivernyk[25], M. Klassen[162], C. Klein[35], L. Klein[170], M.H. Klein[45], S.B. Klein[56], U. Klein[93], A. Klimentov[30], P. Kluit[116], S. Kluth[111], E. Kneringer[79], T.M. Knight[159], A. Knue[49], M. Kobel[50], D. Kobylianskii[173], S.F. Koch[37], M. Kocian[147], P. Kodyš[134], D.M. Koeck[124], T. Koffas[35], O. Kolay[50], I. Koletsou[4], T. Komarek[87], K. Köneke[55], A.X.Y. Kong[1], T. Kono[119], N. Konstantinidis[97], P. Kontaxakis[56], B. Konya[99], R. Kopeliansky[42], S. Koperny[86a], R. Koppenhofer[54], K. Korcyl[87], K. Kordas[156,z], A. Korn[97], S. Korn[55], I. Korolkov[13], N. Korotkova[38], B. Kortman[116], O. Kortner[111], S. Kortner[111], W.H. Kostecka[117], M. Kostov[29a], V.V. Kostyukhin[145], A. Kotsokechagia[37], A. Kotwal[51], A. Koulouris[37], A. Kourkoumeli-Charalampidi[73a,73b], E. Kourlitis[111], O. Kovanda[124], R. Kowalewski[169], W. Kozanecki[124], A.S. Kozhin[38], V.A. Kramarenko[38], G. Kramberger[94], P. Kramer[25], M.W. Krasny[128], A. Krasznahorkay[104], A. C. Kraus[117], J.W. Kraus[175], J.A. Kremer[48], N. B. Krengel[145], T. Kresse[50], L. Kretschmann[175], J. Kretzschmar[93], P. Krieger[159], K. Krizka[21], K. Kroeninger[49], H. Kroha[111], J. Kroll[132],

JHEP10(2026)219

J. Kroll[129], K.S. Krowpman[108], U. Kruchonak[39], H. Krüger[25], N. Krumnack[80], M.C. Kruse[51], O. Kuchinskaia[39], S. Kuday[3a], S. Kuehn[37], R. Kuesters[54], T. Kuhl[48], V. Kukhtin[39], Y. Kulchitsky[39], S. Kuleshov[138d,138b], J. Kull[1], E. V. Kumar[110], M. Kumar[34j], N. Kumari[48], P. Kumari[160b], A. Kupco[132], A. Kupich[38], O. Kuprash[54], H. Kurashige[85], L.L. Kurchaninov[160a], O. Kurdysh[4], A. Kurova[38], M. Kuze[139], A.K. Kvam[104], J. Kvita[123], N.G. Kyriacou[140], M. Laassiri[30], C. Lacasta[167], F. Lacava[75a,75b], H. Lacker[19], D. Lacour[128], E. Ladygin[39], A. Lafarge[41], B. Laforge[128], T. Lagouri[176], F.Z. Lahbabi[36a], S. Lai[55,37], W. S. Lai[97], I.K. Lakomiec[55], J.E. Lambert[169], S. Lammers[68], W. Lampl[7], C. Lampoudis[156], G. Lamprinoudis[170], A.N. Lancaster[117], U. Landgraf[54], M.P.J. Landon[95], V.S. Lang[54], A.J. Lankford[163], F. Lanni[37], C. S. Lantz[166], K. Lantzsch[25], A. Lanza[73a], M. Lanzac Berrocal[167], T. Lari[71a], D. Larsen[17], L. Larson[11], F. Lasagni Manghi[24b], M. Lassnig[37], S.D. Lawlor[143], R. Lazaridou[163], M. Lazzaroni[71a,71b], E. T. T. Le[163], H. D. M. Le[108], E.M. Le Boulicaut[176], L.T. Le Pottier[18a], B. Leban[24b,24a], F. Ledroit-Guillon[60], T.F. Lee[160b], L.L. Leeuw[34h], M. Lefebvre[169], C. Leggett[18a], G. Lehmann Miotto[37], M. Leigh[56], W.A. Leight[104], W. Leinonen[115], A. Leisos[156,aa], M.A.L. Leite[82c], C.E. Leitgeb[19], R. Leitner[134], K.J.C. Leney[45], T. Lenz[25], S. Leone[74a], C. Leonidopoulos[52], A. Leopold[148], J. LePage-Bourbonnais[35], R. Les[108], C.G. Lester[33], M. Levchenko[38], J. Levêque[4], L.J. Levinson[173], G. Levrini[24b,24a], M.P. Lewicki[87], C. Lewis[140], D.J. Lewis[4], L. Lewitt[143], A. Li[30], B. Li[141a], C-Q. Li[111], C. Li[107], H. Li[141a], H. Li[102], H. Li[15], H. Li[62], H. Li[141a], J. Li[142a], L. Li[142a], R. Li[176], S. Li[142b,142a], T. Li[5], Y. Li[14], Z. Li[14,113c], Z. Li[62], S. Liang[14,113c], Z. Liang[14], M. Liberatore[136], B. Liberti[76a], G. B. Libotte[82d], K. Lie[64c], J. Lieber Marin[82e], H. Lien[68], H. Lin[107], S. F. Lin[149], L. Linden[110], R.E. Lindley[7], J.H. Lindon[37], J. Ling[61], E. Lipeles[129], A. Lipniacka[17], A. Lister[168], J.D. Little[68], B. Liu[14], B.X. Liu[113b], D. Liu[154], D. Liu[137], E. H. L. Liu[21], H. Liu[113b], J.K.K. Liu[118], K. Liu[142b], K. Liu[142b], M. Liu[62], M.Y. Liu[62], P. Liu[141a], Q. Liu[147], S. Liu[149], X. Liu[141a], Y. Liu[113b,113c], Y. Liu[166], Y.L. Liu[141a], Y.W. Liu[62], Z. Liu[66,ab], S.L. Lloyd[95], E.M. Lobodzinska[48], P. Loch[7], E. Lodhi[159], K. Lohwasser[143], E. Loiacono[48], J. D. Lomas[21], I. Longarini[163], R. Longo[166], A. Lopez Solis[13], N.A. Lopez-canelas[7], N. Lorenzo Martinez[4], A.M. Lory[110], M. Losada[84b], G. Löschcke Centeno[4], X. Lou[47a,47b], X. Lou[14,113c], P.A. Love[92], M. Lu[66], S. Lu[129], Y.J. Lu[152], H.J. Lubatti[140], C. Luci[75a,75b], F.L. Lucio Alves[113a], F. Luehring[68], B. S. Lunday[129], O. Lundberg[148], J. Lunde[37], N.A. Luongo[6], M.S. Lutz[169], A.B. Lux[26], D. Lynn[30], R. Lysak[132], V. Lysenko[133], E. Lytken[99], V. Lyubushkin[39], T. Lyubushkina[39], M.M. Lyukova[149], H. Ma[30], K. Ma[62], L.L. Ma[141a], W. Ma[62], Y. Ma[122], J.C. MacDonald[101], B. Maček[94], P.C. Machado De Abreu Farias[82e], D. Macina[37], R. Madar[41], T. Madula[97], J. Maeda[85], T. Maeno[30], P.T. Mafa[34f], H. Maguire[143], M. Maheshwari[33], V. Maiboroda[66], A. Maio[131a,131b,131d], K. Maj[86a], O. Majersky[48], S. Majewski[124], R. Makhmanazarov[38], N. Makovec[66], V. Maksimovic[16], B. Malaescu[128], J. Malamant[126], Pa. Malecki[87], V.P. Maleev[38], F. Malek[60,ac], M. Mali[94], D. Malito[96], A. Maloizel[5], A. Malvezzi Lopes[82d], S. Malyukov[39], J. Mamuzic[94], G. Mancini[53], M. N. Mancini[27], G. Manco[73a,73b], S.S. Mandarry[150], I. Mandić[94], L. Manhaes de Andrade Filho[82a], I.M. Maniatis[173], J. Manjarres Ramos[90], D.C. Mankad[173],

JHEP10(2026)219

A. Mann[110], T. Manoussos[37], M.N. Mantinan[40], S. Manzoni[37], L. Mao[142a], X. Mapekula[34c], A. Marantis[156], R.R. Marcelo Gregorio[95], G. Marchiori[5], C. Marcon[71a], E. Maricic[16], M. Marinescu[48], S. Marium[48], M. Marjanovic[121], A. Markhoos[54], M. Markovitch[66], M. K. Maroun[104], M. C. Marr[146], G. T. Marsden[102], E.J. Marshall[92], Z. Marshall[18a], S. Marti-Garcia[167], J. Martin[97], T.A. Martin[135], V.J. Martin[52], B. Martin dit Latour[17], S. Martin-Haugh[135], L. Martinelli[75a,75b], P. Martinez Agullo[167], V.I. Martinez Outschoorn[104], P. Martinez Suarez[37], G. Martinovicova[134], V.S. Martoiu[28b], A.C. Martyniuk[97], A. Marzin[37], D. Mascione[78a,78b], L. Masetti[101], J. Masik[102], A.L. Maslennikov[39], S.L. Mason[42], P. Massarotti[72a,72b], P. Mastrandrea[74a,74b], A. Mastroberardino[44b,44a], T. Masubuchi[125], T.T. Mathew[124], J. Matousek[134], D.M. Mattern[49], K. Mauer[48], J. Maurer[28b], T. Maurin[59], A.J. Maury[66], C. Mavungu Tsava[103], D.A. Maximov[38], A. E. May[102], E. Mayer[41], R. Mazini[34j], S.M. Mazza[137], E. Mazzeo[37], J.P. Mc Gowan[169], S.P. Mc Kee[107], C.A. Mc Lean[6], C.C. McCracken[168], E.F. McDonald[106], L. F. Mcelhinney[92], J.A. Mcfayden[150], R.P. McGovern[129], R.P. Mckenzie[34j], D.J. Mclaughlin[97], S.J. McMahon[135], C.M. Mcpartland[93], R.A. McPherson[169,n], S. Mehlhase[110], A. Mehta[93], D. Melini[167], B.R. Mellado Garcia[34j], A.H. Melo[55], F. Meloni[48], A.M. Mendes Jacques Da Costa[102], L. Meng[92], S. Menke[111], M. Mentink[37], E. Meoni[44b,44a], G. Mercado[117], S. Merianos[156], C. Merlassino[69a,69c], C. Meroni[71a,71b], J. Metcalfe[6], A.S. Mete[6], E. Meuser[101], C. Meyer[68], J-P. Meyer[136], Y. Miao[113a], R.P. Middleton[135], M. Mihovilovic[66], L. Mijović[52], G. Mikenberg[173], M. Mikestikova[132], M. Mikuž[94], H. Mildner[101], A. Milic[37], D.W. Miller[40], E. H. Miller[147], A. Milov[173], D.A. Milstead[47a,47b], T. Min[113a], A.A. Minaenko[38], I.A. Minashvili[153b], A.I. Mincer[118], B. Mindur[86a], M. Mineev[39], Y. Mino[88], L.M. Mir[13], M. Miralles Lopez[59], M. Mironova[18a], M. Missio[41], A. Mitra[171], V.A. Mitsou[167], Y. Mitsumori[112], P.S. Miyagawa[95], T. Mkrtchyan[37], M. Mlinarevic[97], T. Mlinarevic[97], M. Mlynarikova[134], L. Mlynarska[86a], C. Mo[142a], S. Mobius[20], M. H. Mohamed Farook[114], S. Mohapatra[42], M.F. Mohd Soberi[52], S. Mohiuddin[122], G. Mokgatitswane[34j], L. Moleri[173], U. Molinatti[127], L.G. Mollier[20], B. Mondal[132], S. Mondal[134], K. Mönig[48], E. Monnier[103], L. Monsonis Romero[167], A. Montella[47a,47b], M. Montella[120], F. Montereali[77a,77b], F. Monticelli[91], S. Monzani[69a,69c], A. Morancho Tarda[43], N. Morange[66], M. Moreno Llácer[167], C. Moreno Martinez[56], J.M. Moreno Perez[23b], P. Morettini[57b], S. Morgenstern[37], M. Morii[61], M. Morinaga[157], F. Morodei[75a,75b], P. Moschovakos[37], B. Moser[54], M. Mosidze[153b], T. Moskalets[45], P. Moskvitina[115], J. Moss[32], T. Motta Quirino[82d], A. Moussa[36d], Y. Moyal[173], H. Moyano Gomez[13], E.J.W. Moyse[104], T.G. Mroz[87], S. Muanza[103], M. Mucha[25], J. Mueller[130], G.A. Mullier[165], A.J. Mullin[33], J.J. Mullin[51], A.C. Mullins[45], A.E. Mulski[61], D.P. Mungo[159], D. Munoz Perez[167], F.J. Munoz Sanchez[102], W.J. Murray[171,135], E. Musajan[62], M. Muškinja[94], C. Mwewa[48], A.G. Myagkov[38,j], A.J. Myers[8], G. Myers[107], M. Myska[133], B.P. Nachman[147], K. Nagai[127], K. Nagano[83], R. Nagasaka[157], J.L. Nagle[30,ad], E. Nagy[103], A.M. Nairz[37], Y. Nakahama[83], K. Nakamura[83], K. Nakkalil[5], A. Nandi[63b], H. Nanjo[125], E.A. Narayanan[45], Y. Narukawa[157], I. Naryshkin[38], L. Nasella[71a,71b], S. Nasri[84c], C. Nass[25], G. Navarro[23a], A. Nayaz[19], P.Y. Nechaeva[38], S. Nechaeva[24b,24a], F. Nechansky[132], L. Nedic[127], A. Negri[73a,73b],

JHEP10(2026)219

M. Negrini[24b], C. Nellist[116], C. Nelson[105], K. Nelson[107], S. Nemecek[132], M. Nessi[37,ae], M.S. Neubauer[166], J. Newell[93], P.R. Newman[21], Y.W.Y. Ng[166], B. Ngair[84b], H.D.N. Nguyen[109], J.D. Nichols[121], R.B. Nickerson[127], R. Nicolaidou[136], J. Nielsen[137], M. Niemeyer[55], J. Niermann[37], N. Nikiforou[37], V. Nikolaenko[38,j], I. Nikolic-Audit[128], P. Nilsson[30], G. Ninio[155], A. Nisati[75a], R. Nisius[111], N. Nitika[173], E.K. Nkadimeng[34b], T. Nobe[157], D. Noll[147], T. Nommensen[151], M.B. Norfolk[143], B.J. Norman[35], L.C. Nosler[18a], M. Noury[36a], J. Novak[94], T. Novak[94], P. Novotny[173], R. Novotny[133], L. Nozka[123], K. Ntekas[163], D. Ntounis[147], N.M.J. Nunes De Moura Junior[82b], A.P. O'Neill[20], J. Ocariz[128], I. Ochoa[131a], A. Odella Rodriguez[13], S. Oerdek[48], J.T. Offermann[40], A. Ogrodnik[87], A. Oh[102], C.C. Ohm[148], H. Oide[83], M.L. Ojeda[37], Y. Okumura[157], L.F. Oleiro Seabra[131a], I. Oleksiyuk[56], G. Oliveira Correa[13], D. Oliveira Damazio[30], J.L. Oliver[1], R. Omar[68], Ö.O. Öncel[54], Y. Onoda[139], A. Onofre[131a,131e,af], P.U.E. Onyisi[11], M.J. Oreglia[40], D. Orestano[77a,77b], R. Orlandini[77a,77b], R.S. Orr[159], L.M. Osojnak[42], Y. Osumi[112], G. Otero y Garzón[31], H. Otono[89], M. Ouchrif[36d], F. Ould-Saada[126], T. Ovsiannikova[140], M. Owen[59], R.E. Owen[135], V.E. Ozcan[22a], F. Ozturk[87], N. Ozturk[8], S. Ozturk[81], H.A. Pacey[127], K. Pachal[160a], A. Pacheco Pages[13], C. Padilla Aranda[13], G. Padovano[75a,75b], S. Pagan Griso[18a], J. Pampel[25], J. Pan[176], D.K. Panchal[11], C.E. Pandini[60], J.G. Panduro Vazquez[135], H.D. Pandya[1], H. Pang[136], P. Pani[48], G. Panizzo[69a,69c], L. Panwar[128], L. Paolozzi[56], S. Parajuli[166], A. Paramonov[6], C. Paraskevopoulos[53], D. Paredes Hernandez[64b], S.R. Paredes Saenz[52], A. Pareti[73a,73b], K.R. Park[42], T.H. Park[111], F. Parodi[57b,57a], J.A. Parsons[42], U. Parzefall[54], B. Pascual Dias[41], L. Pascual Dominguez[100], E. Pasqualucci[75a], S. Passaggio[57b], F. Pastore[96], P. Patel[87], U.M. Patel[51], J.R. Pater[102], T. Pauly[37], F. Pauwels[134], C.I. Pazos[162], M. Pedersen[126], R. Pedro[131a], S.V. Peleganchuk[38], O. Penc[132], S. Peng[15], G. D. Penn[176], K.E. Penski[110], M. Penzin[38], B.S. Peralva[82d], A.P. Pereira Peixoto[140], L. Pereira Sanchez[147], D.V. Perepelitsa[30,ad], G. Perera[104], E. Perez Codina[37], M. Perganti[10], H. Pernegger[37], S. Perrella[75a,75b], K. Peters[48], R.F.Y. Peters[102], B.A. Petersen[37], T.C. Petersen[43], E. Petit[103], V. Petousis[133], A. R. Petri[71a,71b], T. Petru[134], M. Pettee[18a], A. Petukhov[81], K. Petukhova[37], R. Pezoa[138g], L. Pezzotti[24b,24a], G. Pezzullo[176], L. Pfaffenbichler[37], A. J. Pfleger[79], T. Pham[106], T.M. Pham[174], P.W. Phillips[135], G. Piacquadio[149], E. Pianori[18a], F. Piazza[124], R. Piegaia[31], D. Pietreanu[28b], A.D. Pilkington[102], M. Pinamonti[69a,69c], J.L. Pinfold[2], G. Pinheiro Matos[42], B.C. Pinheiro Pereira[131a], J. Pinol Bel[13], A. E. Pinto Pinoargote[128], L. Pintucci[69a,69c], K. M. Piper[150], A. Pirttikoski[56], D.A. Pizzi[35], L. Pizzimento[64b], A. Plebani[33], M.-A. Pleier[30], V. Pleskot[134], E. Plotnikova[39], G. Poddar[95], R. Poettgen[99], L. Poggioli[128], S. Polacek[134], G. Polesello[73a], A. Poley[146], A. Polini[24b], C.S. Pollard[171], Z.B. Pollock[120], E. Pompa Pacchi[121], N. I. Pond[97], D. Ponomarenko[68], L. Pontecorvo[37], S. Popa[28a], G.A. Popeneciu[28d], A. Poreba[37], D.M. Portillo Quintero[160a], S. Pospisil[133], M. A. Postill[143], P. Postolache[28c], K. Potamianos[171], P.A. Potepa[86a], I.N. Potrap[39], C.J. Potter[33], H. Potti[151], J. Poveda[167], M.E. Pozo Astigarraga[37], R. Pozzi[37], A. Prades Ibanez[76a,76b], S.R. Pradhan[143], J. Pretel[169], D. Price[102], M. Primavera[70a], L. Primomo[69a,69c], M.A. Principe Martin[100], R. Privara[123], T. Procter[86b], M.L. Proffitt[140],

JHEP10(2026)219

N. Proklova[129], K. Prokofiev[64c], G. Proto[111], J. Proudfoot[6], M. Przybycien[86a], W.W. Przygoda[86b], A. Psallidas[46], J.E. Puddefoot[143], D. Pudzha[53], H. I. Purnell[1], D. Pyatiizbyantseva[115], J. Qian[107], R. Qian[108], D. Qichen[127], Y. Qin[13], T. Qiu[52], A. Quadt[55], M. Queitsch-Maitland[102], G. Quetant[56], R.P. Quinn[168], G. Rabanal Bolanos[61], D. Rafanoharana[111], F. Raffaeli[76a,76b], J.L. Rainbolt[40], S. Rajagopalan[30], E. Ramakoti[39], L. Rambelli[57b,57a], I.A. Ramirez-Berend[35], K. Ran[107,113c], D. S. Rankin[129], N.P. Rapheeha[34j], H. Rasheed[28b], A. Rastogi[18a], S. Rave[101], S. Ravera[57b,57a], B. Ravina[37], I. Ravinovich[173], M. Raymond[37], A.L. Read[126], N.P. Readioff[143], D.M. Rebuzzi[73a,73b], A. S. Reed[59], K. Reeves[27], D. Reikher[37], A. Rej[49], C. Rembser[37], H. Ren[62], M. Renda[28b], F. Renner[48], A.G. Rennie[59], M. Repik[56], A.L. Rescia[57b,57a], S. Resconi[71a], M. Ressegotti[57b], S. Rettie[116], W.F. Rettie[35], M. M. Revering[33], O.L. Rezanova[39], P. Reznicek[134], H. Riani[36d], N. Ribaric[51], B. Ricci[69a,69c], E. Ricci[78a,78b], R. Richter[111], S. Richter[47a,47b], E. Richter-Was[86b], M. Ridel[128], S. Ridouani[36d], P. Rieck[118], P. Riedler[37], E.M. Riefel[47a,47b], J. O. Rieger[116], M. Rimoldi[34c], L. Rinaldi[24b,24a], P. Rincke[165,55], G. Ripellino[165], I. Riu[13], J.C. Rivera Vergara[169], F. Rizatdinova[122], E. Rizvi[95], B.R. Roberts[40], S.S. Roberts[137], D. Robinson[33], A. Robson[59], A. Rocchi[76a,76b], C. Roda[74a,74b], F.A. Rodriguez[117], S. Rodriguez Bosca[37], Y. Rodriguez Garcia[23a], A.M. Rodríguez Vera[117], S. Roe[37], J.T. Roemer[37], O. Røhne[126], R.A. Rojas[37], C.P.A. Roland[128], A. Romaniouk[79], E. Romano[73a,73b], M. Romano[24b], A.C. Romero Hernandez[166], N. Rompotis[93], L. Roos[128], S. Rosati[75a], B.J. Rosser[40], E. Rossi[127], E. Rossi[72a,72b], L.P. Rossi[61], L. Rossini[54], R. Rosten[120], M. Rotaru[28b], R. Roth[37], D. Rousseau[66], D. Rousso[48], S. Roy-Garand[159], A. Rozanov[103], Z. M. A. Rozario[59], Y. Rozen[154], A. Rubio Jimenez[167], V.H. Ruelas Rivera[19], T.A. Ruggeri[1], A. Ruggiero[127], A. Ruiz-Martinez[167], A. Rummler[37], G.B. Rupnik Boero[37], Z. Rurikova[54], N.A. Rusakovich[39], S. Ruscelli[49], H.L. Russell[169], G. Russo[75a,75b], J.P. Rutherfoord[7], S. Rutherford Colmenares[118], M. Rybar[134], P. Rybczynski[86a], A. Ryzhov[45], F. Safai Tehrani[75a], S. Saha[1], B. Sahoo[173], A. Saibel[167], B. T. Saifuddin[121], M. Saimpert[136], G.T. Saito[82c], M. Saito[157], T. Saito[157], A. Sala[71a,71b], A. Salnikov[147], J. Salt[167], A. Salvador Salas[155], F. Salvatore[150], A. Salzburger[37], D. Sammel[54], E. Sampson[92], D. Sampsonidis[156,z], D. Sampsonidou[124], M.A.A. Samy[59], J. Sánchez[167], V. Sanchez Sebastian[167], H. Sandaker[126], C.O. Sander[48], J.A. Sandesara[174], M. Sandhoff[175], C. Sandoval[23b], L. Sanfilippo[63a], D.P.C. Sankey[135], T. Sano[88], A. Sansoni[53], M. Santana Queiroz[18b], L. Santi[37], C. Santoni[41], H. Santos[131a,131b], E. Sanzani[24b,24a], K.A. Saoucha[84d], J.G. Saraiva[131a,131d], J. Sardain[7], O. Sasaki[83], K. Sato[161], C. Sauer[37], E. Sauvan[4], P. Savard[159,s], R. Sawada[157], C. Sawyer[135], L. Sawyer[98], A. M. Sayed[27], C. Sbarra[24b], A. Sbrizzi[24b,24a], T. Scanlon[97], J. Schaarschmidt[140], U. Schäfer[101], A.C. Schaffer[66,45], D. Schaile[110], R.D. Schamberger[149], C. Scharf[19], M.M. Schefer[20], V.A. Schegelsky[38], D. Scheirich[134], M. Schernau[138f], C. Scheulen[56], C. Schiavi[57b,57a], M. Schioppa[44b,44a], B. Schlag[147], S. Schlenker[37], J. Schmeing[175], E. Schmidt[111], M. A. Schmidt[175], K. Schmieden[25], C. Schmitt[101], N. Schmitt[101], S. Schmitt[48], N.A. Schneider[110], L. Schoeffel[136], A. Schoening[63b], P.G. Scholer[35], E. Schopf[145], M. Schott[25], S. Schramm[56], T. Schroer[56], H-C. Schultz-Coulon[63a], M. Schumacher[54], B.A. Schumm[137], Ph. Schune[136],

JHEP10(2026)219

H.R. Schwartz[7], A. Schwartzman[147], T.A. Schwarz[107], Ph. Schwemling[136], R. Schwienhorst[108], F.G. Sciacca[20], A. Sciandra[30], G. Sciolla[27], S. A. Scoville[130], F. Scuri[74a], C.D. Sebastiani[37], K. Sedlaczek[117], S.C. Seidel[114], B.D. Seidlitz[42], C. Seitz[48], J.M. Seixas[82b], G. Sekhniaidze[72a], L. Selem[128], N. Semprini-Cesari[24b,24a], A. Semushin[177], D. Sengupta[56], V. Senthilkumar[167], L. Serin[66], M. Sessa[72a,72b], H. Severini[121], F. Sforza[57b,57a], A. Sfyrla[56], Q. Sha[14], H. Shaddix[117], A.H. Shah[33], R. Shaheen[148], J.D. Shahinian[129], M. Shamim[37], L.Y. Shan[14], M. Shapiro[18a], A. Sharma[37], A.S. Sharma[168], P. Sharma[30], P.B. Shatalov[38], K. Shaw[150], S.M. Shaw[102], Q. Shen[14], D.J. Sheppard[146], P. Sherwood[97], L. Shi[97], X. Shi[14], S. Shimizu[83], I.P.J. Shipsey[127,†], S. Shirabe[89], M. Shiyakova[39,ag], M.J. Shochet[40], D.R. Shope[126], B. Shrestha[121], S. Shrestha[120,ah], I. Shreyber[39], M.J. Shroff[105], P. Sicho[132], A.M. Sickles[166], E. Sideras Haddad[34j,164], A. C. Sidley[116], A. Sidoti[24b], F. Siegert[50], Dj. Sijacki[16], F. Sili[62], J.M. Silva[52], I. Silva Ferreira[82b], M.V. Silva Oliveira[30], S.B. Silverstein[47a], S. Simion[66], R. Simoniello[37], E.L. Simpson[102], H. Simpson[150], L.R. Simpson[6], S. Simsek[81], S. Sindhu[55], S. Singh[30], S. N. Singh[27], S. Sinha[48], S. Sinha[102], M. Sioli[24b,24a], K. Sioulas[9], I. Siral[37], E. Sitnikova[48], J. Sjölin[47a,47b], A. Skaf[55], E. Skorda[21], P. Skubic[121], M. Slawinska[87], I. Slazyk[17], I. Sliusar[126], V. Smakhtin[173], B.H. Smart[135], S.Yu. Smirnov[138b], Y. Smirnov[34c], L.N. Smirnova[38,j], O. Smirnova[99], A.C. Smith[42], J.L. Smith[102], M. B. Smith[35], R. Smith[147], H. Smitmanns[101], M. Smizanska[92], K. Smolek[133], P. Smolyanskiy[133], A.A. Snesarev[39], H.L. Snoek[116], R. M. Snyder[51], S. Snyder[30], R. Sobie[169,n], A. Soffer[155], C.A. Solans Sanchez[37], E.Yu. Soldatov[39], U. Soldevila[167], A.A. Solodkov[34j], S. Solomon[27], A. Soloshenko[39], K. Solovieva[54], O.V. Solovyanov[41], P. Sommer[50], A. Sonay[13], A. Sopczak[133], A.L. Sopio[52], F. Sopkova[29b], J. D. Sorenson[114], I.R. Sotarriva Alvarez[139], V. Sothilingam[63a], O. J. Soto Sandoval[138c,138b], S. Sottocornola[68], R. Soualah[84a], Z. Soumaimi[36e], D. South[48], N. Soybelman[173], S. Spagnolo[70a,70b], D. Sperlich[54], B. Spisso[72a,72b], L. Splendori[103], M. Spousta[134], E.J. Staats[35], R. Stamen[63a], E. Stanecka[87], W. Stanek-Maslouska[48], M.V. Stange[50], B. Stanislaus[18a], M.M. Stanitzki[48], E.A. Starchenko[38], G.H. Stark[137], J. Stark[90], P. Staroba[132], P. Starovoitov[84d], R. Staszewski[87], C. Stauch[110], G. Stavropoulos[46], A. Stefl[37], A. Stein[101], P. Steinberg[30], B. Stelzer[146,160a], H.J. Stelzer[130], O. Stelzer[160a], H. Stenzel[58], T.J. Stevenson[150], G.A. Stewart[37], G. Stoicea[28b], M. Stolarski[131a], S. Stonjek[111], A. Straessner[50], J. Strandberg[148], S. Strandberg[47a,47b], M. Stratmann[175], M. Strauss[121], T. Strebler[103], P. Strizenec[29b], R. Ströhmer[170], D.M. Strom[124], R. Stroynowski[45], A. Strubig[47a,47b], S.A. Stucci[30], B. Stugu[17], J. Stupak[121], N.A. Styles[48], D. Su[147], S. Su[62], X. Su[62], D. Suchy[29a], A. D. Sudhakar Ponnu[55], L. Sudit[173], Y. Sue[83], K. Sugizaki[129], V.V. Sulin[38], D.M.S. Sultan[127], L. Sultanaliyeva[25], S. Sultansoy[3b], S. Sun[174], W. Sun[14], S. Sundar Raman[168], N. Sur[99], N. Suri Jr[176], M.R. Sutton[150], M. Svatos[132], P. N. Swallow[33], M. Swiatlowski[160a], A. Swoboda[37], I. Sykora[29a], M. Sykora[134], T. Sykora[134], D. Ta[101], K. Tackmann[48,ai], A. Taffard[163], R. Tafirout[160a], Y. Takubo[83], M. Talby[103], A.A. Talyshev[38], N.M. Tamir[155], A. Tanaka[157], J. Tanaka[157], R. Tanaka[66], M. Tanasini[149], Z. Tao[168], S. Tapia Araya[138g], S. Tapprogge[101], A. Tarek Abouelfadl Mohamed[37], S. Tarem[154], K. Tariq[14], G. Tarna[37], G.F. Tartarelli[71a],

JHEP10(2026)219

M. J. Tartarin[90], P. Tas[134], M. Tasevsky[132], E. Tassi[44b,44a], A.C. Tate[166], Y. Tayalati[36e,aj], G.N. Taylor[106], W. Taylor[160b], R.J. Taylor Vara[167], A.S. Tegetmeier[90], P. Teixeira-Dias[96], J.J. Teoh[159], K. Terashi[157], J. Terron[100], S. Terzo[13], M. Testa[53], R.J. Teuscher[159,n], A. Thaler[79], O. Theiner[56], T. Theveneaux-Pelzer[103], J.P. Thomas[21], E.A. Thompson[18a], P.D. Thompson[21], E. Thomson[129], R. E. Thornberry[45], C. Tian[62], Y. Tian[56], V. Tikhomirov[81], Yu.A. Tikhonov[39], S. Timoshenko[38], D. Timoshyn[134], E.X.L. Ting[1], P. Tipton[176], A. Tishelman-Charny[30], K. Todome[139], S. Todorova-Nova[134], L. Toffolin[69a,69c], M. Togawa[83], J. Tojo[89], S. Tokár[29a], O. Toldaiev[68], G. Tolkachev[103], M. Tomoto[83], L. Tompkins[147], E. Torrence[124], H. Torres[90], D. I. Torres Arza[138g], E. Torró Pastor[167], M. Toscani[31], C. Tosciri[40], M. Tost[11], D.R. Tovey[143], T. Trefzger[170], P.M. Tricarico[13], A. Tricoli[30], I.M. Trigger[160a], S. Trincaz-Duvoid[128], D.A. Trischuk[169], A. Tropina[39], D. Truncali[76a,76b], L. Truong[34c], M. Trzebinski[87], A. Trzupek[87], F. Tsai[149], M. Tsai[107], A. Tsiamis[156], P.V. Tsiareshka[39], S. Tsigaridas[160a], A. Tsirigotis[156,aa], V. Tsiskaridze[153a], E.G. Tskhadadze[153a], Y. Tsujikawa[88], I.I. Tsukerman[38], V. Tsulaia[18a], K. Tsuri[119], D. Tsybychev[149], Y. Tu[64b], A. Tudorache[28b], V. Tudorache[28b], S. B. Tuncay[127], S. Turchikhin[57b,57a], I. Turk Cakir[3a], R. Turra[71a], T. Turtuvshin[39,ak], P.M. Tuts[42], Y. Uematsu[83], F. Ukegawa[161], P.A. Ulloa Poblete[138c,138b], G. Unal[37], A. Undrus[30], J. Urban[29b], P. Urrejola[138e], G. Usai[8], R. Ushioda[158], M. Usman[109], F. Ustuner[52], Z. Uysal[81], V. Vacek[133], B. Vachon[105], T. Vafeiadis[37], A. Vaitkus[97], C. Valderanis[110], E. Valdes Santurio[47a,47b], M. Valente[37], S. Valentinetti[24b,24a], A. Valero[167], E. Valiente Moreno[167], A. Vallier[90], J.A. Valls Ferrer[167], D. R. Van Arneman[116], R. Van Den Broucke[128], A. Van Der Graaf[49], H. Z. Van Der Schyf[34j], P. Van Gemmeren[6], M. Van Rijnbach[37], S. Van Stroud[97], I. Van Vulpen[116], P. Vana[134], M. Vanadia[76a,76b], U. M. Vande Voorde[148], W. Vandelli[37], E.R. Vandewall[147], D. Vannicola[155], L. Vannoli[53], R. Vari[75a], M. Varma[176], E.W. Varnes[7], C. Varni[79], D. Varouchas[66], L. Varriale[167], K.E. Varvell[151], M.E. Vasile[28b], L. Vaslin[83], M. D. Vassilev[147], A. Vasyukov[39], L. M. Vaughan[122], R. Vavricka[134], T. Vazquez Schroeder[13], J. Veatch[32], V. Vecchio[102], M.J. Veen[104], I. Veliscek[30], I. Velkovska[94], L.M. Veloce[159], F. Veloso[131a,131c], A.G. Veltman[52], S.H. Venetianer[162], S. Veneziano[75a], A. Ventura[70a,70b], A. Verbytskyi[111], M. Verducci[74a,74b], C. Vergis[95], M. Verissimo De Araujo[82b], W. Verkerke[116], J.C. Vermeulen[116], C. Vernieri[147], M. Vessella[163], M.C. Vetterli[146,s], A. Vgenopoulos[101], N. Viaux Maira[138g,al], T. Vickey[143], O.E. Vickey Boeriu[143], G.H.A. Viehhauser[127], L. Vigani[63b], M. Vigl[111], M. Villa[24b,24a], M. Villaplana Perez[167], E.M. Villhauer[40], E. Vilucchi[53], M. Vincent[167], M.G. Vincter[35], A. Visibile[116], A. Visive[116], C. Vittori[37], I. Vivarelli[24b,24a], M.I. Vivas Albornoz[48], E. Voevodina[111], F. Vogel[110], J.C. Voigt[50], P. Vokac[133], Yu. Volkotrub[86b], L. Vomberg[25], E. Von Toerne[25], B. Vormwald[37], K. Vorobev[51], M. Vos[167], K. Voss[145], M. Vozak[37], L. Vozdecky[121], N. Vranjes[16], M. Vranjes Milosavljevic[16], M. Vreeswijk[116], N.K. Vu[142b,142a], R. Vuillermet[37], O. Vujinovic[101], I. Vukotic[40], I. K. Vyas[35], J.F. Wack[33], A. Wada[112], S. Wada[161], C. Wagner[147], J.M. Wagner[18a], W. Wagner[175], S. Wahdan[175], H. Wahlberg[91], C. H. Waits[121], J. Walder[135], R. Walker[110], K. Walkingshaw Pass[59], W. Walkowiak[145], A. Wall[129], E.J. Wallin[99], T. Wamorkar[147], K. Wandall-Christensen[167], A. Wang[62], A.Z. Wang[137], C. Wang[48], C. Wang[11],

JHEP10(2026)219

H. Wang[18a], J. Wang[64c], P. Wang[102], P. Wang[97], R. Wang[61], R. Wang[107], R. Wang[6], S. Wang[14], S.M. Wang[152], T. Wang[115], T. Wang[62], W.T. Wang[127], X. Wang[166], X. Wang[142a], X. Wang[48], Y. Wang[149], Y. Wang[114], Z. Wang[107], Z. Wang[142b], Z. Wang[107], C. Wanotayaroj[83], A. Warburton[105], A.L. Warnerbring[145], S. Waterhouse[96], A.T. Watson[21], H. Watson[52], M.F. Watson[21], E. Watton[37], G. Watts[140], B.M. Waugh[97], J. M. Webb[54], C. Weber[30], M.S. Weber[20], C. Wei[62], Y. Wei[54], A.R. Weidberg[127], E.J. Weik[118], J. Weingarten[49], C. Weiser[54], C.J. Wells[48], T. Wenaus[30], T. Wengler[37], N.S. Wenke[111], N. Wermes[25], M. Wessels[63a], A.M. Wharton[92], A. White[8], A.S. White[37], M.J. White[1], D. Whiteson[163], L. Wickremasinghe[125], W. Wiedenmann[174], M. Wielers[135], R. Wierda[148], C. Wiglesworth[43], H.G. Wilkens[37], J. J. H. Wilkinson[33], S. Williams[33], S. Willocq[104], B.J. Wilson[102], D.J. Wilson[102], P.J. Windischhofer[40], F.I. Winkel[31], F. Winklmeier[124], B.T. Winter[54], M. Wittgen[147], M. Wobisch[98], T. Wojtkowski[60], Z. Wolffs[116], J. Wollrath[37], M.W. Wolter[87], H. Wolters[131a,131c], M.C. Wong[137], E.L. Woodward[42], S.D. Worm[48], B.K. Wosiek[87], K.W. Woźniak[87], S. Wozniewski[55], K. Wraight[59], C. Wu[159], C. Wu[21], J. Wu[157], M. Wu[113b], M. Wu[115], S. Wu[14,am], S.L. Wu[174], X. Wu[62], Y. Wu[62], Y.Q. Wu[159], Z. Wu[4], Z. Wu[113a], J. Wuerzinger[111], T.R. Wyatt[102], B.M. Wynne[52], S. Xella[43], L. Xia[113a], M. Xie[62], A. Xiong[124], D. Xu[14], H. Xu[62], L. Xu[62], R. Xu[129], T. Xu[107], W. Xu[113a], Y. Xu[140], Z. Xu[52], R. Xue[130], B. Yabsley[151], S. Yacoob[11], Y. Yamaguchi[83], E. Yamashita[157], H. Yamauchi[161], T. Yamazaki[18a], Y. Yamazaki[85], S. Yan[59], Z. Yan[104], H.J. Yang[142a,142b], H.T. Yang[62], S. Yang[62], X. Yang[37], X. Yang[14], Y. Yang[157], Y. Yang[62], W-M. Yao[18a], C. L. Yardley[150], J. Ye[14], S. Ye[30], X. Ye[62], Y. Yeh[97], I. Yeletskikh[39], B. Yeo[18b], M.R. Yexley[97], T. P. Yildirim[127], K. Yorita[172], C. Young[147], C.J.S. Young[37], I.N.L. Young[59], N.D. Young[124], Y. Yu[62], J. Yuan[14,113c,am], M. Yuan[107], R. Yuan[142b], L. Yue[97], M. Zaazoua[62], B. Zabinski[87], I. Zahir[36a], A. Zaio[57b,57a], Z.K. Zak[87], T. Zakareishvili[167], S. Zambito[56], J.A. Zamora Saa[138d], J. Zang[157], R. Zanzottera[71a,71b], O. Zaplatilek[133], C. Zeitnitz[175], H. Zeng[14], D.T. Zenger Jr[27], O. Zenin[38], T. Ženiš[29a], S. Zenz[95], D. Zerwas[66], B. Zhang[171], D.F. Zhang[143], G. Zhang[14,am], J. Zhang[141a], J. Zhang[6], L. Zhang[62], L. Zhang[113a], P. Zhang[14,113c], R. Zhang[113a], S. Zhang[90], T. Zhang[157], Y. Zhang[140], Y. Zhang[97], Y. Zhang[62], Y. Zhang[113a], Z. Zhang[18a], Z. Zhang[141a], Z. Zhang[66], H. Zhao[140], T. Zhao[141a], Y. Zhao[35], Z. Zhao[62], Z. Zhao[62], A. Zhemchugov[39], J. Zheng[113a], K. Zheng[166], X. Zheng[62], Z. Zheng[147], D. Zhong[166], B. Zhou[107], B. Zhou[142b,142a], H. Zhou[7], N. Zhou[142a], Y. Zhou[15], Y. Zhou[113a], Y. Zhou[7], J. Zhu[107], X. Zhu[142b], Y. Zhu[142a], X. Zhuang[14], K. Zhukov[68], N.I. Zimine[39], J. Zinsser[63b], M. Ziolkowski[145], L. Živković[16], A. Zoccoli[24b,24a], K. Zoch[61], A. Zografos[37], T.G. Zorbas[143], O. Zormpa[46], L. Zwalinski[37]

[1] *Department of Physics, University of Adelaide, Adelaide, Australia*
[2] *Department of Physics, University of Alberta, Edmonton AB, Canada*
[3a] *Department of Physics, Ankara University, Ankara, Türkiye*
[3b] *Division of Physics, TOBB University of Economics and Technology, Ankara, Türkiye*
[4] *LAPP, Université Savoie Mont Blanc, CNRS/IN2P3, Annecy, France*
[5] *APC, Université Paris Cité, CNRS/IN2P3, Paris, France*
[6] *High Energy Physics Division, Argonne National Laboratory, Argonne IL, U.S.A.*
[7] *Department of Physics, University of Arizona, Tucson AZ, U.S.A.*

JHEP10(2026)219

[8] Department of Physics, University of Texas at Arlington, Arlington TX, U.S.A.
[9] Physics Department, National and Kapodistrian University of Athens, Athens, Greece
[10] Physics Department, National Technical University of Athens, Zografou, Greece
[11] Department of Physics, University of Texas at Austin, Austin TX, U.S.A.
[12] Institute of Physics, Azerbaijan Academy of Sciences, Baku, Azerbaijan
[13] Institut de Física d'Altes Energies (IFAE), Barcelona Institute of Science and Technology, Barcelona, Spain
[14] Institute of High Energy Physics, Chinese Academy of Sciences, Beijing, China
[15] Physics Department, Tsinghua University, Beijing, China
[16] Institute of Physics, University of Belgrade, Belgrade, Serbia
[17] Department for Physics and Technology, University of Bergen, Bergen, Norway
[18a] Physics Division, Lawrence Berkeley National Laboratory, Berkeley CA, U.S.A.
[18b] University of California, Berkeley CA, U.S.A.
[19] Institut für Physik, Humboldt Universität zu Berlin, Berlin, Germany
[20] Albert Einstein Center for Fundamental Physics and Laboratory for High Energy Physics, University of Bern, Bern, Switzerland
[21] School of Physics and Astronomy, University of Birmingham, Birmingham, U.K.
[22a] Department of Physics, Bogazici University, Istanbul, Türkiye
[22b] Department of Physics Engineering, Gaziantep University, Gaziantep, Türkiye
[22c] Department of Physics, Istanbul University, Istanbul, Türkiye
[23a] Facultad de Ciencias y Centro de Investigaciónes, Universidad Antonio Nariño, Bogotá, Colombia
[23b] Departamento de Física, Universidad Nacional de Colombia, Bogotá, Colombia
[24a] Dipartimento di Fisica e Astronomia A. Righi, Università di Bologna, Bologna, Italy
[24b] INFN Sezione di Bologna, Italy
[25] Physikalisches Institut, Universität Bonn, Bonn, Germany
[26] Department of Physics, Boston University, Boston MA, U.S.A.
[27] Department of Physics, Brandeis University, Waltham MA, U.S.A.
[28a] Transilvania University of Brasov, Brasov, Romania
[28b] Horia Hulubei National Institute of Physics and Nuclear Engineering, Bucharest, Romania
[28c] Department of Physics, Alexandru Ioan Cuza University of Iasi, Iasi, Romania
[28d] National Institute for Research and Development of Isotopic and Molecular Technologies, Physics Department, Cluj-Napoca, Romania
[28e] National University of Science and Technology Politechnica, Bucharest, Romania
[28f] West University in Timisoara, Timisoara, Romania
[28g] Faculty of Physics, University of Bucharest, Bucharest, Romania
[29a] Faculty of Mathematics, Physics and Informatics, Comenius University, Bratislava, Slovak Republic
[29b] Department of Subnuclear Physics, Institute of Experimental Physics of the Slovak Academy of Sciences, Kosice, Slovak Republic
[30] Physics Department, Brookhaven National Laboratory, Upton NY, U.S.A.
[31] Universidad de Buenos Aires, Facultad de Ciencias Exactas y Naturales, Departamento de Física, y CONICET, Instituto de Física de Buenos Aires (IFIBA), Buenos Aires, Argentina
[32] California State University, CA, U.S.A.
[33] Cavendish Laboratory, University of Cambridge, Cambridge, U.K.
[34a] Department of Physics, University of Cape Town, Cape Town, South Africa
[34b] iThemba Labs, Western Cape, South Africa
[34c] Department of Mechanical Engineering Science, University of Johannesburg, Johannesburg, South Africa
[34d] National Institute of Physics, University of the Philippines Diliman (Philippines), Philippines
[34e] Department of Physics, Stellenbosch University, Matieland, South Africa
[34f] University of KwaZulu-Natal, School of Agriculture and Science, Mathematics, Westville, South Africa
[34g] University of South Africa, Department of Physics, Pretoria, South Africa
[34h] University of Pretoria, Department of Mechanical and Aeronautical Engineering, Pretoria, South Africa
[34i] University of Zululand, KwaDlangezwa, South Africa
[34j] School of Physics, University of the Witwatersrand, Johannesburg, South Africa

JHEP10(2026)219

[35] Department of Physics, Carleton University, Ottawa ON, Canada
[36a] Faculté des Sciences Ain Chock, Université Hassan II de Casablanca, Morocco
[36b] Faculté des Sciences, Université Ibn-Tofail, Kénitra, Morocco
[36c] Faculté des Sciences Semlalia, Université Cadi Ayyad, LPHEA-Marrakech, Morocco
[36d] LPMR, Faculté des Sciences, Université Mohamed Premier, Oujda, Morocco
[36e] Faculté des sciences, Université Mohammed V, Rabat, Morocco
[36f] Institute of Applied Physics, Mohammed VI Polytechnic University, Ben Guerir, Morocco
[37] CERN, Geneva, Switzerland
[38] Affiliated with an institute formerly covered by a cooperation agreement with CERN
[39] Affiliated with an international laboratory covered by a cooperation agreement with CERN
[40] Enrico Fermi Institute, University of Chicago, Chicago IL, U.S.A.
[41] LPC, Université Clermont Auvergne, CNRS/IN2P3, Clermont-Ferrand, France
[42] Nevis Laboratory, Columbia University, Irvington NY, U.S.A.
[43] Niels Bohr Institute, University of Copenhagen, Copenhagen, Denmark
[44a] Dipartimento di Fisica, Università della Calabria, Rende, Italy
[44b] INFN Gruppo Collegato di Cosenza, Laboratori Nazionali di Frascati, Italy
[45] Physics Department, Southern Methodist University, Dallas TX, U.S.A.
[46] National Centre for Scientific Research "Demokritos", Agia Paraskevi, Greece
[47a] Department of Physics, Stockholm University, Sweden
[47b] Oskar Klein Centre, Stockholm, Sweden
[48] Deutsches Elektronen-Synchrotron DESY, Hamburg and Zeuthen, Germany
[49] Fakultät Physik, Technische Universität Dortmund, Dortmund, Germany
[50] Institut für Kern- und Teilchenphysik, Technische Universität Dresden, Dresden, Germany
[51] Department of Physics, Duke University, Durham NC, U.S.A.
[52] SUPA — School of Physics and Astronomy, University of Edinburgh, Edinburgh, U.K.
[53] INFN e Laboratori Nazionali di Frascati, Frascati, Italy
[54] Physikalisches Institut, Albert-Ludwigs-Universität Freiburg, Freiburg, Germany
[55] II. Physikalisches Institut, Georg-August-Universität Göttingen, Göttingen, Germany
[56] Département de Physique Nucléaire et Corpusculaire, Université de Genève, Genève, Switzerland
[57a] Dipartimento di Fisica, Università di Genova, Genova, Italy
[57b] INFN Sezione di Genova, Italy
[58] II. Physikalisches Institut, Justus-Liebig-Universität Giessen, Giessen, Germany
[59] SUPA — School of Physics and Astronomy, University of Glasgow, Glasgow, U.K.
[60] LPSC, Université Grenoble Alpes, CNRS/IN2P3, Grenoble INP, Grenoble, France
[61] Laboratory for Particle Physics and Cosmology, Harvard University, Cambridge MA, U.S.A.
[62] Department of Modern Physics and State Key Laboratory of Particle Detection and Electronics, University of Science and Technology of China, Hefei, China
[63a] Kirchhoff-Institut für Physik, Ruprecht-Karls-Universität Heidelberg, Heidelberg, Germany
[63b] Physikalisches Institut, Ruprecht-Karls-Universität Heidelberg, Heidelberg, Germany
[64a] Department of Physics, Chinese University of Hong Kong, Shatin, N.T., Hong Kong, China
[64b] Department of Physics, University of Hong Kong, Hong Kong, China
[64c] Department of Physics and Institute for Advanced Study, Hong Kong University of Science and Technology, Clear Water Bay, Kowloon, Hong Kong, China
[65] Department of Physics, National Tsing Hua University, Hsinchu, Taiwan
[66] IJCLab, Université Paris-Saclay, CNRS/IN2P3, 91405, Orsay, France
[67] Centro Nacional de Microelectrónica (IMB-CNM-CSIC), Barcelona, Spain
[68] Department of Physics, Indiana University, Bloomington IN, U.S.A.
[69a] INFN Gruppo Collegato di Udine, Sezione di Trieste, Udine, Italy
[69b] ICTP, Trieste, Italy
[69c] Dipartimento Politecnico di Ingegneria e Architettura, Università di Udine, Udine, Italy
[70a] INFN Sezione di Lecce, Italy
[70b] Dipartimento di Matematica e Fisica, Università del Salento, Lecce, Italy
[71a] INFN Sezione di Milano, Italy

JHEP10(2026)219

[71b] Dipartimento di Fisica, Università di Milano, Milano, Italy
[72a] INFN Sezione di Napoli, Italy
[72b] Dipartimento di Fisica, Università di Napoli, Napoli, Italy
[73a] INFN Sezione di Pavia, Italy
[73b] Dipartimento di Fisica, Università di Pavia, Pavia, Italy
[74a] INFN Sezione di Pisa, Italy
[74b] Dipartimento di Fisica E. Fermi, Università di Pisa, Pisa, Italy
[75a] INFN Sezione di Roma, Italy
[75b] Dipartimento di Fisica, Sapienza Università di Roma, Roma, Italy
[76a] INFN Sezione di Roma Tor Vergata, Italy
[76b] Dipartimento di Fisica, Università di Roma Tor Vergata, Roma, Italy
[77a] INFN Sezione di Roma Tre, Italy
[77b] Dipartimento di Matematica e Fisica, Università Roma Tre, Roma, Italy
[78a] INFN-TIFPA, Italy
[78b] Università degli Studi di Trento, Trento, Italy
[79] Universität Innsbruck, Department of Astro and Particle Physics, Innsbruck, Austria
[80] Department of Physics and Astronomy, Iowa State University, Ames IA, U.S.A.
[81] Istinye University, Sariyer, Istanbul, Türkiye
[82a] Departamento de Engenharia Elétrica, Universidade Federal de Juiz de Fora (UFJF), Juiz de Fora, Brazil
[82b] Universidade Federal do Rio De Janeiro COPPE/EE/IF, Rio de Janeiro, Brazil
[82c] Instituto de Física, Universidade de São Paulo, São Paulo, Brazil
[82d] Rio de Janeiro State University, Rio de Janeiro, Brazil
[82e] Federal University of Bahia, Bahia, Brazil
[83] KEK, High Energy Accelerator Research Organization, Tsukuba, Japan
[84a] Khalifa University of Science and Technology, Abu Dhabi, United Arab Emirates
[84b] New York University Abu Dhabi, Abu Dhabi, United Arab Emirates
[84c] United Arab Emirates University, Al Ain, United Arab Emirates
[84d] University of Sharjah, Sharjah, United Arab Emirates
[85] Graduate School of Science, Kobe University, Kobe, Japan
[86a] AGH University of Krakow, Faculty of Physics and Applied Computer Science, Krakow, Poland
[86b] Marian Smoluchowski Institute of Physics, Jagiellonian University, Krakow, Poland
[87] Institute of Nuclear Physics Polish Academy of Sciences, Krakow, Poland
[88] Faculty of Science, Kyoto University, Kyoto, Japan
[89] Research Center for Advanced Particle Physics and Department of Physics, Kyushu University, Fukuoka, Japan
[90] L2IT, Université de Toulouse, CNRS/IN2P3, UPS, Toulouse, France
[91] Instituto de Física La Plata, Universidad Nacional de La Plata and CONICET, La Plata, Argentina
[92] Physics Department, Lancaster University, Lancaster, U.K.
[93] Oliver Lodge Laboratory, University of Liverpool, Liverpool, U.K.
[94] Department of Experimental Particle Physics, Jožef Stefan Institute and Department of Physics, University of Ljubljana, Ljubljana, Slovenia
[95] Department of Physics and Astronomy, Queen Mary University of London, London, U.K.
[96] Department of Physics, Royal Holloway University of London, Egham, U.K.
[97] Department of Physics and Astronomy, University College London, London, U.K.
[98] Louisiana Tech University, Ruston LA, U.S.A.
[99] Fysiska institutionen, Lunds universitet, Lund, Sweden
[100] Departamento de Física Teorica C-15 and CIAFF, Universidad Autónoma de Madrid, Madrid, Spain
[101] Institut für Physik, Universität Mainz, Mainz, Germany
[102] School of Physics and Astronomy, University of Manchester, Manchester, U.K.
[103] CPPM, Aix-Marseille Université, CNRS/IN2P3, Marseille, France
[104] Department of Physics, University of Massachusetts, Amherst MA, U.S.A.
[105] Department of Physics, McGill University, Montreal QC, Canada
[106] School of Physics, University of Melbourne, Victoria, Australia

JHEP10(2026)219

[107] Department of Physics, University of Michigan, Ann Arbor MI, U.S.A.
[108] Department of Physics and Astronomy, Michigan State University, East Lansing MI, U.S.A.
[109] Group of Particle Physics, University of Montreal, Montreal QC, Canada
[110] Fakultät für Physik, Ludwig-Maximilians-Universität München, München, Germany
[111] Max-Planck-Institut für Physik (Werner-Heisenberg-Institut), München, Germany
[112] Graduate School of Science and Kobayashi-Maskawa Institute, Nagoya University, Nagoya, Japan
[113a] Department of Physics, Nanjing University, Nanjing, China
[113b] School of Science, Shenzhen Campus of Sun Yat-sen University, China
[113c] University of Chinese Academy of Science (UCAS), Beijing, China
[114] Department of Physics and Astronomy, University of New Mexico, Albuquerque NM, U.S.A.
[115] Institute for Mathematics, Astrophysics and Particle Physics, Radboud University/Nikhef, Nijmegen, Netherlands
[116] Nikhef National Institute for Subatomic Physics and University of Amsterdam, Amsterdam, Netherlands
[117] Department of Physics, Northern Illinois University, DeKalb IL, U.S.A.
[118] Department of Physics, New York University, New York NY, U.S.A.
[119] Ochanomizu University, Otsuka, Bunkyo-ku, Tokyo, Japan
[120] Ohio State University, Columbus OH, U.S.A.
[121] Homer L. Dodge Department of Physics and Astronomy, University of Oklahoma, Norman OK, U.S.A.
[122] Department of Physics, Oklahoma State University, Stillwater OK, U.S.A.
[123] Palacký University, Joint Laboratory of Optics, Olomouc, Czech Republic
[124] Institute for Fundamental Science, University of Oregon, Eugene, OR, U.S.A.
[125] Graduate School of Science, University of Osaka, Osaka, Japan
[126] Department of Physics, University of Oslo, Oslo, Norway
[127] Department of Physics, Oxford University, Oxford, U.K.
[128] LPNHE, Sorbonne Université, Université Paris Cité, CNRS/IN2P3, Paris, France
[129] Department of Physics, University of Pennsylvania, Philadelphia PA, U.S.A.
[130] Department of Physics and Astronomy, University of Pittsburgh, Pittsburgh PA, U.S.A.
[131a] Laboratório de Instrumentação e Física Experimental de Partículas — LIP, Lisboa, Portugal
[131b] Departamento de Física, Faculdade de Ciências, Universidade de Lisboa, Lisboa, Portugal
[131c] Departamento de Física, Universidade de Coimbra, Coimbra, Portugal
[131d] Centro de Física Nuclear da Universidade de Lisboa, Lisboa, Portugal
[131e] Departamento de Física, Escola de Ciências, Universidade do Minho, Braga, Portugal
[131f] Departamento de Física Teórica y del Cosmos, Universidad de Granada, Granada (Spain), Spain
[131g] Departamento de Física, Instituto Superior Técnico, Universidade de Lisboa, Lisboa, Portugal
[132] Institute of Physics of the Czech Academy of Sciences, Prague, Czech Republic
[133] Czech Technical University in Prague, Prague, Czech Republic
[134] Charles University, Faculty of Mathematics and Physics, Prague, Czech Republic
[135] Particle Physics Department, Rutherford Appleton Laboratory, Didcot, U.K.
[136] IRFU, CEA, Université Paris-Saclay, Gif-sur-Yvette, France
[137] Santa Cruz Institute for Particle Physics, University of California Santa Cruz, Santa Cruz CA, U.S.A.
[138a] Departamento de Física, Pontificia Universidad Católica de Chile, Santiago, Chile
[138b] Millennium Institute for Subatomic physics at high energy frontier (SAPHIR), Santiago, Chile
[138c] Instituto de Investigación Multidisciplinario en Ciencia y Tecnología, y Departamento de Física, Universidad de La Serena, Chile
[138d] Universidad Andres Bello, Department of Physics, Santiago, Chile
[138e] Universidad San Sebastian, Recoleta, Chile
[138f] Instituto de Alta Investigación, Universidad de Tarapacá, Arica, Chile
[138g] Departamento de Física, Universidad Técnica Federico Santa María, Valparaíso, Chile
[139] Department of Physics, Institute of Science, Tokyo, Japan
[140] Department of Physics, University of Washington, Seattle WA, U.S.A.
[141a] Institute of Frontier and Interdisciplinary Science and Key Laboratory of Particle Physics and Particle Irradiation (MOE), Shandong University, Qingdao, China
[141b] School of Physics, Zhengzhou University, China

JHEP10(2026)219

[142a] State Key Laboratory of Dark Matter Physics, School of Physics and Astronomy, Shanghai Jiao Tong University, Key Laboratory for Particle Astrophysics and Cosmology (MOE), SKLPPC, Shanghai, China
[142b] State Key Laboratory of Dark Matter Physics, Tsung-Dao Lee Institute, Shanghai Jiao Tong University, Shanghai, China
[143] Department of Physics and Astronomy, University of Sheffield, Sheffield, U.K.
[144] Department of Physics, Shinshu University, Nagano, Japan
[145] Department Physik, Universität Siegen, Siegen, Germany
[146] Department of Physics, Simon Fraser University, Burnaby BC, Canada
[147] SLAC National Accelerator Laboratory, Stanford CA, U.S.A.
[148] Department of Physics, Royal Institute of Technology, Stockholm, Sweden
[149] Departments of Physics and Astronomy, Stony Brook University, Stony Brook NY, U.S.A.
[150] Department of Physics and Astronomy, University of Sussex, Brighton, U.K.
[151] School of Physics, University of Sydney, Sydney, Australia
[152] Institute of Physics, Academia Sinica, Taipei, Taiwan
[153a] E. Andronikashvili Institute of Physics, Iv. Javakhishvili Tbilisi State University, Tbilisi, Georgia
[153b] High Energy Physics Institute, Tbilisi State University, Tbilisi, Georgia
[153c] University of Georgia, Tbilisi, Georgia
[154] Department of Physics, Technion, Israel Institute of Technology, Haifa, Israel
[155] Raymond and Beverly Sackler School of Physics and Astronomy, Tel Aviv University, Tel Aviv, Israel
[156] Department of Physics, Aristotle University of Thessaloniki, Thessaloniki, Greece
[157] International Center for Elementary Particle Physics and Department of Physics, University of Tokyo, Tokyo, Japan
[158] Graduate School of Science and Technology, Tokyo Metropolitan University, Tokyo, Japan
[159] Department of Physics, University of Toronto, Toronto ON, Canada
[160a] TRIUMF, Vancouver BC, Canada
[160b] Department of Physics and Astronomy, York University, Toronto ON, Canada
[161] Division of Physics and Tomonaga Center for the History of the Universe, Faculty of Pure and Applied Sciences, University of Tsukuba, Tsukuba, Japan
[162] Department of Physics and Astronomy, Tufts University, Medford MA, U.S.A.
[163] Department of Physics and Astronomy, University of California Irvine, Irvine CA, U.S.A.
[164] University of West Attica, Athens, Greece
[165] Department of Physics and Astronomy, University of Uppsala, Uppsala, Sweden
[166] Department of Physics, University of Illinois, Urbana IL, U.S.A.
[167] Instituto de Física Corpuscular (IFIC), Centro Mixto Universidad de Valencia — CSIC, Valencia, Spain
[168] Department of Physics, University of British Columbia, Vancouver BC, Canada
[169] Department of Physics and Astronomy, University of Victoria, Victoria BC, Canada
[170] Fakultät für Physik und Astronomie, Julius-Maximilians-Universität Würzburg, Würzburg, Germany
[171] Department of Physics, University of Warwick, Coventry, U.K.
[172] Waseda University, Tokyo, Japan
[173] Department of Particle Physics and Astrophysics, Weizmann Institute of Science, Rehovot, Israel
[174] Department of Physics, University of Wisconsin, Madison WI, U.S.A.
[175] Fakultät für Mathematik und Naturwissenschaften, Fachgruppe Physik, Bergische Universität Wuppertal, Wuppertal, Germany
[176] Department of Physics, Yale University, New Haven CT, U.S.A.
[177] Yerevan Physics Institute, Yerevan, Armenia

[a] Also at Department of Physics, King's College London, London, U.K.
[b] Also at Institute of Physics, Azerbaijan Academy of Sciences, Baku, Azerbaijan
[c] Also at Imam Mohammad Ibn Saud Islamic University, Saudi Arabia
[d] Also at Department of Physics, University of Thessaly, Greece
[e] Also at An-Najah National University, Nablus, Palestine
[f] Also at Department of Physics, University of Fribourg, Fribourg, Switzerland
[g] Also at Department of Physics, Westmont College, Santa Barbara, U.S.A.

JHEP10(2026)219

[h] Also at Departament de Fisica de la Universitat Autonoma de Barcelona, Barcelona, Spain
[i] Also at University of Siena, Italy
[j] Also at Affiliated with an institute formerly covered by a cooperation agreement with CERN
[k] Also at The Collaborative Innovation Center of Quantum Matter (CICQM), Beijing, China
[l] Also at Faculty of Physics, Sofia University, 'St. Kliment Ohridski', Sofia, Bulgaria
[m] Also at Università di Napoli Parthenope, Napoli, Italy
[n] Also at Institute of Particle Physics (IPP), Canada
[o] Also at Department of Physics, Bolu Abant Izzet Baysal University, Bolu, Türkiye
[p] Also at Faculty of Physics, University of Bucharest, Romania
[q] Also at Borough of Manhattan Community College, City University of New York, New York NY, U.S.A.
[r] Also at National Institute of Physics, University of the Philippines Diliman (Philippines), Philippines
[s] Also at TRIUMF, Vancouver BC, Canada
[t] Also at Department of Financial and Management Engineering, University of the Aegean, Chios, Greece
[u] Also at Institucio Catalana de Recerca i Estudis Avancats, ICREA, Barcelona, Spain
[v] Also at Henan University, China
[w] Also at Yeditepe University, Physics Department, Istanbul, Türkiye
[x] Also at Institute of Theoretical Physics, Ilia State University, Tbilisi, Georgia
[y] Also at CERN, Geneva, Switzerland
[z] Also at Center for Interdisciplinary Research and Innovation (CIRI-AUTH), Thessaloniki, Greece
[aa] Also at Hellenic Open University, Patras, Greece
[ab] Also at Department of Modern Physics and State Key Laboratory of Particle Detection and Electronics, University of Science and Technology of China, Hefei, China
[ac] Also at Department of Physics, Stellenbosch University, South Africa
[ad] Also at University of Colorado Boulder, Department of Physics, Colorado, U.S.A.
[ae] Also at Département de Physique Nucléaire et Corpusculaire, Université de Genève, Genève, Switzerland
[af] Also at Centre of Physics of the Universities of Minho and Porto (CF-UM-UP), Portugal
[ag] Also at Institute for Nuclear Research and Nuclear Energy (INRNE) of the Bulgarian Academy of Sciences, Sofia, Bulgaria
[ah] Also at Washington College, Chestertown, MD, U.S.A.
[ai] Also at Institut für Experimentalphysik, Universität Hamburg, Hamburg, Germany
[aj] Also at Institute of Applied Physics, Mohammed VI Polytechnic University, Ben Guerir, Morocco
[ak] Also at Institute of Physics and Technology, Mongolian Academy of Sciences, Ulaanbaatar, Mongolia
[al] Also at Millennium Institute for Subatomic physics at high energy frontier (SAPHIR), Santiago, Chile
[am] Also at University of Chinese Academy of Sciences (UCAS), Beijing, China
[†] Deceased

JHEP10(2026)219